ABSTRACT

BOSE, KAKOLI. Folding, Stability and Active Site Conformation of Procaspase-3
(Under the direction of Dr. A. Clay Clark)

We have examined the folding, assembly and active site conformation of a catalytically inactive mutant of procaspase-3 (procaspase-3(C163S)), a homodimeric protein that belongs to the caspase family of proteases. The caspase family, and especially caspase-3, is integral to apoptosis. We show that an uncleavable mutant (D_3A) of procaspase-3 is catalytically active with K_m similar to that of its mature counterpart. We developed limited proteolysis assays using trypsin and V8 proteases, which allow the examination of amino acids in three of five active site loops. In addition, we examined the response of the two tryptophanyl residues in the active site to several quenching agents over the pH range of 3 to 9. Overall, the data suggest that the major conformational change that occurs upon maturation results in formation of the loop bundle between loops L4, L2 and L2'. The pKa's of both catalytic groups decrease as a result of the loop movements. However, loop L3, which comprises the bulk of the substrate-binding pocket, does not appear to be unraveled and solvent exposed, even at lower pH. In order to understand the active site formation in the context of folding, we looked into the equilibrium unfolding of procaspase-3(C163S). The equilibrium unfolding of procaspase-3(C163S) is described by a four-state equilibrium model in which the native dimer undergoes an isomeration to a dimeric intermediate, and the dimeric intermediate dissociates to a monomeric intermediate, which then unfolds. Therefore, dimerization is a folding event and it contributes significantly to the protein

stability (18.8 kcal/mol of 25.8 kcal/mol). Equilibrium unfolding experiments of procaspase-3(C163S) at different pH shows maximum stability at pH 7.2, and a transition from four-state model to a three-state monomer and finally to a two-state monomer model with decrease in pH. This is representative of conformational change and dimer dissociation at lower pH (between pH 5 and 4). The pro-less variant of procaspase-3(C163S) folds reversibly only in 1:1 protein to pro-peptide ratio suggesting it might act as an intramolecular chaperone (IMC).

FOLDING, STABILITY AND ACTIVE SITE CONFORMATION OF PROCASPASE-3

by

Kakoli Bose

A dissertation submitted to the Graduate Faculty of North Carolina State University in partial fulfillment of the requirements for the Degree of Doctor of Philosophy

Molecular and Structural Biochemistry

Raleigh

2003

APPROVED BY:

_____ _____

(Chair of the Advisory Committee)

_____ _____

DEDICATION

I dedicate this work to my father Late Mr. Mohon Lal Ghose for his love and endless support.

BIOGRAPHY

Kakoli Bose grew up in Calcutta, India in a close and happy family with her grandparents, parents and sister. She graduated from Bethune College in Chemistry in 1994. She received her Master of Science degree from Calcutta University in Physical Chemistry in 1996. After that she worked as a high school teacher for one year in India. She joined the Ph. D program in the Biochemistry Department of North Carolina State University in 1999. She worked in Dr. A. Clay Clark's laboratory on folding, stability and active site conformation of procaspase-3. She will receive her Ph. D degree in Biochemistry in May 2004. She will be moving to Boston to reside with her husband Mrinal and daughter Roshnee.

ACKNOWLEDGEMENTS

I would like to thank my advisor Dr. Allan Clay Clark for his guidance and advice. Without him it would have been impossible to make this journey successful. I would also like to extend my gratitude towards my committee members Dr. William Miller, Dr. Carla Mattos and Dr. Timothy Elston for their feedbacks and helpful suggestions. I am thankful to my colleagues Yun-Ru Chen, Cristina Pop, Brett Feeney, Luming He and Randy Durren for their cooperation and constructive comments, especially during the lab meetings. I am grateful to Dr. Carla Mattos, Dr. John Cavanagh and their groups for helping me with crystallography and NMR. I am thankful to Dr. Guy Salvesen of Burnham Institute, California for providing us with the clones of tryptophan mutants of procaspase-3. I would also like to thank my professors for guiding me through these years at NCSU.

I am grateful to my family for encouraging me all along.

TABLE OF CONTENTS

Page

Page

Page

LIST OF FIGURES

Page

Page

Page

Page

LIST OF TABLES

Page

INTRODUCTION: BACKGROUND AND SIGNIFICANCE

Apoptosis and caspases

Apoptosis, a Greek term meaning "dropping of leaves from trees" [1], is an evolutionary conserved, tightly regulated process of cell suicide. In normal tissues, apoptosis provides a delicate balance between cell proliferation and cell death and therefore is important in maintaining homeostasis. However, in abnormal tissues, unregulated apoptosis is symptomatic of numerous diseases, including cancer, autoimmune disease, atherosclerosis and neurodegenerative disorders [2]. Apoptosis was defined based on readily visible morphological changes that occur in cells. These include cytoplasmic shrinkage, blebs on the plasma membrane, and appearance of intracellular inclusions or "apoptotic bodies." The morphological changes are in turn, accompanied by identifiable biochemical changes within the cell that facilitate phagocytosis by neighboring tissue. These include mitochondrial damage, nuclear membrane breakdown, chromatin condensation and DNA fragmentation [3].

There has been huge progress in the last decade in identifying the key components of the intracellular suicidal program [3]. The core of the program has been found in all eumetazoans. Thus, apoptosis is conserved throughout evolution from worm to human. The three major components that have been identified are the Bcl-2 family of proteins, the caspase family of endoproteases, and Apaf-1, which relays signals from the Bcl-2 protein family to caspases. In general, there are two activation cascades that lead to procaspase (zymogen of caspase) processing, and thus apoptosis: the death receptor-ligated pathway and the mitochondrial-initiated pathway. Both mechanisms utilize a

scaffold-mediated activation of a subset of procaspases, the upstream activator caspases. The common theme in these two pathways is that dimerization of the upstream procaspase, mediated by the scaffold, is sufficient for caspase activation because the procaspase dimer has low levels of activity and can autoprocess. This has been referred to as the closed proximity effect [4].

Biochemical studies have demonstrated that three proteins are necessary and sufficient to activate caspase-3, the executioner caspase through the mitochondrial pathway [5; 6]. These include cytochrome-c, Apaf-1, and procaspase-9. Apaf-1 contains three domains, including an amino terminal caspase recognition domain, a nucleotide binding domain and an oligomerization domain. The amino-terminal 85 residues constitute a domain that is homologous to the pro-domains of caspase-1, -2, and –9. The domain functions in caspase recruitment, and thus is referred to as a CARD, caspase recruitment domain. The CARD-CARD interactions are highly specific. In the presence of ATP and upon release of cytochrome-c from the mitochondria, Apaf-1 and cytochrome-c form a multimeric complex. Procaspase-9 is then recruited to the complex, called the apoptosome, and becomes activated through proteolysis. Active site mutants of procaspase-9 are not processed indicating that procaspase activation occurs through autoprocessing. Activated caspase-9 is released from the apoptosome and cleaves the downstream procaspases (-3, -6 and –7). The second mechanism of procaspase processing occurs by activation of the cell surface death receptors, a family of transmembrane proteins belonging to the tumor necrosis factor receptor superfamily. The mammalian death receptor is a member of this family. When the Fas receptor binds its ligand, the activation is translated into intracellular events that lead to caspase activation.

These events include ligand-induced receptor trimerization, recruitment of intracellular receptor-associated proteins, and recruitment of caspases [3]. The cytoplasmic region of Fas contains a death domain (DD), which recruits a DD-containing adapter protein, FADD (Fas associated adapter protein with a death domain). FADD contains two distinct domains, a DD and a homologous death-effector domain (DED), which is critical for recruiting the upstream procaspase-8 and –10. Following recruitment, the procaspase autoprocesses. Activated caspase-8 or –10 cleaves the downstream procaspase-3. While procaspase-1 is not an upstream activator caspase, its activation occurs by a similar mechanism. Procaspase-1 contains a CARD in its pro-domain and binds the adapter protein RICK (RIP-like interacting CLARP kinase). Like other adapters, RICK also contains two domains, an N-terminal serine/throenine kinase, and a C-terminal CARD. The significance of the kinase is currently unknown, but the CARD-CARD interaction leads to procaspase-1 autoprocessing**.** Caspases can also be activated by other proteases such as granzyme B, which is introduced into cells by cytotoxic lymphocytes and triggers apoptosis by cleavage and activation of caspases such as caspase-3 (Figure 1).

Caspases are cysteinyl aspartate specific proteases that have unusual requirement for aspartate at the P1 position of the substrate [7]. Currently, 14 caspases have been identified [8]. Based on genetic and biochemical work, caspases are categorized under three subfamilies [9; 10; 11]. The proteins in subclass I (caspases-1, -4, -5) function primarily in the inflammatory response, whereas proteins in the subclasses II (caspases-3, -7, -2) and III (caspases-6, -8, -9) function primarily in apoptosis. An alternative classification is based on the function of the caspase in the cascade, either activator or executioner. In this classification, the activator caspases (-2, -8, -9, -10) almost exclusively contain long pro-

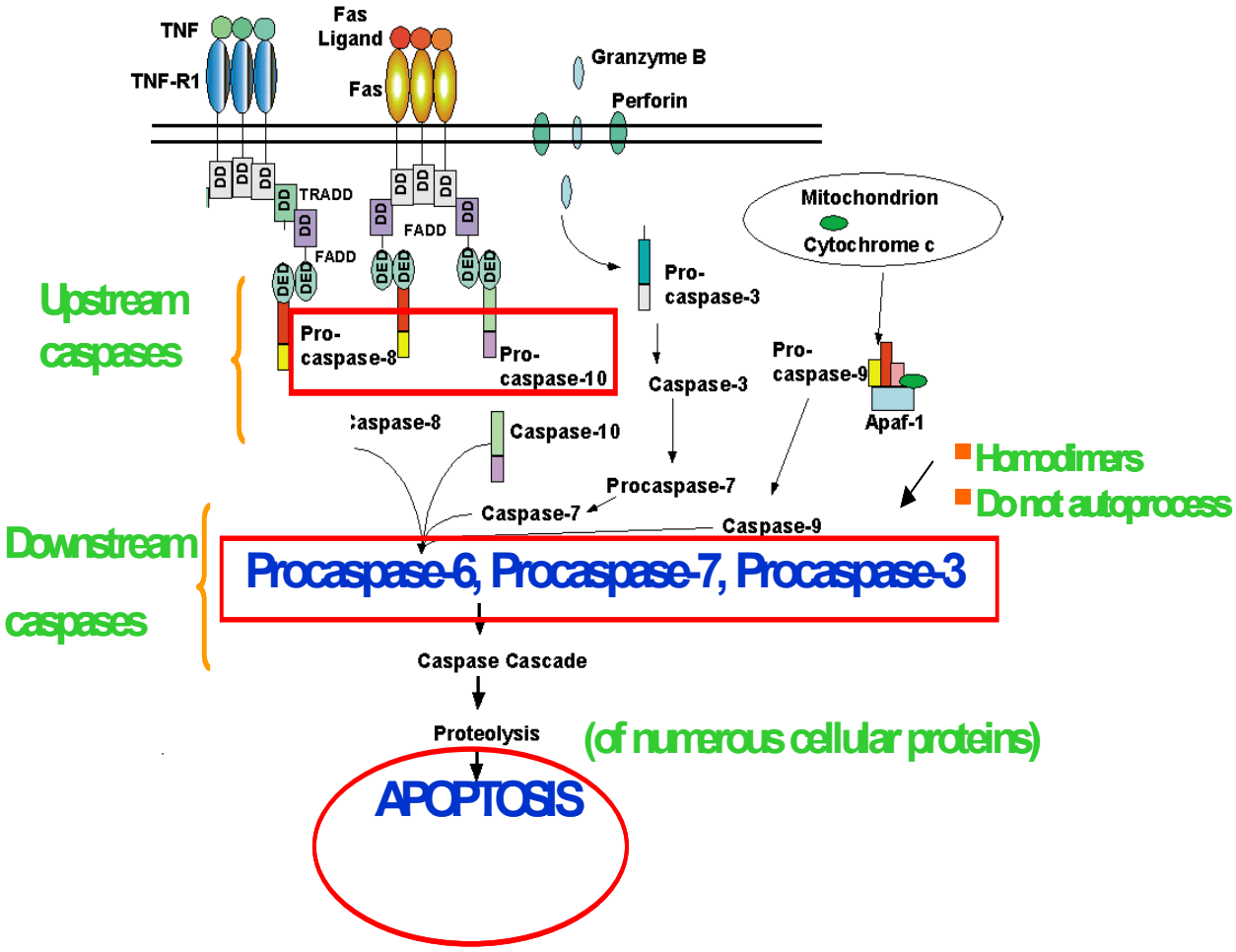

Figure 1. Pathways of caspase activation and initiation

domains (>100 amino-acids), whereas, the executioner caspases (-3, -6, -7) contain short pro-domains (25-30 amino acids). The long pro-domains are responsible for protein-protein interaction whereas, the functions of short pro-domains are currently unknown. Each caspase monomer is made up of a large subunit (~17 kDa) and a small subunit (~12 kDa) with a small linker region in between. The pro-domains vary in size depending on the class it belongs to. The organization of the subunits for procaspase-3 and its pro-less variant (procaspase-3 without the pro-domain) is shown in Figure 2. The phylogenetic relationship among the mammalian caspases is shown in Figure 3.

Caspase structure

Caspases exist in normal cells as inactive zymogens and are activated by proteolytic processing. All caspases have similar folds and share 30-50% amino acid sequence identity [12]. Crystal structures of several caspases [13; 14; 15; 16; 17; 18; 19] demonstrate the structural homology within the family (Figure 4). The mature, enzymatically active caspases are tetramers with M_r of approximately 60 kDa and consist of two copies of each of two non-identical subunits, described as dimers of heterodimers. The subunits are arranged in αβ-βα configurations, where α represents the large subunit, β represents the small subunit, and αβ represents one heterodimeric unit. Interestingly, the two subunits in the αβ heterodimer form a single domain, which consists of a six-stranded β-sheet core flanked by α-helices.

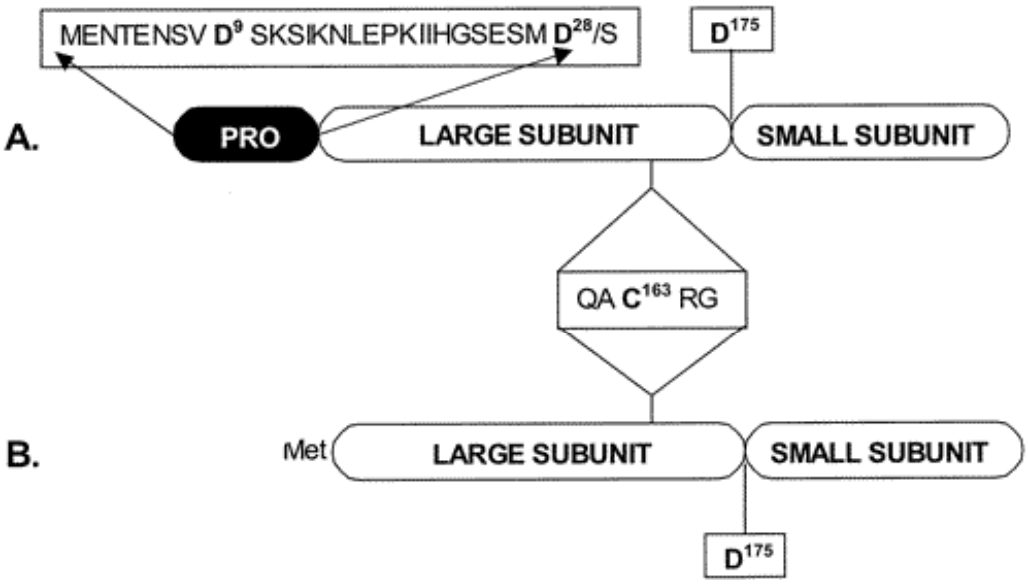

Figure 2. Cartoon demonstrating the structure of procaspase-3 and its pro-less variant. A. Procaspase-3 structure showing the sequence of the pro-domain (28 amino acids), large subunit (17 kDa), and small subunit (12 kDa). B. The figure shows organization of the pro-less variant of procaspase-3. D^{9}, D^{28} and D^{175} are the cleavage sites that are cleaved during zymogen processing. $QAC^{163}RG$ is the active site, C163 being the active site cysteine residue [22].

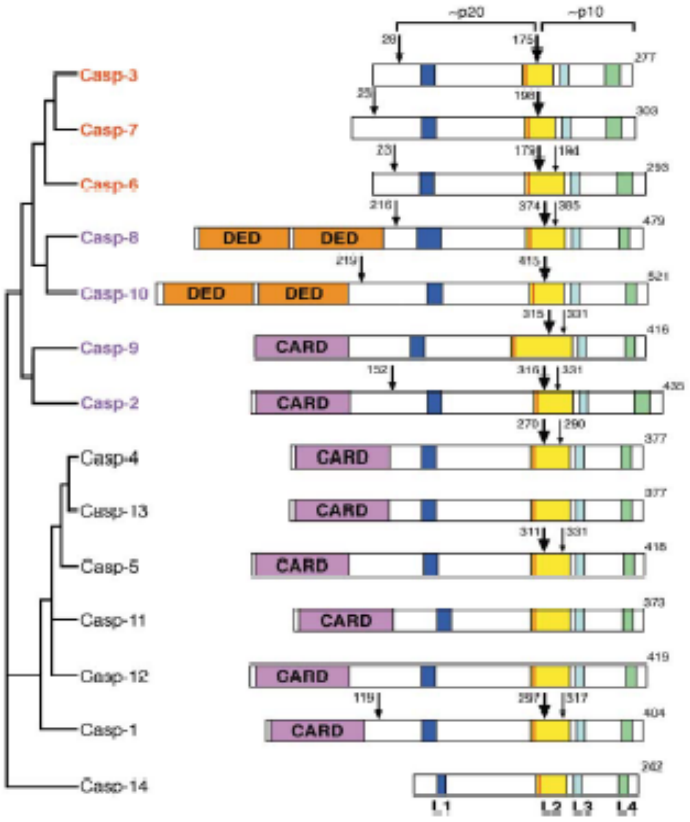

Figure 3. Schematic diagram of the mammalian caspases. Except caspase-11 (mouse), -12 (mouse), and –13 (bovine), all listed caspases are of human origin. Their phylogenetic relationship (*left*) appears to correlate with their function in apoptosis or inflammation. The initiator and activator caspases are labeled in purple and red respectively. The position of the first activation cleavage (between the large and the small subunits) is highlighted with a large arrow while additional sites of cleavage are represented by medium and small arrows. In contrast to the other protease zymogens, removal of the pro-domain of a caspase is unnecessary for its catalytic activity. The four surface loops (L1-L4) that shape the catalytic groove are indicated. The catalytic residue Cys is shown as a red line at the beginning of loop L2. This diagram is scaled according to the lengths of caspases and the location of functional segments [23].

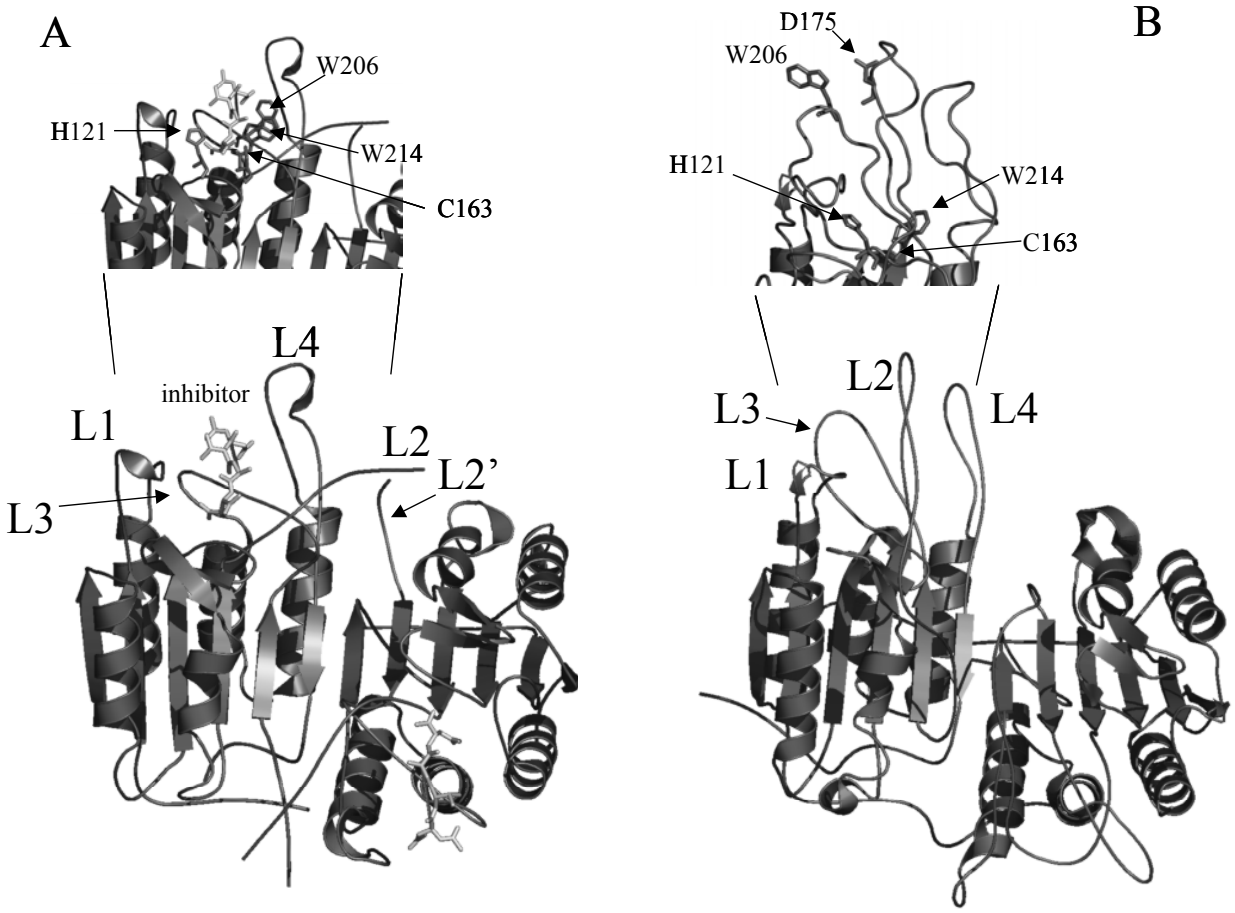

Figure 4. A. Mature caspase-3 (inhibitor bound) structure (PDB id: 1CP3) and B. Procaspase-7 structure (PDB id: 1GQF) generated with *PyMOL* (Delano Scientific, CA). For both A and B, L1 (residues 52-64), L2 (residues 163-175), L2' (residues 176'-192'), L3 (residues 198-213) and L4 (residues 246-263) represent the five active site loops as described in the text. The prime indicates residues from the second heterodimer. The two tryptophan residues (W206 and W214), the cleavage site aspartate residue (D175) and the two catalytic residues (H121 and C163) are highlighted in the inset (caspase-3 numbering). For clarity only one active site is labeled for the two proteins.

Caspase-3- the executioner

Caspase-3 (CPP32, apopain, Yama) is the primary executioner during apoptosis [20; 21] and it has been generally accepted that caspase-3 is the primary death effector protease in humans. Like other caspases it exists as an inactive precursor procaspase-3 that is activated by cleavage in the intersubunit linker at D175 and then slowly at D9 and D28 to remove the pro-domain (Figure 5). The cleavage at D175 is sufficient to allow for full activity [24]. Although a lot of information is available on caspase-3, very little is known about the procaspase.

Caspase-3 contains an active-site pentapeptide QACRG. There is an absolute requirement for an Asp in the P_1 position. However, the residues that form the P_2–P_4 binding pocket are not well conserved, suggesting that they may determine the substrate specificities of the different caspases. The amino acids Cys-163 and His-121 are involved in catalysis. During substrate/inhibitor binding, rearrangement of the active site loops allows the Cys-163 to reorient and form the oxyanion hole. Residues Cys-163, His-121 and Gly-122 interact with the substrate/inhibitor to form a tetrahedral intermediate (Figure 6). The substrate-binding groove is shaped by four surrounding loops, L1-L4 [23]. L1 constitutes one side of the groove, whereas, L4 represents the other side. Loop L3 and the following β hairpin, collectively referred to as L3, are located at the base of the groove. L2, which harbors the catalytic residue C163, is positioned at one end of the groove with the side chain of C163 pointing along the groove, poised for binding and catalysis. L1 and L3 are conserved in length and composition among caspases while L2 and L4 are highly divergent. These four loops determine the sequence specificity of the substrates. All caspases have similar conformation at the substrate-binding groove. The

A. B.

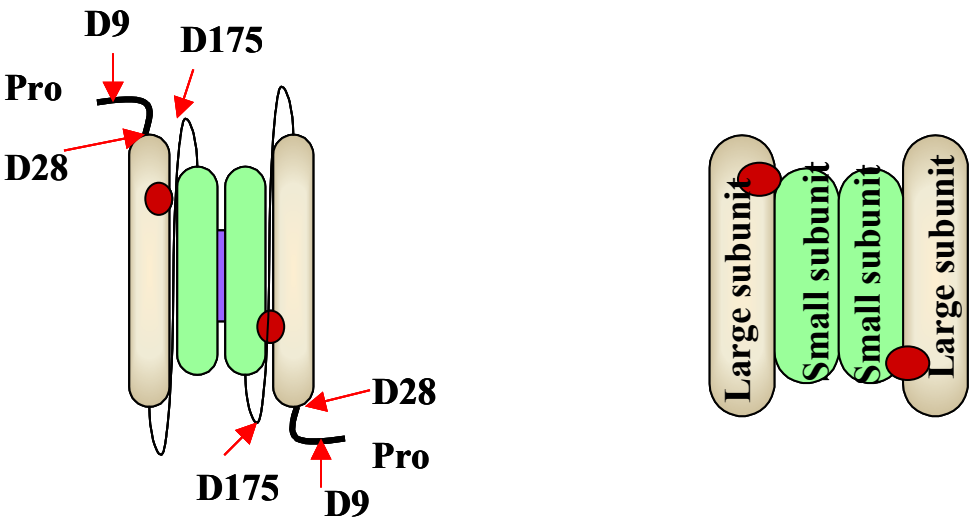

Figure 5. A. Schematic diagram showing arrangement of the two procaspase-3 monomers to form the heterotetramer. The pro-domain and the three processing sites D^{9}, D^{28} and D^{175} are labeled. The red circle represents the active site. The gray blocks are large and the green blocks represent the small subunits. The blue region is the dimer-dimer interface. B. Processed caspase-3 structure.

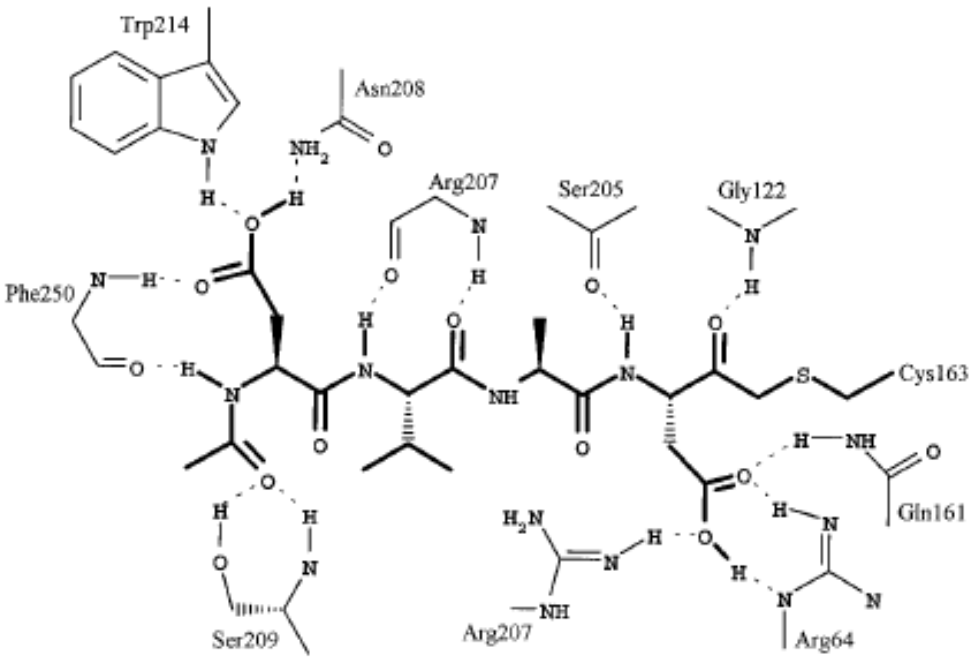

Figure 6. Hydrogen bonds and salt bridges in the CPP32-Ac-DEVD-FMK complex. The inhibitor is covalently linked to the active site Cys 163 via a thioether bond. The inhibitor is shown by thick lines. Hydrogen bonds are represented as dashed lines [19].

conformational similarity at the active site is extended to the surrounding structural elements. Most notably, the loops L4 and L2 from one catalytic subunit are stabilized by the N-terminus (loop L2') of the small subunit of the other catalytic subunit forming a structure called "loop bundle."

Until recently, procaspase-3 was thought to be a monomer and was frequently drawn as a monomer in literature reviews [25]. Work from our laboratory has shown that the protein is dimeric under the protein concentrations found *in vivo* [22]. These results as well as previous studies [25] suggest the model shown in Figure 7 for maturation of procaspase-3. Before processing, two molecules of procaspase-3 form a dimer by association (A), generating a structure similar to that of caspase-3 heterotetramer. The dimeric procaspase-3 is cleaved at D175 to form the maturation intermediate (B). The pro-domain is then cleaved rapidly at D9 (C), then more slowly at D28, generating the mature heterotetramer (D).

While, there are many aspects known about the pathway shown in Figure 7, there remain several unanswered questions. Three of these important questions are the following. (1) Although, the pathway suggests that dimerization is an early event in maturation of the short pro-domain caspases, it is important to understand procaspase-3 dimerization in the context of folding, that is, whether the dimer forms from two native monomers or whether dimerization occurs during folding. (2) What is the function of the short pro-domain in folding and maturation of procaspase-3? (3) Why does not the dimeric procaspase-3 autoprocess? Also, it is interesting to see how folding and active site formation is possibly linked. Previous studies have shown that caspase-1 monomer is not active [26], whereas, in caspase-9 only one active site is active due to movements of

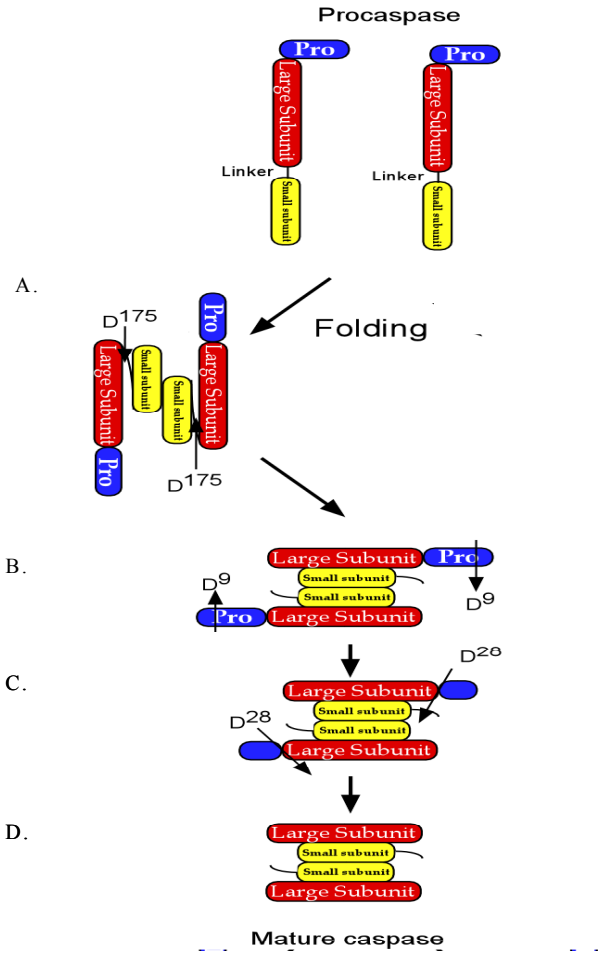

Figure 7. Model for procaspase assembly and maturation. Before processing, two molecules of procaspase form a dimer by association (*Structure* A), generating a structure similar to that of caspase heterotetramer. The dimeric procaspase is cleaved at Asp 175 (caspase-3 numbering) to form the maturation intermediate (*Stucture* B). The pro-domain is then cleaved rapidly at Asp9 (*Structure* C), then more slowly at Asp28 to give the mature heterotetramer (*Structure* D).

residues in the dimer interface. This suggests a coupling between dimerization and active site formation.

In order to find answers to these questions, the folding and assembly of procaspase-3 was examined via urea denaturation studies using spectroscopic probes at different pH. In addition, the studies were performed over a broad pH range. In the broader context, these studies are also important in looking into the folding pathway of large multi-domain proteins. The role of the pro-domain was explored spectroscopically by adding the pro-domain (in different amounts) to the pro-less variant of procaspase-3. The lower activity of procaspase-3 with respect to its mature counterpart and its active site conformation were studied using several biochemical and biophysical techniques and comparing the results with the recently published structure of homologous procaspase-7 [27; 28].

I. Characterization of active site conformation of procaspase-3

Although there is a large pool of procaspase-3 in the cell (~100 nM) [29], it is unclear why the protein is inactive. Moreover, procaspase-3 is known to auto-activate when expressed in *E. coli* cells [19] or *in vitro* [22]. While it remains unclear why procaspase-3 does not auto-process in eukaryotic cells, the activation in *E. coli* is thought to be due to artificially high protein concentrations in those systems.

The structures of several mature caspases, with inhibitors bound, have been solved [13; 14; 15; 16; 17; 18; 19], but until recently, structural information of the procaspases was not available. The structure of procaspase-7, described by Chai *et al*. [27] and Riedl *et al*. [28] has allowed a detailed comparison of the caspase structure as it undergoes maturation [23]. Procaspase-7 is thought to represent the executioner sub-group of caspases, and indeed,

caspases-3 and -7 share a 55% amino acid sequence identity. The structures of mature caspase-3 and of procaspase-7 are summarized in Figure 4 and show that the two proteins are very similar.

The differences between the two forms of the proteins are observed primarily in four surface loops (L1-L4) that comprise the active sites. Three of the loops (L2-L4) undergo conformational changes after zymogen processing. In particular, loop L3, which forms the bulk of the substrate-binding pocket, is found to be unraveled and extends away from the active site. In the mature caspase, this loop moves over 10 Å toward the body of the protein and forms the base of the catalytic groove. Loop L4, which forms one side of the active site, rotates 60° and forms interactions with loop L2. The active-site cysteinyl residue C163 (caspase-3 numbering), which is present at the base of loop L2, is rotated away from solvent, and in the zymogen, loop L2 extends into the intersubunit linker.

Following cleavage at D175 to generate apo-caspase-7, loops L3 and L4 move to positions similar to those found in the holo-enzyme [18]. However, the intersubunit linker, now called loop L2', remains in the "closed" conformation, that is, L2' is folded back into the central cavity, as observed in the procaspase. The binding of substrate/inhibitor induces the conformational change to the fully productive state. Loop L2 reorients so that it interacts with loop L4. This movement changes the orientation of the catalytic cysteine by 90°, positioning the side chain for attack of the substrate, and allows the backbone amides of C163 and G122 to form the oxyanion hole. In addition, loop L2' flips 180° to interact with loops L2 and L4 of the second active site, forming the so-called loop-bundle. Numerous hydrogen bonds and van der Waals interactions in the loop bundle stabilize the active site conformation.

The structures suggest mechanisms for the procaspase dormancy. For example, Riedl *et al.* [28] showed that the C-terminal segment of the intersubunit linker, in particular K186-V189 (caspase-3 numbering), occupies the central cavity of the procaspase dimer interface. The isopropyl side chain of V189 in the "blocking segment" [28] of one monomer prevents the insertion of the "elbow loop" region of loop L3 in the opposite monomer. Insertion of the elbow loop (S198-S205) in the active caspase stabilizes the active site conformation via stacking interactions between Y197, R164, and P201. As a result of positioning the blocking segment in the central cavity, the amino acids in the elbow loop are shifted into the binding pocket. The overall result is that loop L3 is unraveled, and the S1, S2, and S4 subsites are not well formed [28]. The flipping of loop L2' upon substrate/inhibitor binding removes the blocking segment from the central cavity. Thus, the covalent connectivity between the subunits prevents formation of the loop bundle, and the blocking segment prevents formation of the substrate-binding pocket.

The pH-effect that occurs early in apoptosis is due, in part, to pH-induced conformational changes in caspases that increase their rate of activation. Recently, Nicholson and coworkers [30], showed that in *E.coli* cell extracts the rate of autocatalytic processing of procaspase-3 increased as the pH decreased from 7 to 5.5. These results suggest that there is a pH-induced effect on procaspase structure and maturation. Moreover, this was the first study that showed that procaspase-3 is active. Nicholson and coworkers further showed that a tripeptide ^{179}DDD^{181} was important in the pH-dependent mechanism-a mutation of D$^{179\text{-}181}$N abrogates the pH-dependent autoactivation and produces a procaspase-3 protein that rapidly autoactivates at higher pH. Therefore, they show that a tri-aspartate "safety-catch" in the intersubunit linker (D179-D181 affects

procaspase dormancy in a pH-dependent manner [30]. It was suggested that the loop containing the tri-peptide adopts a pH-sensitive conformation that renders the IETD175 cleavage site inaccessible.

Removal of the ionic interactions afforded by the safety-catch results in a marked increase in rates of autoactivation, presumably by exposing D175. Nicholson and coworkers used an active site probe that required catalytic turnover to covalently modify the active site cysteine to show that procaspase-3 is catalytically competent [30]. That procaspase-3 has enzymatic activity is in keeping with results for other procaspases (procaspases-1,-8, -9, for example) [26; 31; 32], which clearly show that the procaspases contain enzymatic activity when the proforms are recruited into the oligomeric scaffolds. However, the results of Nicholson and coworkers [30] appear to contrast with the recent structures of procaspase-7, which demonstrate that peptide substrates cannot be bound properly due to the incomplete or ill formed S1, S2, and S4 subsites.

In order to solve the puzzle and also to understand the active site formation in the context of folding, we looked into the active site conformation of procaspase-3 and compared it with caspase-3 using several biochemical and biophysical probes.

II. Folding and stability of procaspase-3

The clear understanding of a biological concept requires insights from physical chemistry. While it has been observed that biological activity of a protein is dependent on its ability to fold into the correct three-dimensional structure, predicting the correct fold of a protein based solely on its primary sequence, the so-called “protein folding

problem," has been elusive. The problem will become critical in the post-genomic age for gaining precise information on intricate biological functions of proteins.

As first shown by Anfinsen [33] and later pointed out by Baker [34], the simplest case of biological self-organization is the spontaneous self-assembly of protein molecules into a unique three-dimensional structure that carries out biological function. While great interest in this area over the past few decades has resulted in a plethora of experimentation [35], most of the experimental systems have been confined to small single-domain proteins [36]. For most of those proteins, partially ordered non-native conformations, that is, folding intermediates, are not typically observed. The folding could be well modeled as a two-state transition between a denatured state and the ordered native state. While these models provide a framework for solutions to the folding problem, they cannot account for the complexities of folding of multi-domain or multi-subunit proteins. One challenge that underlies protein folding studies in the onset of proteomics is to correlate the functional features found in protein families with the evolutionary conservation of sequence identity [37] as well as conserved structural topology [34]**.** For example, picornaviral 3C cysteine proteinases have a fold similar to chymotrypsin-like serine proteinases [38]. While models of contact order [34] and conservatism [37] have been developed using small proteins with well-characterized two-state folding transitions, eventually these or other models must be extended to larger multi-domain or multi-subunit proteins. Domains are considered as the basic units of protein folding, evolution, and function. Decomposing each protein into modular domains is thus a basic prerequisite for accurate functional classification of biological molecules. A complete understanding of folding and assembly will fully reflect the

balance between local and global interactions, including global interactions between subunits. Moreover, protein folding also has practical applications in the understanding of different pathologies and the development of novel therapeutics to prevent diseases associated with protein misfolding and aggregation. An increasing family of neurodegenerative disorders such as Alzheimer's, Parkinson's and Huntington's diseases, prion encephalopathies and cystic fibrosis is associated with aggregation of misfolded polypeptide chains which are toxic to the cell. Transmissible spongiform encephalopathies or prion-related disorders, occurs due to misfolding of the normal prion protein. Aggregation and deposition are a result of malfunction in protein folding, assembly, and transport, caused by protein mutation and/or changes in the cell environment [39]. The mechanism of protein deposition and aggregation is triggered when the hydrophobic and positively charged regions of the misfolded proteins are exposed. The cells aim to regulate these misfolded and malfunctioning aggregation-prone proteins by degradation mechanisms, such as, proteosomes, and/or by storing them in specialized compartments, for example, Russell bodies and aggresomes. Study of the folding and stability of these proteins will help develop therapeutic strategies for these diseases. Because of these and other considerations, we have examined the folding and assembly of procaspase-3.

III. Role of the short pro-domain in procaspase-3

Although, it is well known that the long pro-domain caspases are involved in protein-protein interactions through their CARD (caspase recruitment domain) domains, the role of the pro-domains in short pro-domain caspases (~ 28 amino acids) are unknown.

Interestingly, after removal of the CARD domain from the long pro-domain caspases like caspase-1, the number of remaining amino acids is similar to the pro-domains of caspase-3, -6 and –7, although the sequence identity is quite low. It is possible that the caspase pro-domains are bifunctional. One is to promote CARD-CARD interaction with other CARD-containing proteins, the other, that involved the remaining 28 amino acids, is still undefined. It might be possible that the short pro-domain acts as a vestigial linker between the CARD domain and the amino terminus of the large subunit. Since the downstream caspases are activated by the upstream caspases, the CARD may have been lost through evolution, whereas, the vestigial linker comprising 28 amino acids is retained. Another possibility is that it attenuates procaspase activity. Salvesen and coworkers [10] as well as our work [22] have shown that the pro-peptide does not affect the activity of the mature caspase and therefore it is not an attenuator of its activity. The third possibility is that the pro-domain acts as an intramolecular chaperone (IMC).

In several classes of proteases, serine, aspartyl, cysteine, and metalloprotease, the proteins are synthesized as pro-peptide dependent zymogens [40]. The pro-regions of those systems have two distinct functions, assisting folding or inhibiting the activity of the protease domain. For example, subtilisin, a serine protease homologous with eukaryotic pro-hormone convertases is synthesized as a zymogen in which the pro-peptide functions as an intramolecular chaperone (IMC) essential for proper activation and secretion of the protease *in vivo*. Moreover, alpha-lytic protease [41; 42] is a precursor containing a 166 amino-acid pro region transiently required for the correct folding of the protease domain. By omitting the pro region in an *in vitro* refolding reaction, an inactive, but folding competent state having an expanded radius yet native-like secondary structure was

trapped. This state is stable for weeks at physiological pH in the absence of denaturant, but rapidly folds to the active, native state on addition of the pro region as a separate polypeptide chain. Anfinsen demonstrated that all the information necessary for folding of a protein into an active conformation resides in the amino acid sequence of that protein [43]. On the other hand, pro-aminopeptidase processing protease (PA protease) is a thermolysin-like metalloprotease, the N-terminal pro-peptide of which acts as an intramolecular chaperone to assist the folding of PA protease and shows inhibitory activity toward its cognate mature enzyme. Moreover, the N-terminal pro-peptide strongly inhibits the autoprocessing of the C-terminal pro-peptide by forming a complex with the folded intermediate pro-PA protease containing the C-terminal pro-peptide.

Based on Anfinsen's observation, the native state of a protein is generally believed to be the global free energy minimum. However, there is increasing evidence that kinetically selected states play a role in the biological function of some proteins. For example, the serpin plasminogen activator inhibitor 1 folds into an active structure and then converts slowly to a more stable, but low activity "latent" conformation [44]. Thus, the folding of plasminogen activator inhibitor 1 is apparently under kinetic control. When alpha-lytic protease [45; 46] and subtilisin are folded in the absence of their pro-peptides, they fold into partially structured molten globule intermediates. These stable but inactive intermediates can convert into active conformations upon addition of their pro-peptides and suggest that pro-peptides promote folding of their proteases by direct stabilization of the rate-limiting folding transition state. Based on these evidences, we looked into the equilibrium folding and unfolding of the pro-less variant of procaspase-3 in presence and absence of the pro-peptide.

MATERIALS AND METHODS

Plasmid Construction

The procaspase-3 gene was amplified by PCR from pET21b-CPP32 [47], kindly provided by Dr. Emad Alnemri, using the primers HC3P32F (GTCGCGGATCATATGGAGAACACTG) and HC3P12R (GTGGTGGTGGTGCTCGAGGTG). This introduced an *Nde*I site at the 5' end of the gene and an *Xho*I site at the 3' end of the gene. The amplified gene product was inserted into pET21b that had been digested with *Nde*I and *Xho*I. This strategy removed 14 amino acids at the amino terminus of procaspase-3 that arise from the vector in pET21b-CPP32. The resulting plasmid, pHC332, produces procaspase-3 with the correct amino terminus. The active site cysteine (Cys163) was mutated to serine using Quick-Change site-directed mutagenesis kit (Stratagene), with the primers HCP3CS1 (5'-CATTATTCAGGCCT**C**CCG<u>C</u>GGTACAGAACTGGACTGTGG-3') and HCP3CS2 (5'-CAGTTCTGTACC<u>G</u>CGG**G**AGGCCTGAATAATGAAAAGTTTGG-3'), and plasmid pET21b-CPP32. This strategy also introduced a unique *Sac*II site (underlined) downstream of the C163S mutation (shown in boldface type). Plasmids were first screened by digestion with *Sac*II, and positive clones were sequenced to confirm the mutation. The mutated gene was cloned into pET21b, as described above, to produce the plasmid pHC33201.

Plasmid pHC32901 was constructed by subcloning the DNA for the procaspase-3 large and small subunits from pHC33201. The primers for PCR amplification were HC3P17F (5'-GCGAATCACATATGTCTGGAATATCCC-3') and HC3P12R (5'-

GTGGTGGTGGTGCTCGAGGTG-3'), generating *Nde*I and *Xho*I sites at the 5' and 3' ends, respectively. The ~750 bp fragment was inserted into pET21b digested with *Nde*I and *Xho*I. The resulting proteins [pro-caspase-3(C163S) and pro-less variant] have carboxyl termini consisting of the sequence Leu-Glu-His_6 that arise from the vector.

Procaspase-3 mutants were created using the Quick-Change site directed mutagenesis kit (Stratagene) and the primers described below. The procaspase-3(D9A,D28A,D175A) mutant was made by a three-step process from plasmid pHC332 [22], harboring the gene for wild-type human procaspase-3. First, D175 was mutated to alanine using primer 1 (5'-GTGGCATTGAGACAG**CTAGC**GGTGTTGATGATG-3') and primer 2 (5'-CATCATCAACACC**GCTAGC**TGTCTCAATGCCAC-3'). In the background of D175A, D28 was mutated to alanine using primer 3 (5'-GGAAGCGAATCAATGG**CCAG**TGGAATATCCCTG-3') and primer 4 (5'-CAGGGATATTCCA**CTGGCCA**TTGATTCGCTTCC-3'). In the background of D28A/D175A, D9 was mutated to alanine using primer 5 (5'-GAAAACTCAGTGG**CTAGC**AAATCCATTAAAAATTTGG-3') and primer 6 (5'-CCAAATTTTTAATGGATTT**GCTAGC**CACTGAGTTTTC-3'). The primers incorporated the following restriction sites for screening mutants. Primers 1 and 2: *Nhe*I; primers 3 and 4: *Bal*I (*Msc*I); primers 5 and 6: *Nhe*I. The mutations are shown in bold, and the restriction sites are underlined. All plasmids were sequenced (both strands) to confirm the mutations. The resulting plasmid is called pHC33209, and we refer to this mutant as procaspase-3(D_3A). All constructs were sequenced (both strands) in order to confirm the correct sequence. The plasmids for procaspase-3(C163A,W206Y) and procaspase-3(C163A,W214V) were kindly provided by Dr. Guy Salvesen (Burnham

Table I: List of buffers used for protein purification, activity measurements and fluorescence studies.

BUFFERS	COMPOSITION
Buffer A	50 mM Tris-HCl, pH 7.9, 100 µg/ml PMSF, 50 µg/ml TLCK, 100 µg/ml TPCK
Buffer B	20 mM Tris-HCl, pH 7.9, 500 mM NaCl, 100 µg/ml PMSF, 50 µg/ml TLCK, 100 µg/ml TPCK
Buffer C	50 mM Tris-HCl, pH 7.9, 250 mM NaCl, 1 mM EDTA, 1 mM EGTA
Buffer D	50 mM KH_2PO_4/K_2HPO_4, pH 7.5, 1 mM DTT, 1 mM EDTA, 1 mM EGTA
Buffer E	50 mM KH_2PO_4/K_2HPO_4, pH 7.9, 250 mM KCl, 1 mM EDTA, 1 mM EGTA
Buffer F	50 mM KH_2PO_4/K_2HPO_4, pH 7.5, 25 mM KCl, 1 mM DTT, 1 mM EDTA, 1 mM EGTA
Buffer G	50 mM Tris-HCl, pH 7.9, 50 mM NaCl, 5 mM imidazole, 50 µg/ml TLCK, 50 µg/ml TPCK, 100 µg/ml PMSF
Buffer H	20 mM Pipes, 100 mM NaCl, 0.1% CHAPS, 10% sucrose, and 10 mM DTT
Phosphate Buffer	50 mM KH_2PO_4/K_2HPO_4, pH 7.2, 1 mM DTT
Citrate Buffer	30 mM sodium citrate/citric acid, pH 4 to pH 6.5, 1 mM DTT
Tris Buffer	30 mM Tris-HCl, pH 7 to pH 9, 1 mM DTT

Institute).

Protein Purification

All steps were performed at 4 °C unless otherwise noted. In separate experiments, human procaspase-3(C163S) and the pro-less variant were purified as C-terminal-$(His)_6$-tagged proteins from *E. coli* BL21(DE3) harboring the plasmid pHC33201 or pHC32901, respectively. The protocols for purification of both proteins were similar. Cells were grown in Fernbach flasks containing 1 L of LB media with 50 μg/ml ampicillin and 0.003% antifoam-C at 30 °C. When the cultures reached an A_{600} of ~1.2, protein expression was induced by the addition of IPTG to a final concentration of 0.1 mM. The cells were harvested after ~16 h by centrifugation at 10000*g* for 15 min (GS-3 rotor). The bacterial pellets were resuspended in buffer A (~10 ml/L of culture) (Table I) and lysed on ice using a French pressure cell (16 000 psi). The supernatant was separated from cell debris by centrifugation at 28000*g* for 30 min (SA-600 rotor). The pellet from this step was washed once with buffer A (5 ml/L of culture) (Table I) and centrifuged for 30 min. The resulting supernatant was combined with the first. The proteins were fractionated between 30% and 80% ammonium sulfate, centrifuged at 22000*g* for 15 min, resuspended in buffer B (Table I) containing 5 mM imidazole, and dialyzed against the same buffer (2 × 80 volumes). The samples were then batch-bound for 2 min to His-bind resin (5 ml) equilibrated in buffer B (Table I) containing 5 mM imidazole, and the resin was loaded onto a column (2 cm diameter). The resin was washed and the protein was eluted using step gradients of imidazole (20, 40, 100, 150, 250, and 500 mM imidazole in buffer B, 50 ml per step). The fractions were analyzed by SDS-PAGE (4-20% gradient

gels). For procaspase-3(C163S), the fractions containing the protein (150-250 mM imidazole) were pooled, concentrated (YM10 membrane), and dialyzed first against buffer C (Table I) and then against buffer D (Table I). For the pro-less variant, the fractions from the His-bind resin containing the protein (100-250 mM imidazole) were pooled, concentrated (YM10 membrane), and dialyzed first against buffer E (Table I) and then buffer F (Table I), respectively (2 × 80 volumes for both buffers). In each case, the sample was applied to a DEAE-Sepharose column (4 cm × 18 cm) that had been equilibrated with buffer D (Table I). The proteins were eluted at a flow rate of 4 ml/min with a linear gradient of 0-400 mM KCl (procaspase-3(C163S)) or 25-250 mM KCl (pro-less variant). Each fraction was tested using a mini-Bradford assay [48], and the positive fractions were analyzed by SDS-PAGE (4-20% gradient gels). The fractions (75-125 mM KCl) containing procaspase-3(C163S) or the pro-less variant (100-150 mM KCl) were pooled, concentrated, and dialyzed overnight against buffer D (Table I) or buffer F (Table I), respectively. The proteins were stored at -80 °C. The protein purity was greater than 95% as assessed by SDS-PAGE.

The concentrations of procaspase-3(C163S) and the pro-less variant were determined using ε_{280} = 26 500 M^{-1} cm^{-1} and ε_{280} = 25 300 M^{-1} cm^{-1}, respectively. The extinction coefficients were determined by the method of Edelhoch [49] and are in good agreement with that determined previously for procaspase-3 [10]. The concentrations shown here are those of the monomers.

For active-site conformation experiments, proteins (procaspase-3(C163S), caspase-3, procaspase-3(D_3A), procaspase-3(C163A, W206Y), procaspase-3(C163A, W214V)), were purified as above with certain modifications. Cells were grown in LB media at 37

^{o}C. After induction with 0.4 mM IPTG at A_{600} ~1.2, the temperature was lowered to 25 ^{o}C. The cells were harvested after 4 h (procaspase-3(D_3A) and caspase-3) or 18 h (all other proteins) of induction. Following lysis, the supernatant was separated from cell debris by centrifugation at 28,000g (SA-600 rotor) for 30 minutes at 4 °C. The supernatant was batch-bound for 30 min to His-bind resin (15 ml) that had been pre-equilibrated in buffer G (Table I). The resin was washed four times with four volumes of buffer G (Table I), then four times with four volumes of buffer G (Table I) containing 80 mM imidazole. After each wash, the resin was centrifuged for two minutes at 500g (SA-600 rotor), and the supernatant was removed. The protein was eluted with buffer G (two times of two volumes each) (Table I) containing 500 mM imidazole, and the fractions were analyzed by SDS-PAGE. The proteins were further purified by DEAE-sepharose chromatography [22].

The activities of mature caspase-3 and of procaspase-3(D_3A) were determined as described [32] using the fluorescent substrate Ac-DEVD-AFC. Assays were performed in buffer H (Table I) at 25 ºC. The total reaction volume was 200 µl, and the final concentration of the enzymes was either 1 nM (caspase-3) or 10 nM (procaspase-3(D_3A)). Samples were excited at 400 nm, and the fluorescence emission was monitored at 505 nm.

Peptide synthesis

The pro-domains of procaspase-3 and procaspase-1 were synthesized from University of North Carolina at Chapel Hill peptide synthesis laboratory.

Reagents

Ampicillin, antifoam-C, bovine serum albumin, carbonic anhydrase, CHAPS, cytochrome *c*, DEAE-Sepharose, dansyl chloride, DMF, DMSO, EDTA, EGTA, glycerol, IPTG, kanamycin, nickel sulfate, PMSF, potassium phosphate (KH_2PO_4 and K_2HPO_4), citric acid, sodium citrate (dihydrate), dithiothreitol (DTT), Trizma base, bovine serum albumin, microcentrifuge tubes, PIPES, potassium iodide, acrylamide Sephacryl-S15, Sephacryl-S100, sodium bicarbonate, TLCK, TPCK and di-isopropyl fluorophosphate (DFP) were obtained from Sigma Chemicals (St. Louis, MO). Ultrapure ammonium sulfate, guanidine hydrochloride and imidazole, were from ICN. Tryptone and yeast extract were from Difco. His-bind resin was from Novagen. Potassium chloride and sucrose were from Mallinckrodt. Acetonitrile and HEPES were from Acros. Ultra-pure urea was purchased from Nacalai Tesque Inc. (Kyoto, Japan). Sodium chloride and glycine were from Fisher. α-cyano-4-hydroxycinnamic acid and sinapinic acid were from Aldrich. V8 protease and trypsin were from Roche Biochemicals. Cesium chloride was from Harshaw. Ac-DEVD-AFC (acetyl-DEVD-7-amino-4-trifluoromethyl coumarin), Ac-DEVD-CHO ((acetyl-DEVD-aldehyde) and Z-VAD-FMK (Z-VAD-fluoromethyl ketone) were purchased from Calbiochem. Ziptip pipette tips were from Millipore.

Stock solutions

Urea stock solutions (10 M) were prepared as described previously [50] in phosphate buffer (Table I). For urea denaturation studies at different pH, urea stock solutions (10 M) were prepared in citrate buffer (Table I) and Tris buffer (Table I). All solutions were prepared fresh for each experiment and were filtered (0.22 μm pore size) prior to use. The

urea concentration of each stock solution was calculated by weight (A) and by refractive index (B) [50], and solutions were used only if the two values were within ±1%.

A. Calculation of molarity of urea by weight measurement

It is practical to express density data in terms of specific gravity, *i.e.* as density relative to the density of water at the same temperature. Although both density and specific gravity are temperature-dependent, the variation in specific gravity is considerably less.

The following empirical equation describes determination of urea concentration at 25 °C.

$$d/d_0 = 1 + 0.2658W + 0.0330W^2$$

where, W is the weight fraction denaturant in the solution, d is the density of the solution and d_0 is the density of water. Therefore, d/d_0 is the specific gravity of the solution. d/d_0 has been found to be 1.103 for 10 M urea solution at 25 °C. This helps to determine the weight of water to be added.

The experiment was done as follows: Urea was weighed out in a beaker of known weight. Reagents for buffer were weighed out with a different balance and added to the urea in the beaker to give a desired molarity of buffer. Water was then added up to a certain weight depending on the specific gravity of the solution (for example, for 25 ml solution, total weight of the solution will be 25*1.103).

B. Calculation of molarity of urea by refractive index measurement

The molarity of urea can be expressed in terms of refractive index of urea solution by the empirical equation as described below:

$$M\ (urea) = 117.66(\Delta N) + 29.753(\Delta N)^2 + 185.56(\Delta N)^3$$

where, ΔN is the difference in refractive index between urea solution and buffer. This is therefore the measure of the refractive index of urea. The refractive indices of the buffer solution as well as the urea solution in the buffer were measured in a refractometer.

Equilibrium unfolding studies

All equilibrium unfolding experiments were performed as described previously [50; 51]. Briefly, stock protein solutions were prepared in phosphate buffer to be ten times the final concentration used in the experiment. Phosphate buffer (Table I), urea from the 10 M stock solution, and stock protein solutions were mixed in 2 ml siliconized microcentrifuge tubes to give final urea concentrations between 0 M and 8 M and the final protein concentrations as indicated in the figure legends. For renaturation experiments, the protein was incubated in 6 M urea-containing phosphate buffer (Table I). After incubation for 1 hour at 25 °C, the protein was added to phosphate buffer (Table I) and urea such that the final urea and protein concentrations were as indicated in the figure legends. All samples were mixed by vortexing. In order to determine that the samples had reached equilibrium, we monitored the fluorescence emission over time for a sample incubated in 4 M urea-containing phosphate buffer (Table I). The results from this experiment (data not shown) demonstrate that the sample equilibrated within 45 minutes at 25 °C as there was no further change in signal after this time. When the protein was

refolded by dilution from 8 M to 0.8 M urea, we observed several kinetic phases, although folding was complete within several hours. For the equilibrium unfolding experiments, the samples were incubated for approximately 24 hours at 25 °C prior to data collection. This incubation time was sufficient to allow all samples to equilibrate.

Fluorescence emission at each denaturant concentration was measured using a PTI C-61 spectrofluorometer (Photon Technology International). Time-based measurements were acquired at excitation wavelengths of 280 nm and 295 nm with fluorescence emission at 320 nm. All measurements were corrected for background signal. Circular dichroism at 228 nm was measured with a Jasco J600A spectropolarimeter using a cuvette of 1 cm path length. The data were averaged for 30 seconds. Both instruments were equipped with thermostatted cell holders, and the temperature was held constant at 25 °C using a circulating water bath.

Equilibrium unfolding studies at different pH

Procaspase-3(C163S) was dialyzed in citrate buffer (Table I) for experiments from pH 4 to pH 6.5 and Tris buffer (Table I) from pH 7 to pH 9. Protein stock solutions at different concentrations as well as solutions for unfolding and renaturation experiments in citrate and Tris buffer were prepared as described before. Fluorescence emission scans were acquired for protein solutions at different urea concentrations at 280 and 295 nm with emissions between 305-400 nm. Circular dichroism experiments were performed at 228 nm as described previously.

Equilibrium unfolding studies of the pro-less variant with different concentrations of the pro-domain

All equilibrium unfolding experiments were performed as described previously [50; 51]. Briefly, stock protein solutions were prepared in phosphate buffer (Table I) to be ten times the final concentration used in the experiment. Phosphate buffer (Table I), urea from the 10 M stock solution, and stock protein solutions were mixed in 2 ml siliconized microcentrifuge tubes to give final urea concentrations between 0 M and 8 M and the final protein concentrations as indicated in the figure legends. For renaturation experiments, the protein was incubated in 6 M urea-containing phosphate buffer (Table I). Peptide solutions (pro-domains of procaspase-1 or procaspase-3) were added at different concentrations (0 μM, 0.1 μM, 0.5 μM, 1 μM, 2 μM and 2.5 μM) before incubation for both renaturation and unfolding experiments. After incubation for 1 hour at 25 °C, the protein was added to phosphate buffer and urea such that the final urea and protein concentrations were as indicated in the figure legends. All samples were mixed by vortexing. For the equilibrium unfolding experiments, the samples were incubated for approximately 24 hours at 25 °C prior to data collection. This incubation time was sufficient to allow all samples to equilibrate.

Fluorescence emission scans were acquired at excitation of 280 nm with fluorescence emissions between 300-400 nm. Relative fluorescence at 320 nm was plotted versus urea concentration. All measurements were corrected for background signal.

Active Site Titration of procaspase-3(D_3A)

Working solutions of tetrapeptide inhibitor Z-VAD-FMK were prepared in buffer H (Table I) at 37 ^{o}C. Procaspase-3(D_3A) stock solution (60 nM) was prepared in assay buffer and incubated for 15 mins at 37 ^{o}C for activation [32]. 20 µl of working solutions of Z-VAD-FMK were added to 30 µl of enzyme solution and incubated for 30 min at 37 ^{o}C. Stock solution of the fluorometric substrate Ac-DEVD-AFC (69 µM) was prepared in assay buffer. Reaction mixtures were prepared with inhibitor-enzyme solution and 130 µl of substrate solution. The total reaction volume was 180 µl, and the final concentrations of the enzyme and substrate were 10 nM and 50 µM respectively. Working solutions of the inhibitor were prepared such that the enzymes to inhibitor ratio were 0, 0.25, 0.5, 1 and 2. Several fluorescence time-based scans (100 seconds) were taken with the reaction mixture having different inhibitor to enzyme ratio. Fluorescence emission was measured at 505 nm after excitation at 400 nm. Plot of the slopes of the initial velocity (v_0) versus ratio of the inhibitor to enzyme concentration was plotted.

Limited Proteolysis with Trypsin

Proteins (all 15 µM) were digested with one fifteenth of their concentration (w/w) of trypsin in a buffer of 20 mM Tris-HCl, pH 7.2, 0.5 mM DTT at 25 °C. After trypsin was added, aliquots were withdrawn at prescribed time intervals, and reactions were inhibited by TLCK (thrice the concentration of trypsin (w/w)). The samples were frozen at -20 °C until analyzed. Samples were analyzed by SDS-PAGE using either 4-25% or 10-25% polyacrylamide gradient gels. In separate experiments, the reversible tetrapeptide caspase-3 inhibitor, Ac-DEVD-CHO (thrice the concentration of the protein) was

included. Protein fragment identification was done by MALDI-TOF mass spectrometry and peptide sequencing as described below.

Limited Proteolysis with V8 Protease

Proteins (all 15 μM) were digested with one fifteenth of their concentration (w/w) of V8 protease in a buffer of 20 mM Tris-HCl, 0.5 mM DTT (for experiments at pH 7.8 and 7.2) or a buffer of 10 mM citrate, 0.5 mM DTT (for experiments at pH 6, 5 and 4), at 25 °C. After the addition of protease, aliquots were withdrawn at prescribed time intervals, and the reactions were inhibited with DFP (thrice the concentration of V8 (w/w)). Samples were frozen at -20 °C until analyzed. Samples were analyzed by SDS-PAGE using either 4-25% or 10-25% polyacrylamide gradient gels. In separate experiments, the irreversible tetrapeptide caspase-3 inhibitor Z-VAD-FMK (thrice the concentration of the protein) was included. Protein fragment identification was done by MALDI-TOF mass spectrometry and peptide sequencing, as described below.

Kinetic analysis of the fragments was done using the ImageQuant software (Molecular Dynamics). The fraction of species relative to the full-length protein at time zero was plotted, and the data were fit to a double exponential equation for bands 1-4 and to a single exponential equation for 16 kDa, 8 kDa and 4 kDa bands.

MALDI-TOF Mass Spectrometry

Experiments were performed with a Bruker Proflex III instrument that is equipped with a nitrogen laser (λ = 337 nm, 3 ns pulse width), deflection capabilities, delayed extraction and an extended flight tube. The mass accuracy for analyte molecules is ±0.1

% with external calibration. Matrices used for these experiments were saturated solutions of sinapinic acid (3,5-dimethoxy-4-hydroxycinnamic acid) or α-cyano-4-hydroxycinnamic acid in acetonitrile, water and TFA (50:50:0.1 (v/v)). Calibration was done with ubiquitin (8 kDa), myoglobin (17 kDa) and bovine serum albumin (66.5 kDa). Samples from the limited proteolysis experiments were crystallized on a target plate with matrix solution (1:1). Desalting of the peptides was done with Ziptip pipette tips. Experiments were performed at 22-26 attenuation and 50 shots. Each experiment was repeated at least 5 times and the average data were collected.

Peptide Sequencing

The gels for trypsin and V8 protease digestions were transferred to PVDF membrane as described [52], and the first five amino-terminal amino acids were determined by Edman degradation (University of Nebraska, Protein Structure Core Facility).

Quenching of Tryptophan Fluorescence Emission

Stock protein solutions were dialyzed against a buffer of 50 mM potassium phosphate, pH 7.2, 1 mM DTT. Stock solutions of acrylamide, KI or CsCl (quenchers) were prepared in the same buffers. Protein solutions (1 μM) were prepared from the stocks, and the quenching agent was added to the final concentrations as shown in the figures. The samples were stirred and incubated for 5 min following each addition of quencher, and the experiments were performed at 25 °C. Samples were excited at 295 nm, and the fluorescence emission was examined from 300-400 nm. Fluorescence emission at 345 nm was used for data analysis. All data were corrected for background

signal. For pH-dependent quenching studies, the following buffers were used: 50 mM sodium citrate (pH 3-6.5), 50 mM potassium phosphate (pH 6.5-7.2), or 50 mM Tris-HCl (pH 7.2-9). All buffers contained 1 mM DTT.

Data Analysis

The fluorescence and circular dichroism studies were modeled using the four state equilibrium model shown in equation 1.

$$N_2 \overset{K_1}{\rightleftarrows} I_2 \overset{K_2}{\rightleftarrows} 2I \overset{K_3}{\rightleftarrows} 2U \qquad \text{(Eq. 1)}$$

In this model, the protein is assumed to be either in the native homodimeric state (N_2), a non-native dimeric state (I_2), a non-native monomeric state (I), an unfolded monomeric state (U), and K_1, K_2, K_3 are the equilibrium constants for the three steps, respectively. If we consider the total molar concentration of the polypeptide chains as P_T, as shown in equation 2,

$$P_T = 2[N_2] + 2[I_2] + [I] + [U] \qquad \text{(Eq. 2)}$$

then the mole fraction of each species can be defined as shown in equations 3-6.

$$f_{N_2} = \frac{2N_2}{P_T} \qquad \text{(Eq. 3)}$$

$$f_{I_2} = \frac{2\,I_2}{P_T} \qquad \text{(Eq. 4)}$$

$$f_I = \frac{I}{P_T} \qquad \text{(Eq. 5)}$$

$$f_U = \frac{U}{P_T} \qquad \text{(Eq. 6)}$$

The sum of all fractions is equal to unity as shown in equation 7.

$$f_{N_2} + f_{I_2} + f_I + f_U = 1 \qquad \text{(Eq. 7)}$$

The equilibrium constants K_1, K_2 and K_3 are related to the mole fraction of each species and to P_T, as shown in equations 8-10.

$$K_1 = \frac{f_{I_2}}{f_{N_2}} \qquad \text{(Eq. 8)}$$

$$K_2 = \frac{2f_I^{\,2}P_T}{f_{I_2}} \qquad \text{(Eq. 9)}$$

$$K_3 = \frac{f_U}{f_I} \qquad \text{(Eq. 10)}$$

Equating equations 8, 9, 10, substituting in terms of f_U, and rearranging yields equation 11.

$$\frac{2f_U{}^2P_T}{K_1K_2K_3{}^2} + \frac{2f_U{}^2P_T}{K_2K_3{}^2} + \frac{f_U}{K_3} + f_U - 1 = 0 \qquad \text{(Eq. 11)}$$

By solving the quadratic equation 11, the fraction of each species is obtained, as shown in equations 12-15.

$$f_U = \frac{-K_1K_2K_3(1+K_3) + \sqrt{K_1{}^2K_2{}^2K_3{}^2(1+K_3)^2 + 8P_T(1+K_1)(K_1K_2K_3{}^2)}}{4P_T(1+K_1)} \qquad \text{(Eq. 12)}$$

$$f_I = \frac{f_U}{K_3} \qquad \text{(Eq. 13)}$$

$$f_{I_2} = \frac{2f_I{}^2P_T}{K_2} \qquad \text{(Eq. 14)}$$

$$f_{N_2} = \frac{f_{I_2}}{K_1} \qquad \text{(Eq. 15)}$$

From equations 12-15 and the relationship

$$\Delta G = -RT\ln(K_{eq}) \quad \text{(Eq. 16)}$$

where R is the gas constant and T is the temperature in Kelvin, one may calculate the equilibrium constant and the values of ΔG at each urea concentration. We assume the free energy change for each step in the reaction to be linearly dependent on denaturant concentration as described earlier [53] (Equations 17-19).

$$\Delta G_1 = \Delta G_1^{H_2O} - m_1[\text{denaturant}] \quad \text{(Eq. 17)}$$

$$\Delta G_2 = \Delta G_2^{H_2O} - m_2[\text{denaturant}] \quad \text{(Eq. 18)}$$

$$\Delta G_3 = \Delta G_3^{H_2O} - m_3[\text{denaturant}] \quad \text{(Eq. 19)}$$

where $\Delta G_1^{H_2O}$, $\Delta G_2^{H_2O}$, and $\Delta G_3^{H_2O}$ are the free energy changes in the absence of denaturant corresponding to K_1, K_2 and K_3, respectively, and m_1, m_2 and m_3 are the cooperativity indices associated with each step. The amplitude of the spectroscopic signal determined at each urea concentration is assumed to be a linear combination of the fractional contribution from each species (equation 20),

$$Y = Y_{N_2}f_{N_2} + Y_{I_2}f_{I_2} + Y_I f_I + Y_U f_U \quad \text{(Eq. 20)}$$

where, Y_{N_2}, Y_{I_2}, Y_I, and Y_U are the amplitudes of the signals for the respective species.

In order to determine the unknown parameters $\Delta G_1^{H_2O}$, $\Delta G_2^{H_2O}$, $\Delta G_3^{H_2O}$, m_1, m_2, and m_3, the ten data sets shown in Figures 15 and 16 were fit simultaneously using Igor Pro. For each spectroscopic signal, the values for Y_{I_2} and Y_I did not vary with changes in P_T. The following values were determined from the fits. For fluorescence emission (280 nm excitation), Y_{I_2}=0.78 and Y_I=-0.16. For circular dichroism at 228 nm, Y_{I_2}=0.85 and Y_I=0.3. For fluorescence emission (295 nm excitation), Y_{I_2}=1.13 and Y_I=0.08. The amplitudes associated with the native form of the protein were assumed to be linearly dependent on urea concentration, as shown in equation 21

$$Y_{N_2} = Y_{N_2'} + m_4[\text{urea}] \qquad \text{(Eq. 21)}$$

where $Y_{N_2'}$ is the amplitude of the signal in the absence of urea for the native species. This correction to the pre-transition baselines (equation 21) had little effect on the free energy or *m*-values determined from the fits. For example, when m_4 was set to zero, $\Delta G_1^{H_2O}$ varied from 8.3 kcal/mol to 7.5 kcal/mol, and m_1 varied from 2.8 kcal/mol/M to 2.65 kcal/mol/M. The remaining parameters were unchanged. These variations in $\Delta G_1^{H_2O}$ and m_1 are within the experimental error. The fits shown in Figures 15 and 16 as well as the values reported in the text reflect the pre-transition baseline corrections. Due to the lack of a sufficient number of data points in the post-transition regions, no corrections were made to the post-transition baselines, and the values of Y_U were set to zero, in agreement

with the normalized experimental data shown in the Figures 15 and 16. The values of P_T were not allowed to vary during the fitting process.

For equilibrium studies at different pH, average emission wavelength was determined for each fluorescence emission scans [54] using equation 22,

$$< \lambda >= \sum_{i=1}^{N} (I_i \lambda_i) \Big/ \sum_{i=1}^{N} (I_i) \qquad \text{(Eq. 22)}$$

where **<λ>** is the average emission wavelength, and I_i is the fluorescence emission at wavelength λ_i.

Data were fitted to the four-state model as described above from pH 8.5 to pH 4.75. Data for pH 4.5 and 4.2 were fitted to a three-state monomer[55] (as shown in equation 23).

$$N \overset{K_1}{\rightleftarrows} I \overset{K_2}{\rightleftarrows} U \qquad \text{(Eq. 23)}$$

In this model, the protein is assumed to be either in the native monomeric state (N), a non-native monomeric intermediate state (I), an unfolded monomeric state (U), and K_1 and K_2 are the equilibrium constants for the two steps, respectively.

Data for pH 4 were fitted to a two-state monomer [56] (as shown in equation 24).

$$N \overset{K}{\rightleftarrows} U \qquad \text{(Eq. 24)}$$

In this model, the protein is assumed to be either in the native monomeric state (N) or in an unfolded monomeric state (U), and K is the equilibrium constant for the unfolding process.

Global fit of the data with Igor Pro

Data for equilibrium unfolding studies at different pH were fit globally with Igor Pro. For data between 8.5 and 4.75, six parameters were fit globally such that their values would be same for different concentrations at a particular pH. They are $\Delta G_1^{H_2O}$, m_1, $\Delta G_2^{H_2O}$, m_2, $\Delta G_3^{H_2O}$ and m_3. Initial guesses for $Y_{U'}$, $Y_{I_2'}$, $Y_{I'}$ were held constant for each pH so that during the fitting process those values would remain constant. The procedure file for four-state model is shown in Figure 8.

Data for pH 4.5 and 4.2 were also fit globally with the three-state monomer model described above. The global parameters for these two parameters were $\Delta G_1^{H_2O}$, m_1, $\Delta G_2^{H_2O}$ and m_2. For pH 4.5, $Y_{N'}$ was held constant, while, for pH 4.2, both $Y_{N'}$ as well as $Y_{U'}$ were held constant. The procedure file for three-state model is shown in Figure 9.

For data at pH 4, global fit was applied to $\Delta G_1^{H_2O}$ and m_1. None of the parameters were held during the fitting process. The procedure file for the fit is shown in Figure 10.

Fits to the fluorescence quenching data

For acrylamide and CsCl quenching, the data were fit to the Stern-Volmer equation, accounting for static and dynamic quenching [57].

For quenching by iodide, the percent quenching ($\Delta F/F_0$)*100 was plotted versus the concentration of KI, and the data were fit to equation 25:

$$(\Delta F/F_0)*100 = (100* K_{SV} f_a[Q])/(1 + K_{SV}[Q]) \qquad \text{(Eq. 25)}$$

where, ΔF is the change in fluorescence emission at each concentration of quencher (KI),

```
Wave w

    Variable x

    Variable    K1=EXP(-((w[0]+w[1]*x)/(0.001987*298)))
    Variable    K2=EXP(-((w[2]+w[3]*x)/(0.001987*298)))
    Variable    K3=EXP(-((w[4]+w[5]*x)/(0.001987*298)))
    Variable    Fu=(-
(K1*K2*K3+K1*K2*K3^2)+sqrt((K1*K2*K3+K1*K2*K3^2)^2+8*K1*K2*K3^2*w[6
]*(1+K1)))/(4*w[6]*(1+K1))
    Variable    Fi=Fu/K3
    Variable    Fb=(2*Fi^2*w[6])/K2
    Variable    Fd=Fb/K1
    Variable    Yd=w[7]+w[8]*x
    Variable    Yu=w[9]+w[10]*x
    Variable    y=Yd*Fd+(w[11]+w[12]*x)*Fb+(w[13]+w[14]*x)*Fi+Yu*Fu

    Return y

End
```

Figure 8. Procedure file for four-state equilibrium unfolding model of procaspase-3(C163S). w[0] is $\Delta G_1^{H_2O}$, w[1] is m_1, w[2] is $\Delta G_2^{H_2O}$, w[3] is m_2, w[4] is $\Delta G_3^{H_2O}$, w[5] is m_3, w[6] is P_T, w[7] is $Y_{N_2'}$, w[8] is m_4, w[9] is $Y_{U'}$, w[10] is m_5, w[11] is $Y_{I_2'}$, w[12] is m_6, w[13] is $Y_{I'}$, w[14] is m_7. Fd, Fb, Fi and Fd represent fractions of native, dimeric intermediate, monomeric intermediate and the unfolded species respectively. Yb and Yu represent amplitude of the native and the unfolded species respectively. All parameters have been described earlier.

```
Wave w

    Variable x

    Variable    K1=EXP(-((w[0]+w[1]*x)/(0.001987*298)))
    Variable    K2=EXP(-((w[2]+w[3]*x)/(0.001987*298)))
    Variable    Fb=1/(1+K1+K1*K2)
    Variable    Fi=K1/(1+K1+K1*K2)
    Variable    Fu=(K1*K2)/(1+K1+K1*K2)
    Variable    Yb=w[4]+w[5]*x
    Variable    Yu=w[6]+w[7]*x
    Variable    y=Yb*Fb+(w[8]+w[9]*x)*Fi+Yu*Fu

    Return y

    End
```

Figure 9. Procedure file for three-state monomer model of procaspase-3(C163S). w[4] is $Y_{N'}$, w[5] is m_3, w[6] is $Y_{U'}$, w[7] is m_4, w[8] is $Y_{I'}$, w[9] is m_5. Fu is the fraction of the unfolded species. The other parameters are as described earlier.

```
Wave w

    Variable x

    Variable    K=EXP(-((w[0]-w[1]*x)/(0.001987*298)))
    Variable    Fu=K/(1+K)
    Variable    Fb=1-Fu
    Variable    Yb=w[2]+w[3]*x
    Variable    Yu=w[4]+w[5]*x
    Variable    y=Yb*Fb+Yu*Fu

    Return y
```

Figure 10. Procedure file for two-state monomer model of procaspase-3(C163S). w[2] is $Y_{N'}$, w[3] is m_2, w[4] is $Y_{U'}$, w[5] is m_3. The other parameters have been defined earlier.

F_0 is the fluorescence intensity of the protein in absence of quencher, K_{SV} is the Stern-Volmer constant, [Q] is the quencher concentration and f_a is the fraction of the initial fluorescence emission that is accessible to the quencher.

The Stern-Volmer constants (K_{SV}), determined from the fits described by equation 25, over the pH range of 2.5 to 9, were plotted versus pH. The data were fit to equation 26:

$$K_{SV} = A + \left[\Delta K_{SV_1} * 10^{n_1(pH-pKa_1)} / \left(1 + 10^{n_1(pH-pKa_1)}\right)\right] + \left[\Delta K_{SV_2} * 10^{n_2(pH-pKa_2)} / \left(1 + 10^{n_2(pH-pKa_2)}\right)\right]$$

(Eq. 26)

where, K_{SV} is the Stern-Volmer constant, A is the value of K_{SV} at the lowest pH, ΔK_{SV_1} and ΔK_{SV_2} represent the changes in the Stern-Volmer constant for each transition, n_1 and n_2 are the number of protons titrated in each transition, and pKa_1 and pKa_2 are the apparent *pK's* of the transitions.

Derivation of the modified form of Stern-Volmer Equation

$$F_0 = F_{0,a} + F_{o,b}$$

and

$$F = \frac{F_{0a}}{1 + K_A[Q]} + \frac{F_{0b}}{1 + K_B[Q]}$$

$$\Delta F = F_0 - F$$

$$= F_{oa} + F_{ob} - \frac{F_{0a}}{1 + K_A[Q]} - \frac{F_{0b}}{1 + K_B[Q]}$$

$$= F_{0a}\left(1 - \frac{1}{1 + K_A[Q]}\right) + F_{0b}\left(1 - \frac{1}{1 + K_B[Q]}\right)$$

$$= F_{0a}\left(\frac{K_A[Q]}{1 + K_A[Q]}\right) + F_{0b}\left(\frac{K_B[Q]}{1 + K_B[Q]}\right)$$

$$\frac{F_0}{\Delta F} = \frac{F_{0a} + F_{0b}}{F_{0a}\left(\frac{K_A[Q]}{1 + K_A[Q]}\right) + F_{0b}\left(\frac{K_B[Q]}{1 + K_B[Q]}\right)}$$

and

$$\frac{\Delta F}{F_0} = \frac{F_{0a}\left(\frac{K_A[Q]}{1 + K_A[Q]}\right) + F_{0b}\left(\frac{K_B[Q]}{1 + K_B[Q]}\right)}{F_{0a} + F_{0b}}$$

$$= \frac{F_{0a}\left(\frac{K_A[Q]}{1 + K_A[Q]}\right)}{F_{0a} + F_{0b}} + \frac{F_{0b}\left(\frac{K_B[Q]}{1 + K_B[Q]}\right)}{F_{0a} + F_{0b}};$$

$$\text{since } f_a = \frac{F_{0a}}{F_{0a} + F_{0b}}$$

$$\text{and } f_b = \frac{F_{0b}}{F_{0a} + F_{0b}}$$

$$\text{then } \frac{\Delta F}{F_0} = f_a\left(\frac{K_a[Q]}{1 + K_a[Q]}\right) + f_b\left(\frac{K_b[Q]}{1 + K_b[Q]}\right)$$

where, 'F_0' and 'F' are fluorescence without and with the quencher respectively. 'a' and 'b' are two populations of tryptophan that are not equally accessible to the quencher. 'f_a' is fraction of species 'a'. [Q] is the quencher concentration. 'K_a' and 'K_b' are quenching constants for the two species.

Derivation of equation for percent quenching

$$\frac{F_0}{F} = 1 + K_{SV}[Q]$$

and

$$\frac{F_0}{\Delta F} = \frac{1}{f_a K[Q]} + \frac{1}{f_a}$$

$$= \frac{f_a + f_a K[Q]}{K[Q] f_a^2}$$

$$= \frac{f_a \{1 + K[Q]\}}{f_a^2 K[Q]}$$

$$= \frac{\{1 + K[Q]\}}{f_a K[Q]};$$

$$\frac{\Delta F}{F_0} = \frac{K[Q] f_a}{1 + K[Q]}$$

$$Percent\ Quenching = \left(\frac{\Delta F}{F_0}\right) * 100 = \frac{100 * K[Q] f_a}{1 + K[Q]}$$

K_{SV} is the Stern Volmer constant. Since, the data were not improved using two tryptophan populations, percent quenching was determined using single tryptophan population.

RESULTS

I. Characterization of active site conformation of procaspase-3

Nicholson and coworkers [30] demonstrated that procaspase-3 is catalytically competent by using an active site probe that required catalytic turnover to covalently modify the active site cysteinyl residue. While the catalytic parameters were not described, they concluded that procaspase-3 contains sufficient activity to carry out autolytic cleavage. To examine the catalytic parameters of procaspase-3, our lab generated a mutant in which the three aspartate residues that are cleaved during processing were mutated to alanine (D9A,D28A,D175A). This mutant, called procaspase-3(D_3A), is comparable to the D9E,D28E,D175E triple mutant and the D28A,D175A double mutant described by Nicholson and coworkers [30], who showed that the mutations prevented autoprocessing. The active-site catalytic residues (C163 and H121) were kept intact, thus generating an uncleavable procaspase-3 with the active-site cysteine unchanged.

The activity of procaspase-3(D_3A) was measured by our lab and the results were compared with mature caspase-3. The data demonstrate that procaspase-3(D_3A) binds the tetrapeptide substrate and is catalytically active, although the activity is much lower than that of the mature caspase-3. The steady-state parameters, K_m and k_{cat}, were calculated and the results show that the values of K_m are comparable in the two proteins, 2.2 ± 0.5 μM for caspase-3 and 3.5 ± 0.8 μM for procaspase-3(D_3A). The catalytic efficiency, k_{cat}, for procaspase-3(D_3A) is about 130 fold lower than that of the mature caspase-3. Overall, the specificity constant (k_{cat}/K_m) is ~200 fold lower in the procaspase compared to the mature caspase-3. It has been shown that both active sites in the caspase-3 heterotetramer

are catalytically active [32]. We find that this is also true for procaspase-3(D_3A) (data not shown).

Limited Trypsin Proteolysis. We examined the conformation of procaspase-3 and of caspase-3 by limited trypsin proteolysis. A time-course analysis of the procaspase-3(C163S) digestion with trypsin showed several discrete cleavages (Figure 11, panel A). Also, minor contaminants of ~24 kDa and ~15 kDa were observed in the stock protein (time zero in Figures 11A and Figure 12A) for procaspase-3(C163S). Our laboratory shows that there was no reaction of these bands with a caspase-3 antibody raised against the large subunit, demonstrating that the proteins were from *E. coli* rather than processed procaspase-3(C163S) (data not shown).

We analyzed the digests by MALDI-TOF mass spectrometry, and the results showed protein fragments of 25 kDa, 16 kDa, 9.5 kDa and 4 kDa, consistent with the bands observed by SDS-PAGE. Representative figures are shown in Figure 11, panel B (full length protein) and panel C (tryptic fragments). The N-terminal five amino acids of these fragments were sequenced, and this allowed an unambiguous assignment of the cleavage sites in the protein. The results show that the protein is cleaved at K57/R64 to generate the 25 and 4 kDa fragments. Cleavage of the 25 kDa fragment at R207 generates the 16 kDa and 9.5 kDa fragments.

Two of the three residues are found in the active site. Both K57 and R64 reside in loop L1, where R64 forms part of the S1 binding pocket. R207 is in loop L3 and makes contacts in both the S1 and S3 binding sites. We consider the cleavages at K57 and R64

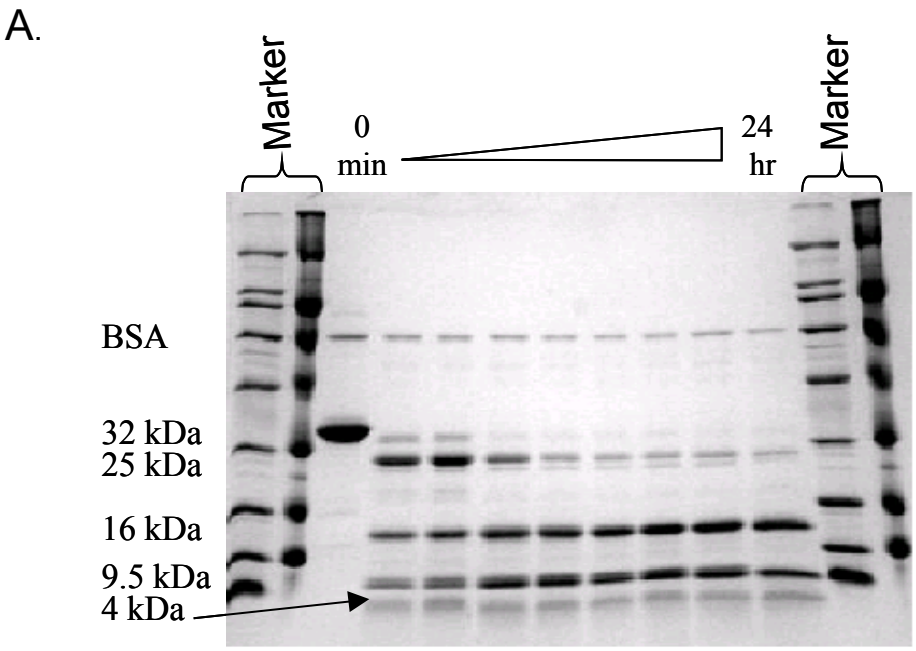

Figure 11. *Panel* A. Trypsin digestion of procaspase-3(C163S) at pH 7.2. The 32 kDa band represents the full-length procaspase-3(C163S), whereas the 25 kDa, 16 kDa, 9.5 kDa and 4 kDa bands are the cleavage products as described in the text. Known amount of BSA was added to the gel for normalization.

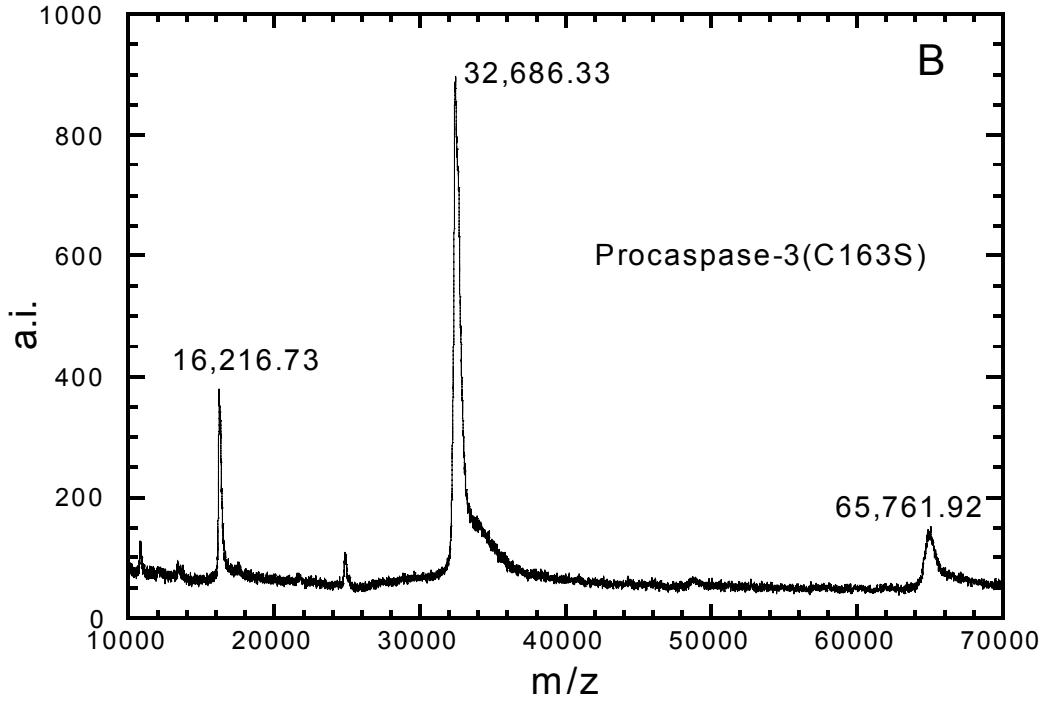

Figure 11. *Panel* B. MALDI-TOF mass spectrometric analysis of procaspase-3(C163S). The ~32 kDa band represents full-length protein (monomer), while the 16 kDa and ~65 kDa peaks represent doubly ionized and dimeric species respectively.

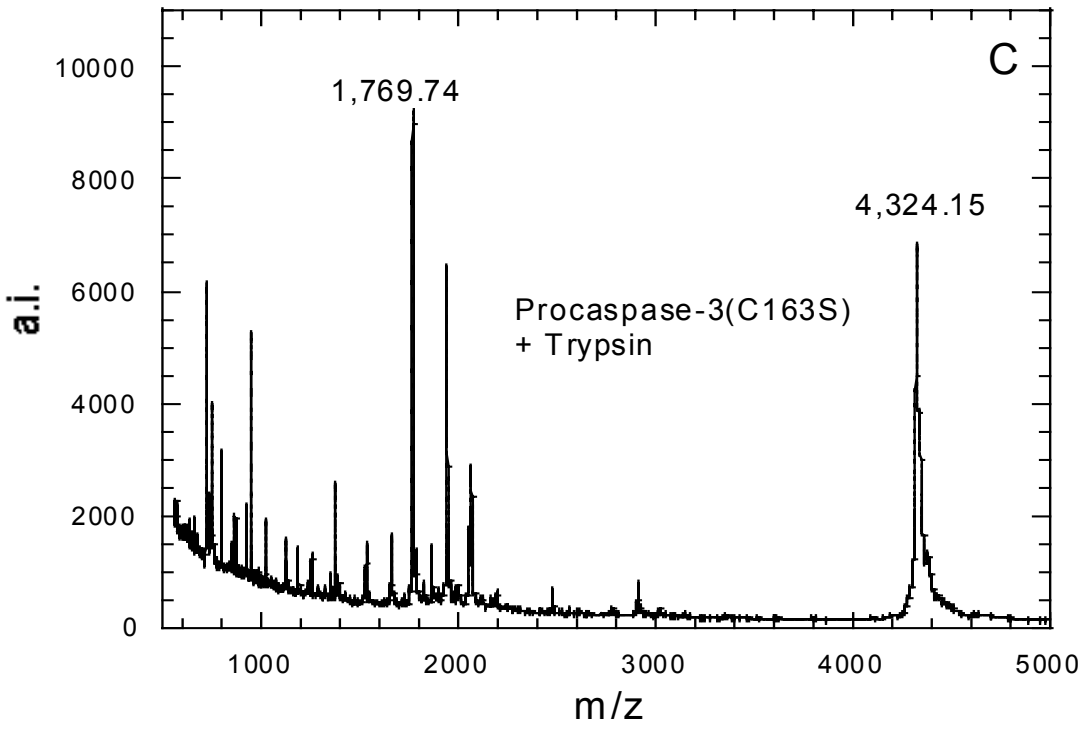

Figure 11. *Panel* C. MALDI-TOF mass spectrometric analysis of tryptic fragments (overnight digestion) of procaspase-3(C163S). The 4 kDa band is as described in the text.

to be equivalent. Under these conditions, the cleavages at K57/R64 occur with $t_{½} < 2$ minutes, while the cleavage at R207 occurs with $t_{½} \sim 75$ minutes. In the presence of inhibitor (Figure 11, panel D), only R207 is protected from cleavage by trypsin.

One interpretation of the results shown in Figure 11A is that R207, on loop L3, is less accessible to trypsin than are K57 and R64 on loop L1. However, it is possible that flanking residues and local structures may affect cleavage efficiency. Le Bonniec and coworkers [58] addressed this issue by examining the specificity of several proteases. They concluded that trypsin was the most efficient but least selective protease when compared to factor Xa and to thrombin. Of the five sites on the substrate (P3-P3', excluding P1), the P1' site exhibited the highest selectivity index for trypsin, although the value of 80 was significantly lower than that of thrombin. Based on the values published by Le Bonniec and coworkers, one can estimate that there is little difference in selectivity between the flanking sequences of K57 (FHK(57)STG), R64 (TSR(64)SGT) and R207 (SWR(207)NSK). The predicted selectivity would differ by at most a factor of three between R207 and K57/R64. This difference is not sufficient to account for the factor of >40 in $t_{½}$. Thus, we suggest that the slower cleavage of R207 by trypsin demonstrates that the residue is less accessible than are K57 and R64.

The limited trypsin digests of caspase-3 (Figure 11, panel E) also show that both the large subunit (17 kDa) and the small subunit (12 kDa) are cleaved rapidly by the protease. In caspase-3, cleavage at K57/R64 in the large subunit gives a doublet at ~12 kDa and a band of 3.3 kDa (S29-K57). The small subunit is cleaved at R207, giving rise to 9.5 kDa (N208-H285) and 3.6 kDa (S176-R207) bands. Note that the 3.6 kDa and 3.3

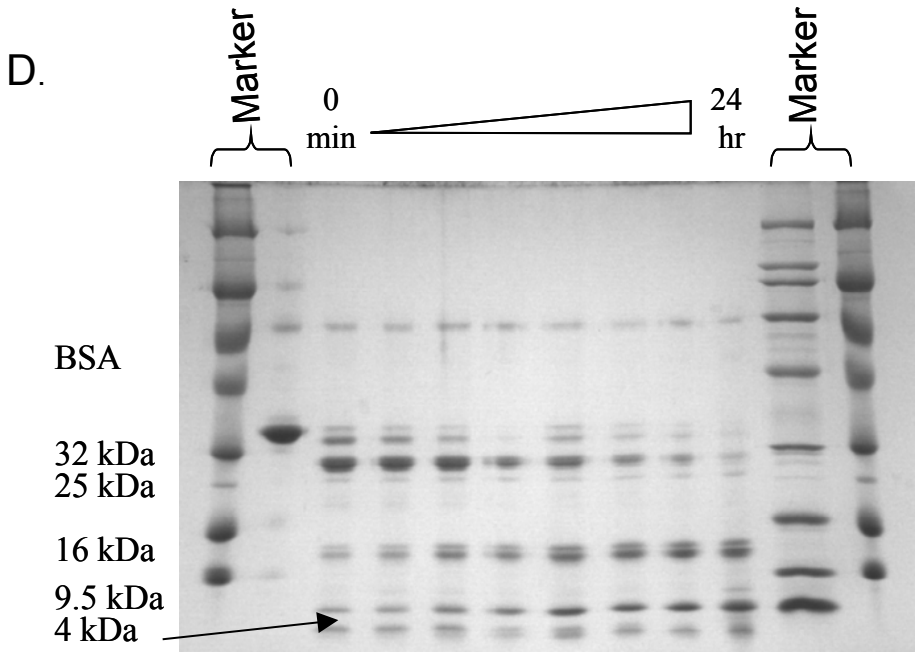

Figure 11. *Panel* D. Trypsin digestion of procaspase-3(C163S) at pH 7.2 in presence of tetrapeptide inhibitor Ac-DEVD-CHO (3 times its concentration). The 32 kDa band represents the full-length procaspase-3(C163S), whereas the 25 kDa, 16 kDa, 9.5 kDa and 4 kDa bands are the cleavage products as described in the text. Known amount of BSA was added to the gel for normalization.

kDa bands are not visible in the gel shown in Figure 11E although they are readily observed by MALDI-TOF (data not shown).

In the mature caspase-3, the cleavage at R207 was significantly faster ($t_{½}$ < 2 minutes) when compared to that of procaspase-3 ($t_{½}$ ~ 75 minutes), suggesting that the site becomes more accessible to the protease upon maturation of the procaspase. The rate of cleavage at K57/R64 remained fast in the mature caspase ($t_{½}$ < 2 minutes). Experiments using less trypsin suggest that the cleavages occur about ten fold faster in caspase-3 when compared to the procaspase (Figure 11, panel F). As with the procaspase, R207 was protected in the presence of inhibitor (Figure 11, panel G).
Overall, the data suggest that processing of the zymogen results in a more open active site conformation in the mature caspase that allows greater access to trypsin.

Limited Proteolysis with V8 Protease. We examined the conformation of procaspase-3 and of caspase-3 by limited V8 proteolysis, which cleaves C-terminal to glutamate and aspartate residues. The time-course analysis of V8 digestion of procaspase-3(C163S) at pH 7 is shown in Figure 12, panel A and demonstrates four closely spaced bands between ~27 and 32 kDa. These fragments are referred to as band 1 through 4, with band 1 being the full-length protein. These fragments were further cleaved into fragments of 16 kDa, 8.5 kDa and 4 kDa.

As with the trypsin studies described above, we used MALDI-TOF mass spectrometry and N-terminal sequencing to unambiguously assign the cleavages to residues D9, E25, E98, E106, E173, D190, E248 and D253. Representative figure for MALDI-TOF mass spectrometry is shown in Figure 12, panel B. The first cleavage occurs at E248 and D253, resulting in two fragments of ~29 kDa and 4 kDa. The larger

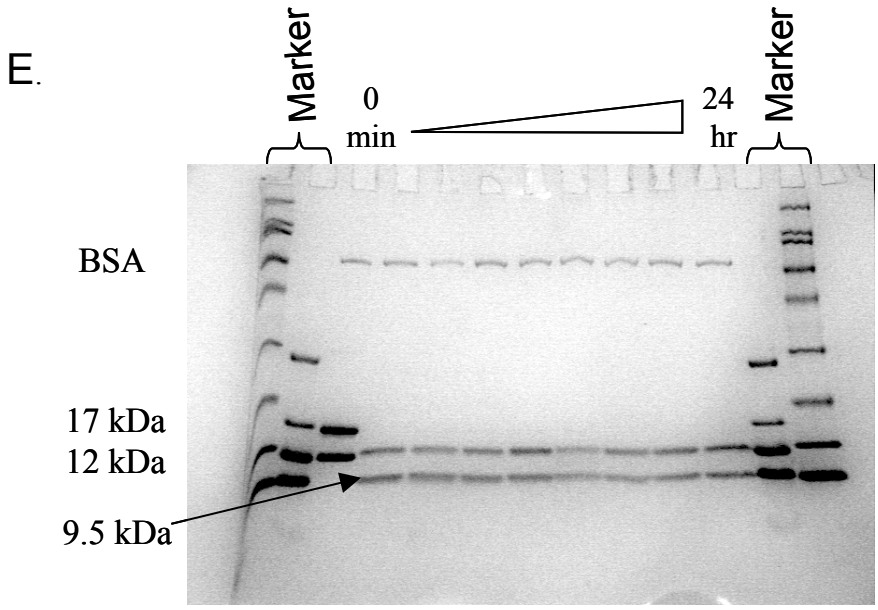

Figure 11. *Panel* E. Trypsin digestion of mature caspase-3 at pH 7.2. The 17 kDa and the 12 kDa bands represent the large and small subunits, respectively. The 9.5 kDa band represents the cleavage product as described in the text. Known amount of BSA was added to the gel for normalization.

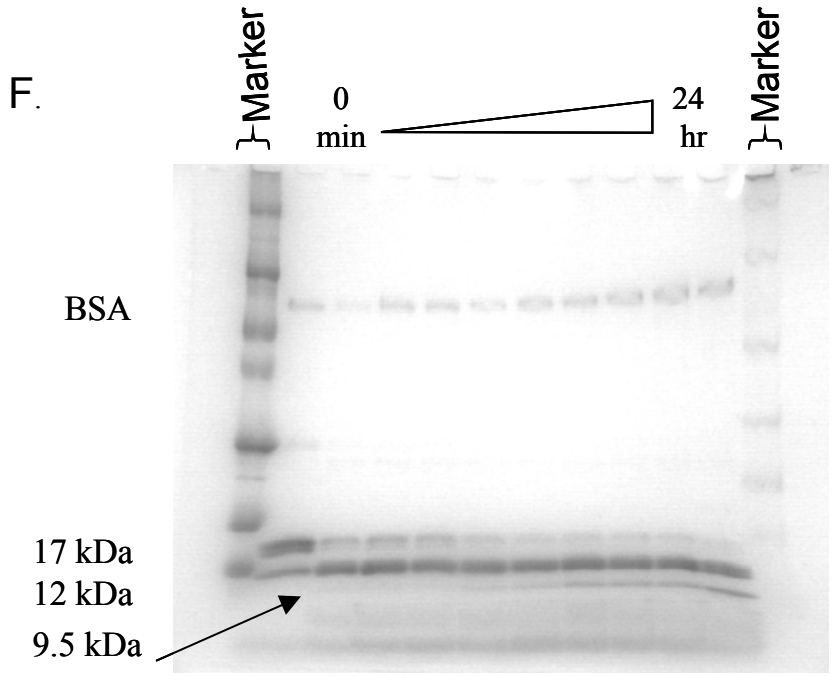

Figure 11. *Panel* F. Trypsin digestion of mature caspase-3 at pH 7.2 ($1/10^{th}$ trypsin concentration as used for gel described in figure 1E). The 17 kDa band and the doublet at 12 kDa represent the large subunit, small subunit and the cleaved large subunit respectively. The 9.5 kDa band represents the cleavage product as described in the text. Known amount of BSA was added to the gel for normalization.

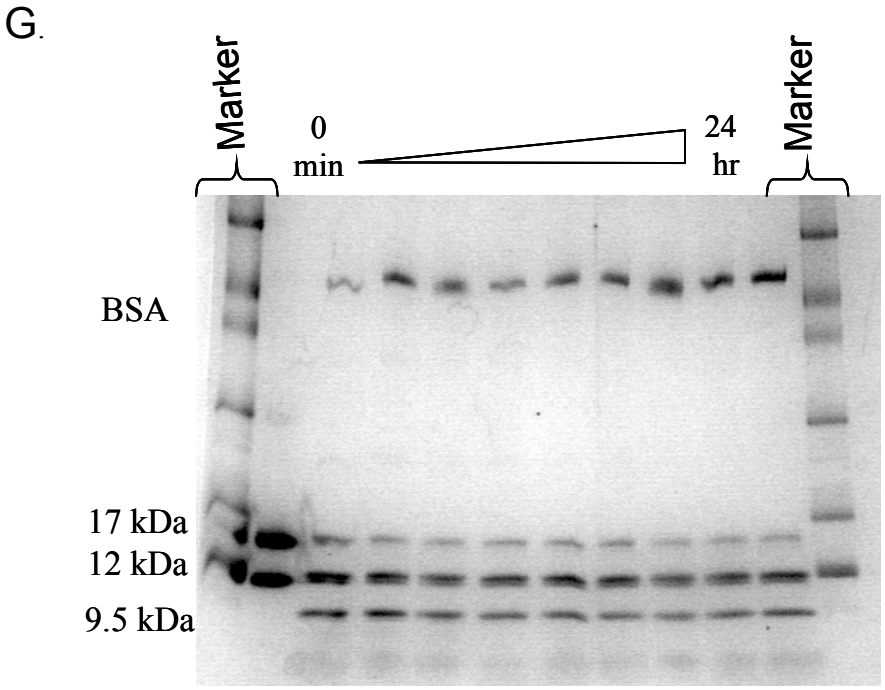

Figure 11. *Panel* G. Trypsin digestion of mature caspase-3 at pH 7.2 in presence of its tetrapeptide inhibitor Ac-DEVD-CHO. The 17 kDa band and the doublet at 12 kDa represent the large subunit, small subunit and the cleaved large subunit respectively. The 9.5 kDa band represents the cleavage product as described in the text. Known amount of BSA was added to the gel for normalization.

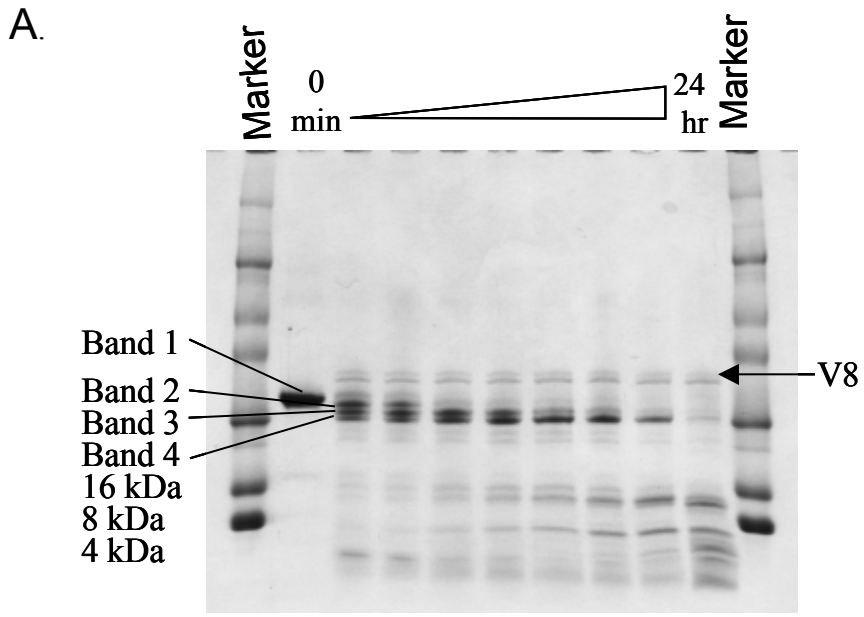

Figure 12. *Panel* A. V8 protease (Endo-Glu C) digests of procaspase-3(C163S) at pH 7. **Band 1**: full-length procaspase-3(C163S), **Band 2**: cleavage at D248/E253, **Band 3**: cleavage at D9, **Band 4**: cleavage at E25, **16 kDa, 8 kDa**: cleavage at D190, E98, E106, **4 kDa**: cleavage at D248/E253.

B.

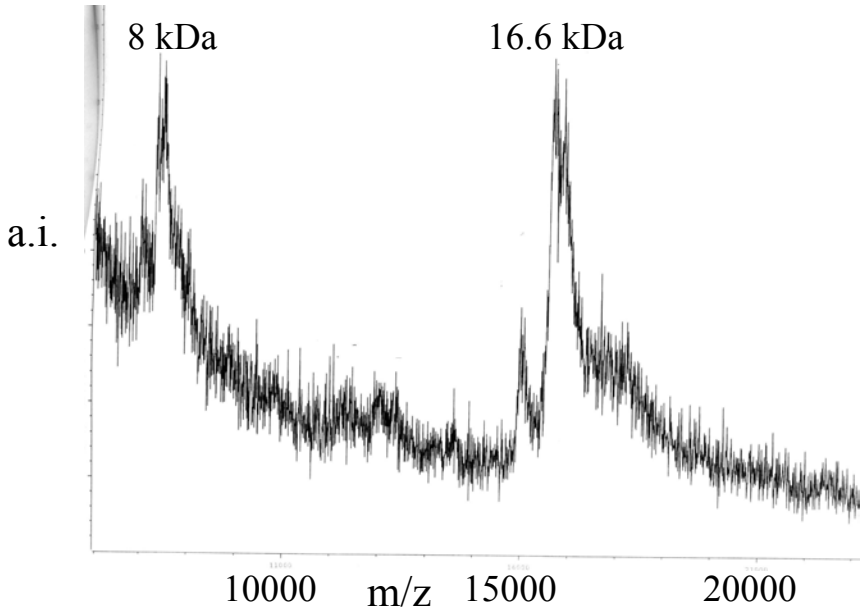

Figure 12. *Panel* B. MALDI-TOF mass spectrometric analysis of V8 protease digests (overnight) of procaspase-3(C163S). The 16 kDa and 8 kDa peaks represent the fragments as described in the text.

band is referred to as band 2, and band 2 is further cleaved at D9 and then at E25, both of which are in the pro-domain, to give bands 3 and 4, respectively. Band 4 is then cleaved simultaneously at positions 98/106 and 173/190, giving rise to a mixture of ~16 kDa and ~8.5 kDa bands. The presence of inhibitor did not result in significant protection of the cleavage sites (data not shown).

For mature caspase-3, the results of limited V8 proteolysis are shown in Figure 12, panel C. Overall, the same cleavages occur as for the procaspase, with the exceptions noted below. Importantly, no new cleavage sites appear upon zymogen processing. The results demonstrate three major bands (Figure 12 C). The large subunit (17 kDa) is trimmed at the C-terminus, possibly at E173 (removing two residues) or at D169 (removing six residues) or at E167 (removing eight residues). This produces a doublet cleaved at E272, which removes the his-tag at the C-terminus, producing a doublet consisting of two fragments of ~12 kDa. The small subunit is cleaved further at E248/D253, resulting in an ~8 kDa fragment. The 4 kDa fragment is observed only in the overnight digests because cleavage at E272 results in two ~2 kDa fragments. Both of these fragments are observed by MALDI-TOF. Interestingly, the cleavages at E98 and E106 and at D190 are not observed in caspase-3.

The results of the limited proteolysis studies (trypsin and V8) are shown in Figure 12, panel D. The data are mapped onto the structure of mature caspase-3 to show the positions of the residues that are cleaved. As shown in this figure, E248 and D253 reside in loop L4, whereas E173 and D190 are in loops L2 and L2', respectively. Residues E98 and E106 reside on the surface of the protein, away from the active site. In caspase-3 [19],

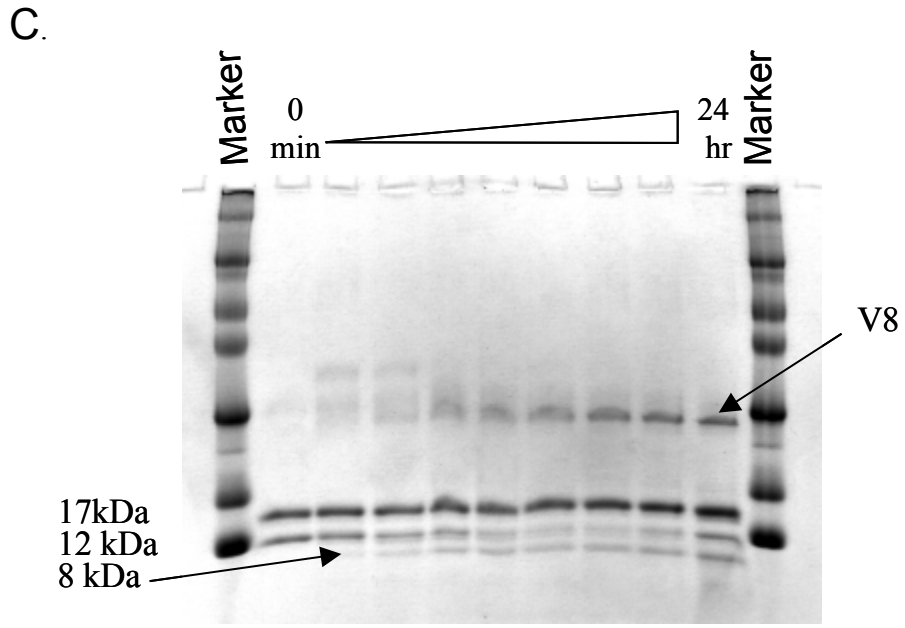

Figure 12. *Panel* C. V8 protease digests of mature caspase-3 at pH 7. 17 kDa band region shows a doublet for the full-length and trimmed large subunit. Bands at 12 kDa show the small subunit and the small subunit with cleaved his-tag. The 8 kDa band is due to the cleavage of small subunit at E248/D253.

D.

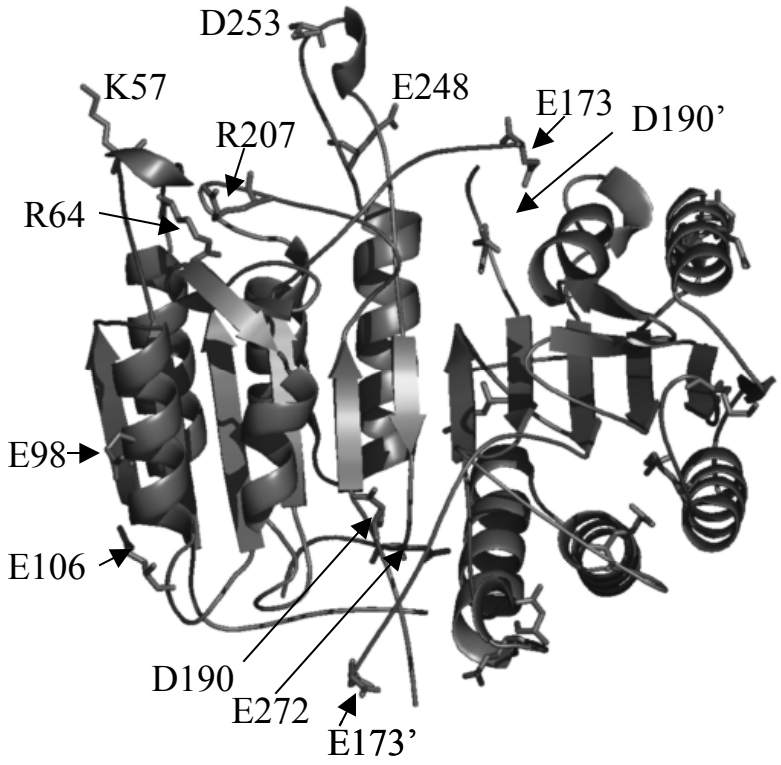

Figure 12. *Panel* D. Trypsin and V8 protease cleavage sites of procaspase-3(C163S) are mapped onto the caspase-3 structure. The structure was generated using the program *PyMOL* (Delano Scientific, CA). The cleavages at K57, R64 and R207 are by trypsin and E98, E106, E173, D190, E248, D253, E272 are by V8 protease. The prime indicates residues from the second heterodimer. Note that the inhibitor has been removed and only half of the protein is labeled for clarity.

consisting of the full-length and trimmed large subunits. The small subunit (12 kDa) is E106 is observed to interact with R86, which resides on β-strand 2. This strand is the outside-most strand in the β-sheet, the edge of which is exposed to solvent. These results suggest that the salt bridge between R86 and E106 is not formed in the procaspase. Residue D190 is C-terminal to the blocking segment (K186-V189) described above, so it is worth noting the changes at this site. Residue D190 is not cleaved in caspase-3, suggesting that the exposed L2' loop in procaspase-3 becomes less accessible for cleavage after zymogen processing. In caspase-3, D190 is within 3.3 Å of K137, on helix 3, whereas the distance is about 7.4 Å between D190 and K137 in procaspase-7. Overall, the data are consistent with movements in loop L2' upon maturation.

One of the advantages of V8 protease is that it is active over a broad pH range, with maximum activities around pH 4.0 and 7.8 [59]. The activity varies only about 1.5-fold over this pH range. This allowed us to examine the cleavage of procaspase-3(C163S) and of caspase-3 between pH 8 and 4. These experiments were undertaken for two reasons. First, in the two structural studies [18; 28] the crystals were grown at pH 5.6 or pH 5.8. Second, Nicholson and coworkers [30] showed that the rate of autoactivation was pH-dependent, with a maximum rate obtained at pH~5.5. The results for procaspase-3(C163S) are shown in Figures 12, panels E-H for pH 8, 6, 5 and 4 respectively. With respect to the four closely spaced bands (bands 1-4) of procaspase-3, the rates of the cleavages increased with a decrease in pH from 7 to 5. The rates of disappearance of bands 1-4 increased about 20-fold from pH 7 to 5. This suggests greater accessibility to the protease at E248/D253, D9, and E25. We have shown previously that the pro-domain of procaspase-3 binds to the protease domain at site(s) away from the active site,

although the binding site(s) has not been identified [22]. The data presented here suggest that the binding is pH-dependent. That is, the pro-domain may be unbound and more solvent-exposed at lower pH, which allows faster cleavage by V8 protease. In addition, the data suggest a conformational change in loop L4 (E248/D253) at pH 5 that results in faster cleavage by the protease. As described below, this correlates with a change in the environments of the tryptophanyl residues in the active site.

Between pH 8 and 5, the cleavage of band 4 to generate the 16 kDa and 8 kDa bands occurred at approximately the same rate. This suggests that the accessibility to V8 protease of the E98/E106 and E173/D190 sites does not change significantly over this pH range.

A second significant change occurred between pH 5 and 4, where at pH 4 the protein was more resistant to digestion. Over the time course of the experiment, we observed only band 1 and band 2, that is, cleavage at E248/D253. The data show that there was no cleavage in the pro-domain (D9 or E25), nor were there cleavages at E98/E106 or E173/D190. The results suggest that with the exception of loop L4, the protein undergoes a conformational change between pH 5 and 4 that results in a protection of the remaining sites of proteolysis.

In our experiments, the proteins were cleaved as described above for pH 7 (Figure 12A), and the intensities of the bands were quantitated at each time point. The data were then normalized relative to that of the full-length protein at time zero. Representative data for pH 7 are shown in Figure 12, panel I for the seven major species, bands 1-4, 16 kDa, 8 kDa, and 4 kDa fragments. The data for bands 1-4 were fit to a double exponential

E.

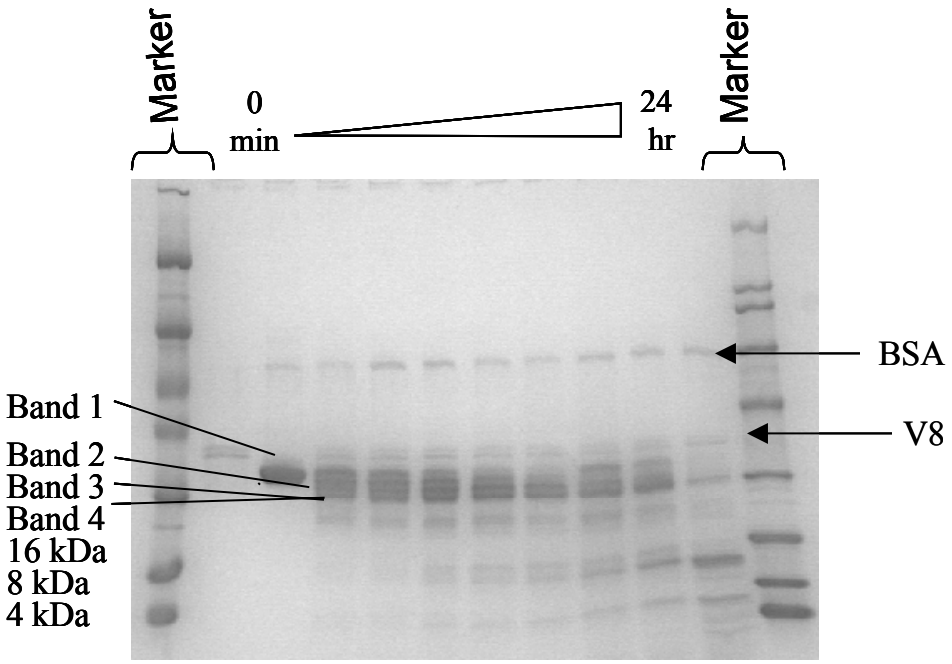

Figure 12. *Panel* E. V8 protease (Endo-Glu C) digests of procaspase-3(C163S) at pH 8. The bands are as described earlier.

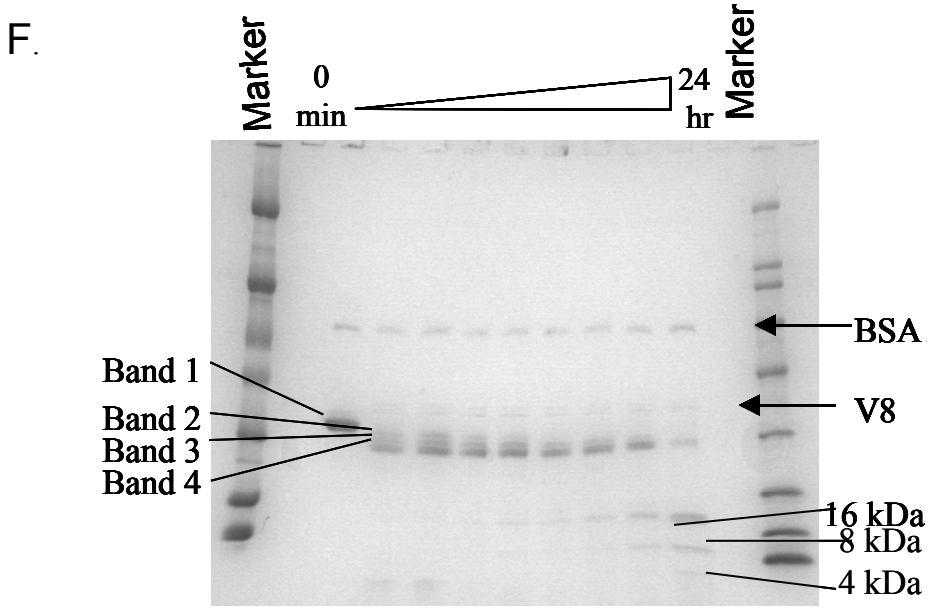

Figure 12. *Panel* F. V8 protease (Endo-Glu C) digests of procaspase-3(C163S) at pH 6. The bands are as described earlier.

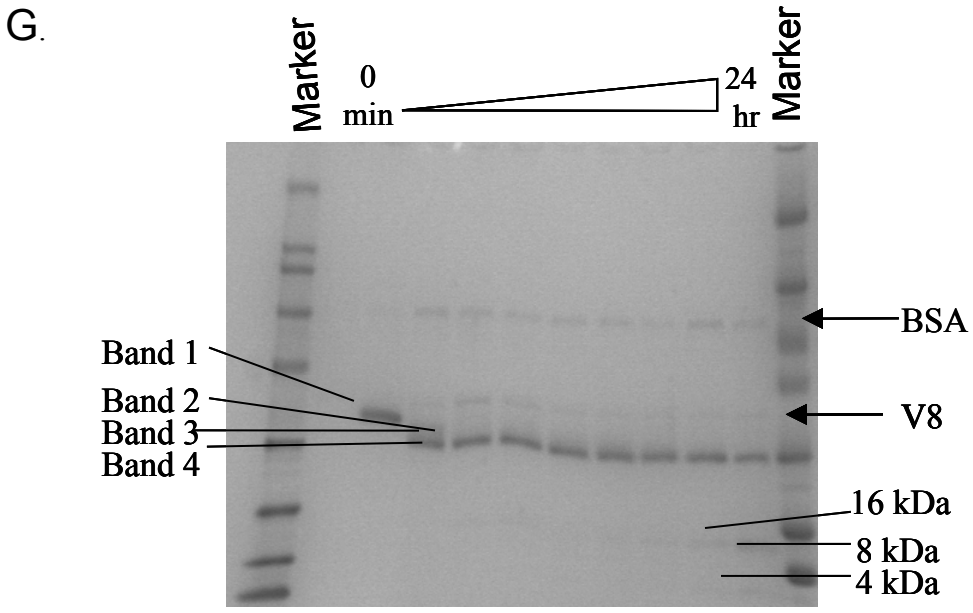

Figure 12. *Panel* G. V8 protease (Endo-Glu C) digests of procaspase-3(C163S) at pH 5. The bands are as described earlier.

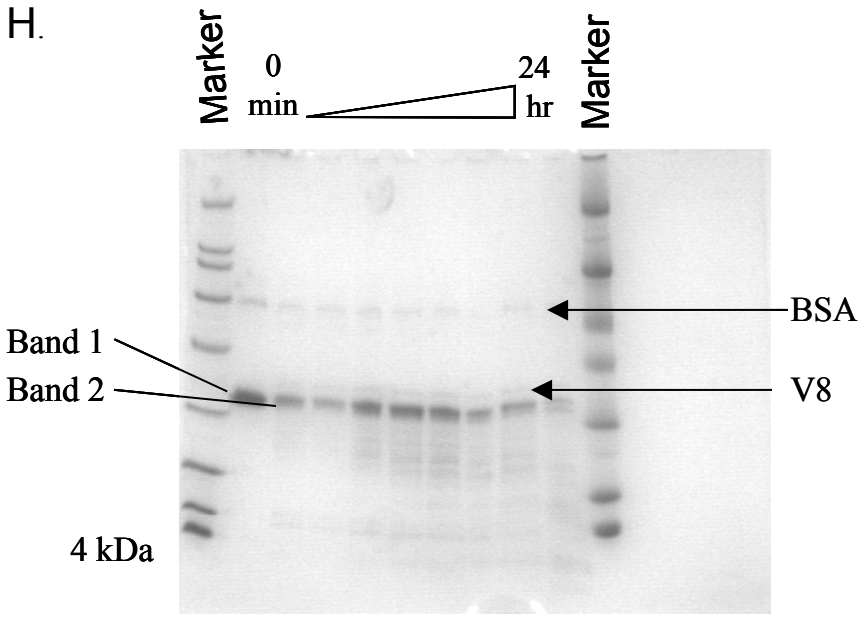

Figure 12. *Panel* H. V8 protease (Endo-Glu C) digests of procaspase-3(C163S) at pH 4. The bands 1 and 2 and 4 kDa bands are as described earlier.

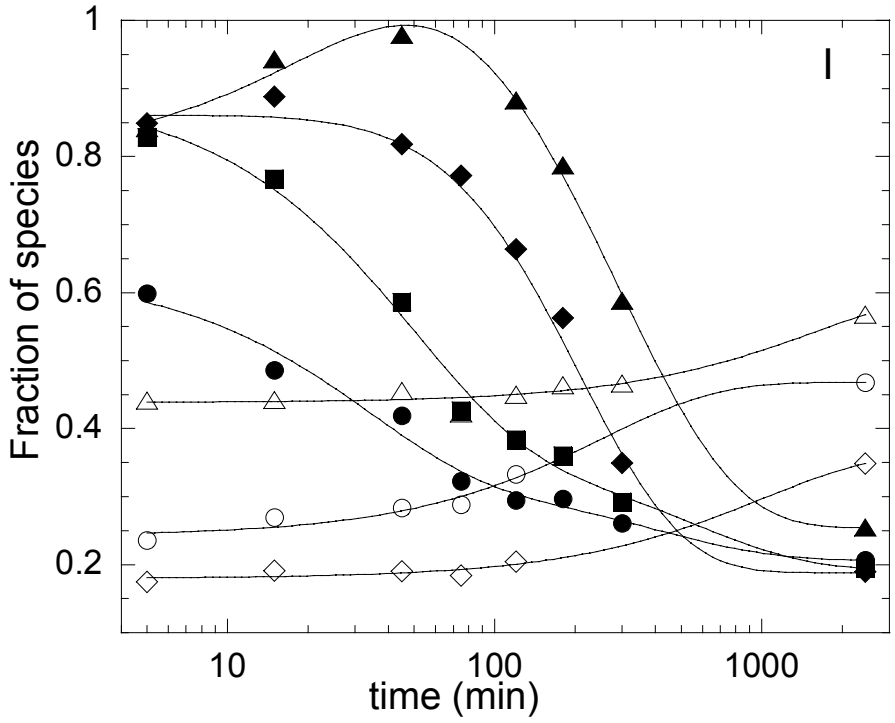

Figure 12. *Panel* I. Fraction of species versus time for procaspase-3(C163S) at pH 7. The bands are shown as follows: band 1 (●), band 2 (■), band 3 (◆), band 4 (▲), 16 kDa band (○), 8 kDa band (◇), 4 kDa band (△). Solid lines represent fits of the data as described under Materials and Methods. Bands 1-4 were fitted to a double exponential equation while the 16 kDa, 8 kDa and 4 kDa bands were fitted to a single exponential equation.

equation and for 16 kDa, 8 kDa, and 4 kDa fragments to a single exponential equation in order to obtain kobs, the apparent rate of change for each species. These rates were then plotted versus pH, and the results are shown in Figure 12, panel J. While this analysis allows us to summarize a large amount of data, we consider this to be a qualitative rather than a quantitative description of the results.

In comparison with procaspase-3(C163S), the mature caspase-3 was cleaved faster at the E248/D253 sites at pH 4 compared to the cleavage rates at higher pH (Figure 12, panel K). For example, cleavage at E248/D253 occurred with t½ ~3 hours at pH 4 versus t½ >8 hours at pH 7, so that at pH 4 the 12 kDa small subunit disappeared in the overnight samples. This can be compared to the data in Figure 12 C, which show that the small subunit persists after overnight digestion. In contrast to the data at pH 7, there was less cleavage at E272, which eliminated the ~12 kDa doublet and resulted in the appearance of the 4 kDa fragment in the early time points. Overall, the data show that for both the procaspase and the mature caspase, cleavage at E248/D253 occurs faster at lower pH compared to pH 7. This is consistent with a pH-dependent conformational change in loop L4.

Fluorescence Quenching. Each monomer of the procaspase-3 dimer contains two tryptophanyl residues, W206 and W214, both of which are in the active site. According to the structures of procaspase-7, W206, in loop L3, is completely solvent exposed (see Figure 4). Upon maturation, loop L3 moves into the active site such that W206 stacks onto W214, a movement of about 10 Å.

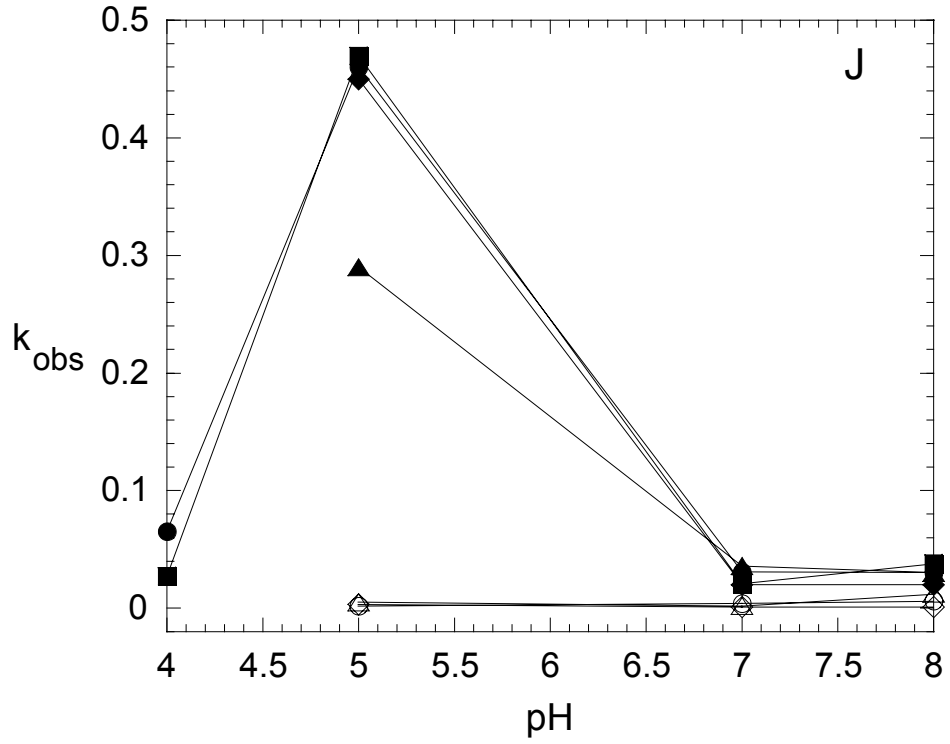

Figure 12. Panel J. Plot of k_{obs} versus pH for the procaspase-3(C163S) fragments. The bands are shown as follows: band 1 (●), band 2 (■), band 3 (◆), band 4 (▲), 16 kDa band (○), 8 kDa band (◇), 4 kDa band (△). The rates of disappearance (k_{obs}) of the bands 1-4 and the rates of formation (k_{obs}) of the 16 kDa, 8 kDa and 4 kDa bands from the fits were plotted against pH. The points are joined by solid lines.

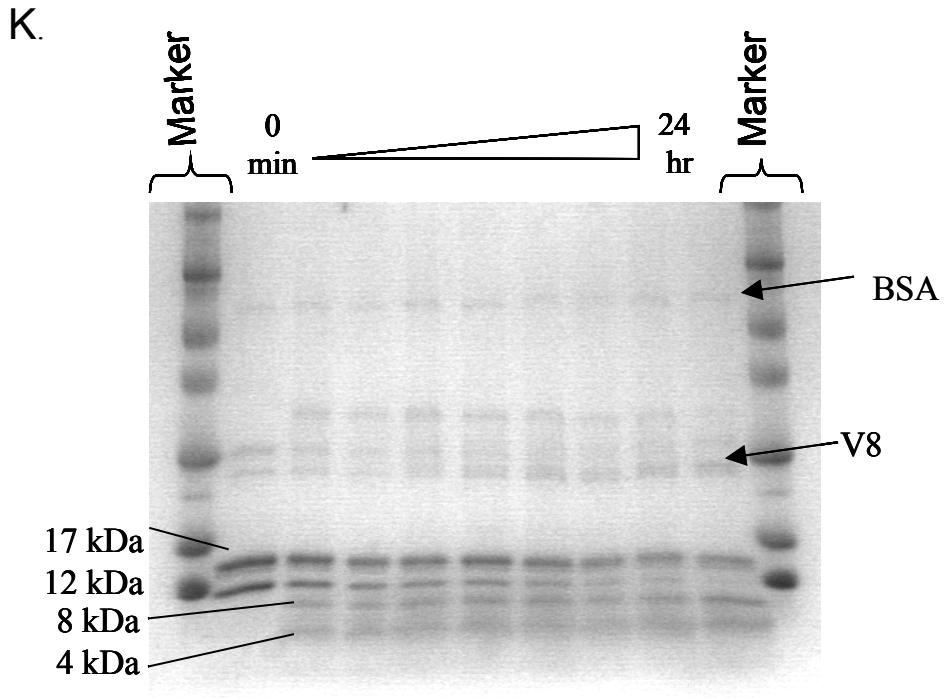

Figure 12. *Panel* K. V8 protease digests of mature caspase-3 at pH 4. The bands are as described in figure 12C. The 4 kDa band is due to the cleavage of the small subunit at E248/D253 giving rise to the 8 kDa and 4 kDa fragments. Known amount of BSA was added to the gel for normalization.

We examined the fluorescence emission of two mutants of procaspase-3 in which the tryptophans were replaced to generate W206Y or W214V. Both mutants were in the context of an active site mutation, C163A. The results are shown in Figure 13, panel A. Overall, there was a decrease in fluorescence emission for both mutants, but surprisingly, the fluorescence emissions were blue-shifted compared to that of procaspase-3(C163S). The wavelength maximum for caspase-3, procaspase-3(C163S), procaspase-3(C163A,W206Y) and procaspase-3(C163A,W214V) are 342 nm, 340 nm, 337 nm and 335 nm, respectively. The results are unexpected because the structure of procaspase-7 predicts that procaspase-3(C163A,W214V) would have a red-shifted fluorescence emission compared to the wild-type procaspase if loop L3, containing W206, were unraveled and solvent exposed.

The fluorescence emission of procaspase-3(C163S) and of procaspase-3(D_3A) in the presence or absence of inhibitor, were similar (data not shown). If binding of inhibitor induced W206, on loop L3, to move 10 Å to stack on W214, then the movement should be reflected by a change in fluorescence emission. These results suggest that the environments of the tryptophans change little upon inhibitor binding. In Figure 11C we noted the protection of R207 from trypsin proteolysis in the presence of inhibitor. The results suggested either that loop 3 was inserted into the active site before inhibitor binding, and hence R207 was protected, or that the binding of inhibitor facilitated the correct conformation of loop L3. These results suggest that the binding of inhibitor does not facilitate movement of loop L3, but rather the loop is inserted into the active site in the apo-procaspase.

Because of these results, we examined the accessibility of the tryptophans to quenching by potassium iodide, and the experiments were performed over the pH range of 9 to 3. Representative data for procaspase-3(C163S), caspase-3, procaspase-3(C163A, W206Y) and procaspase-3(C163A, W214V) are shown in Figure 13, panels B, C, D, E respectively. The data at each pH were fit to equation 26, as described in Methods, to determine the Stern-Volmer quenching constant, K_{SV}. The constants were plotted versus pH, and the results are shown in (Figure 13F, upper panel**)** for procaspase-3(C163S), caspase-3, procaspase-3(C163A, W206Y) and procaspase-3(C163A, W214V). For all proteins at pH>8, values for K_{SV} are ~3-8. Both caspase-3 and procaspase-3 demonstrate two transitions, although one transition results in the opposite effect for the proteins. For example, between pH 9 and 6, K_{SV} increases to ~13 for procaspase-3, whereas it decreases from ~8 to ~6 for caspase-3. Although the transition is small for caspase-3, it is reproducible. The transition results in an increased accessibility to iodide in the case of procaspase-3 and a decrease in iodide accessibility for the mature caspase-3. In contrast to these two proteins, the two tryptophan mutants demonstrate a single transition. All four proteins show a cooperative increase in K_{SV} between pH 6 and 3, with the final values between ~18 and 25.

The data shown in Figure 13F were fit to equation 24, as described in Methods, to determine the apparent pK's for the transitions. In the case of the tryptophan mutants, a modified form of equation 3 was used to account for the single transition. For the first transition, the pKa's for procaspase-3(C163S) and mature caspase-3 were 4.1±0.3 and 4.0±0.2, respectively. The pKa's for procaspase-3(C163A,W206Y) and procaspase-

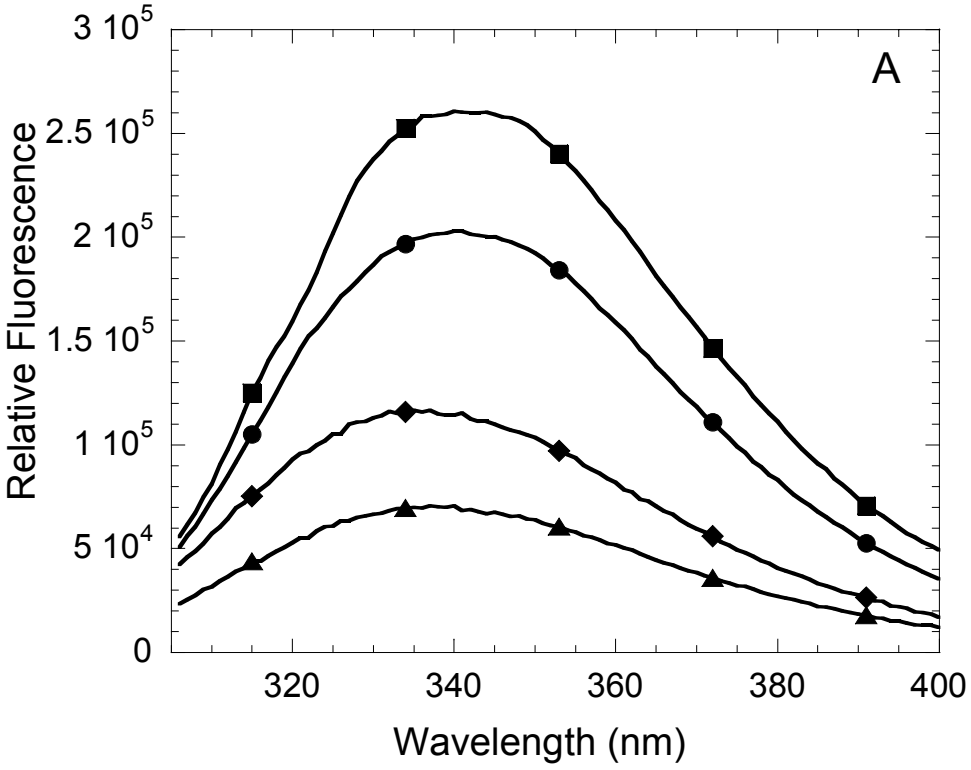

Figure 13. *Panel* A. Fluorescence emission scans of procaspase-3(C163S) (●), mature caspase-3 (■), procaspase-3(C163A,W206Y) (▲), procaspase-3(C163A,W214V) (♦). Samples were excited at 295 nm and emission was monitored between 305-400 nm.

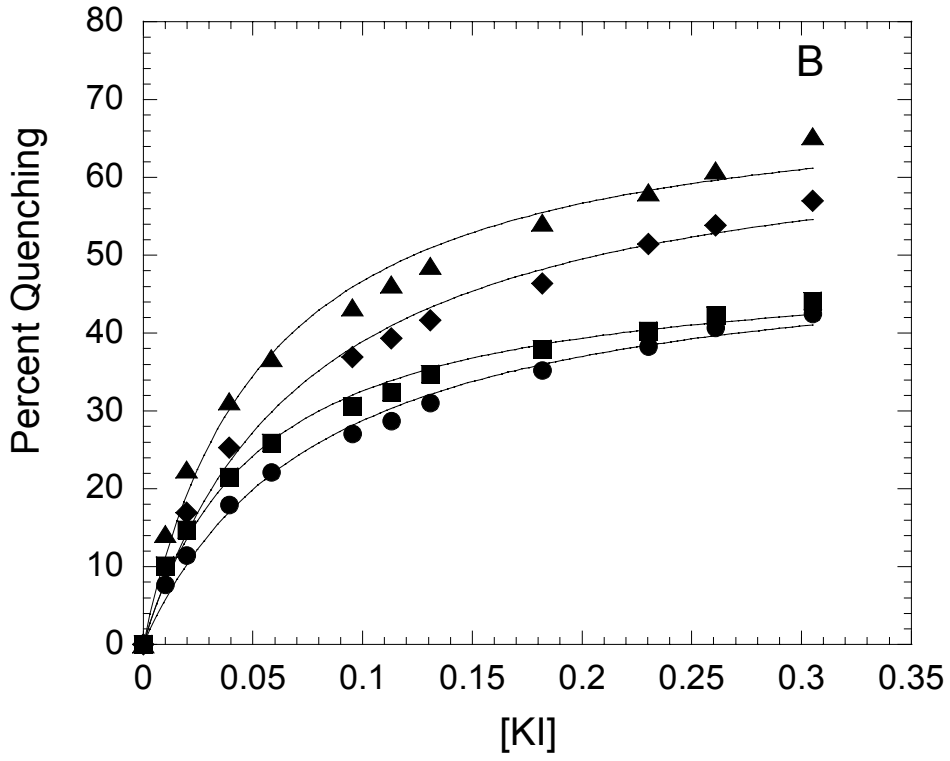

Figure 13. *Panel* B. Plot of percent quenching of procaspase-3(C163S) versus [KI] at pH 7.2 (●), pH 6 (■), pH 5 (◆), pH 4 (▲). Percent quenching is calculated using equation 25 as described in Materials and Methods. The data were fit to equation 26 of Materials and Methods.

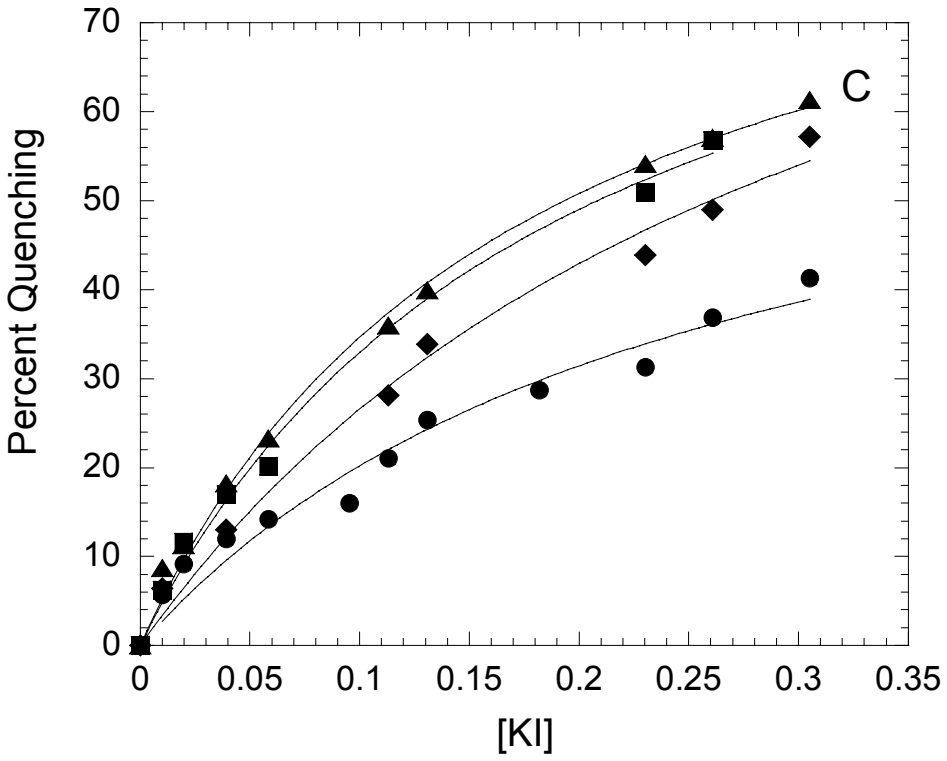

Figure 13. *Panel* C. Plot of percent quenching of mature caspase-3 versus [KI] at pH 7.2 (●), pH 6 (■), pH 5 (◆), pH 4 (▲). Percent quenching is calculated using equation 25 as described in Materials and Methods. The data were fit to equation 26 of Materials and Methods.

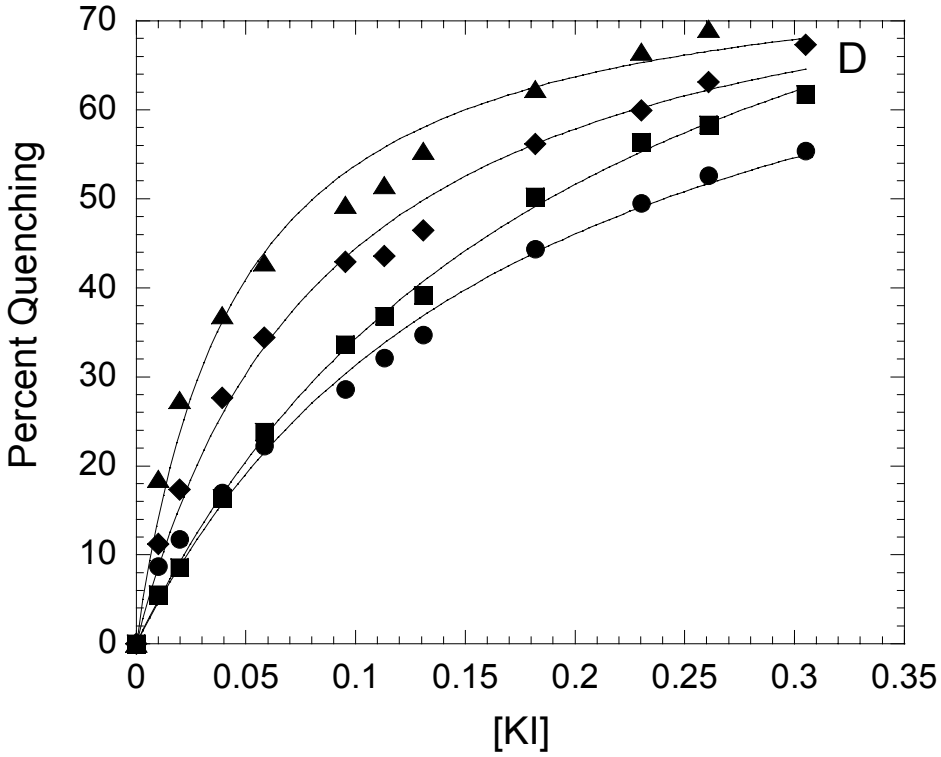

Figure 13. *Panel* D. Plot of percent quenching of procaspase-3(C163A, 206Y) versus [KI] at pH 7.2 (●), pH 6 (■), pH 5 (◆), pH 4 (▲). Percent quenching is calculated using equation 25 as described in Materials and Methods. The data were fit to equation 26 of Materials and Methods.

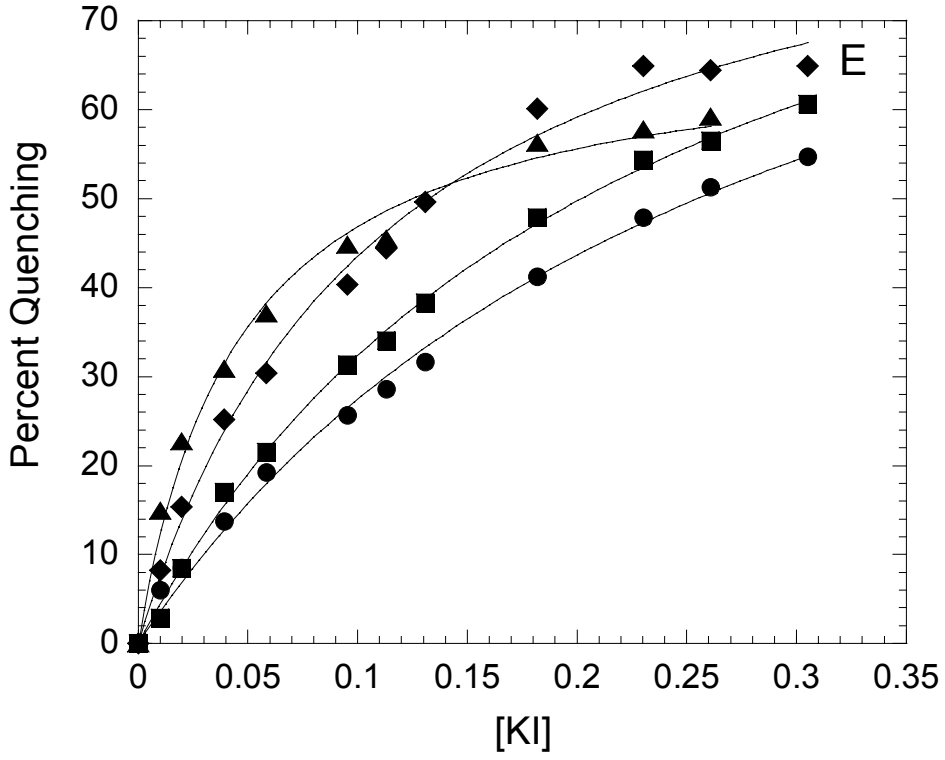

Figure 13. *Panel* E. Plot of percent quenching of procaspase-3(C163A, 214V) versus [KI] at pH 7.2 (●), pH 6 (■), pH 5 (◆), pH 4 (▲). Data were fit to equation 25 as described in Materials and Methods.

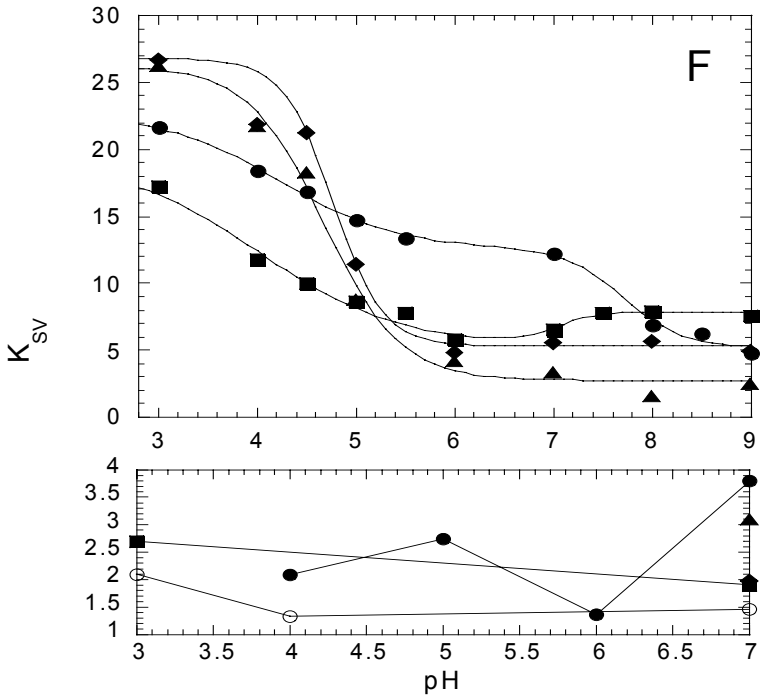

Figure 13. *Panel* F. *Upper panel.* Stern-Volmer quenching constants (K_{SV}) by iodide vs. pH for procaspase-3(C163S) (●), procaspase-3(C163A,W206Y) (▲), procaspase-3(C163A,W214V) (◆) and mature caspase-3 (■). *Lower panel.* Stern-Volmer quenching constants (K_{SV}) by acrylamide vs. pH for procaspase-3(C163S) (●), procaspase-3(C163A,W206Y) (▲), procaspase-3(C163A,W214V) (◆) and mature caspase-3 (■). Stern-Volmer quenching constants (K_{SV}) by CsCl vs. pH for procaspase-3(C163S) (○). Data were fit to equation 26 as described in Materials and Methods.

3(C163S,W214V) were 4.8±0.1 and 4.7±0.03, respectively. These results are consistent with the titration of one or more acidic groups that affect the environment of the tryptophanyl residues in the active sites. It is not clear why the pKa's are higher for the tryptophanyl mutants or why these proteins demonstrate a single transition, but the data suggest that removal of one tryptophan changes the environment of the second tryptophan. The second transition for mature caspase-3 has a pKa of 7.2±0.4, whereas that for procaspase-3 is 7.7±0.4. The second transition is consistent with the titration of a histidyl residue, which again, affects the environment of the tryptophanyl residues in the active sites.

The results also are consistent with an increased solvent exposure of the tryptophanyl side-chains as the pH is lowered. To examine this, we used acrylamide and cesium chloride as quenching agents. The results for acrylamide quenching at pH 7, are shown in Figure 13, panel G. The data demonstrate that there is little quenching of the fluorescence emission by this quenching agent. Moreover, there are no differences among the four proteins. For comparison, procaspase-3(C163S) was unfolded in 8 M urea-containing buffer, and the data demonstrate an increase in the Stern-Volmer quenching constant for the unfolded protein due to the exposure of the tryptophanyl side chains.
These results would be expected for native procaspase-3(C163A,W214V) if W206 were solvent exposed in the native protein. As with potassium iodide, the experiments with acrylamide were performed over the pH range of 7 to 4 for procaspase-3(C163S) (Figure 13, panel H**)** and at pH 7 and pH 3 for caspase-3 (Figure 13, panel I**)**. The data demonstrate that there was no change in K_{SV} for acrylamide over this pH range. In addition, we repeated the experiments using cesium chloride as the quenching agent, and

the results were the same as for acrylamide (Figure 13F, lower panel). There was no change in K_{SV} from pH 7 to 3. Representative figure for procaspase-3(C163S) quenching by CsCl at pH 7 and 4 is shown in Figure 13, panel J. These results suggest that the conformational change that occurs between pH 6 and 4 likely affects the microenvironment of the tryptophanyl residues so that the tryptophans are more accessible to quenching by iodide. That is, at lower pH, the negative charge(s) around the tryptophans decreases, resulting in increased quenching by the negatively charged iodide ion.

Overall, the results demonstrate that the tryptophans are not exposed to solvent, even at the lower pH. This interpretation is consistent with the results of the limited trypsin proteolysis, presented above, in which it was shown that at pH 7.2 R207 in loop L3 is cleaved more slowly than R64, in loop L1, and is protected upon substrate binding. While the precise groups that are responsible for the transitions are not known, the protonation/deprotonation of the groups affects the environment of the tryptophanyl residues in the active site. Protonation of the acidic group may be responsible for the increase in K_{SV} for iodide quenching (Figure 13B) and may explain why there is no increase in K_{SV} for cesium or acrylamide at lower pH. Overall, the data suggest that one or more salt bridges affect the stability of the active site.

II. Folding and stability of procaspase-3

The monomeric procaspase-3 consists of 277 amino acids (M_r=31,577 Da). Under some conditions, such as the high protein concentrations found in heterologous

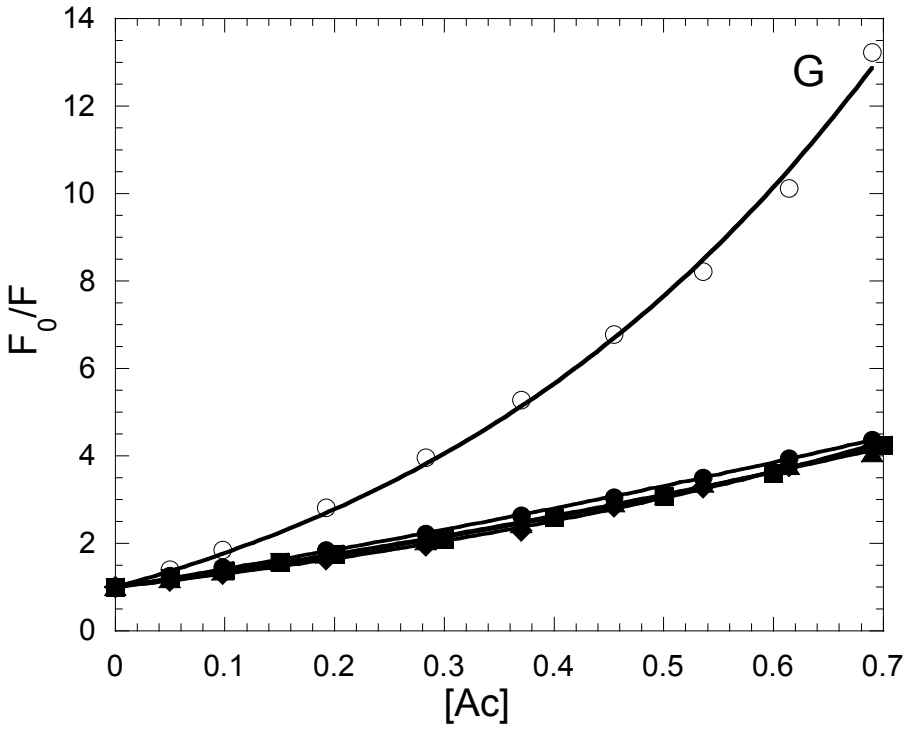

Figure 13. *Panel* G. Acrylamide quenching of procaspase-3(C163S) (●), procaspase-3(C163A,W206Y) (▲), procaspase-3(C163A,W214V) (◆), mature caspase-3 (■) and procaspase-3(C163S) in 8 M urea-containing buffer (○), at pH 7. Data were fit to modified Stern-Volmer equation as described in the text.

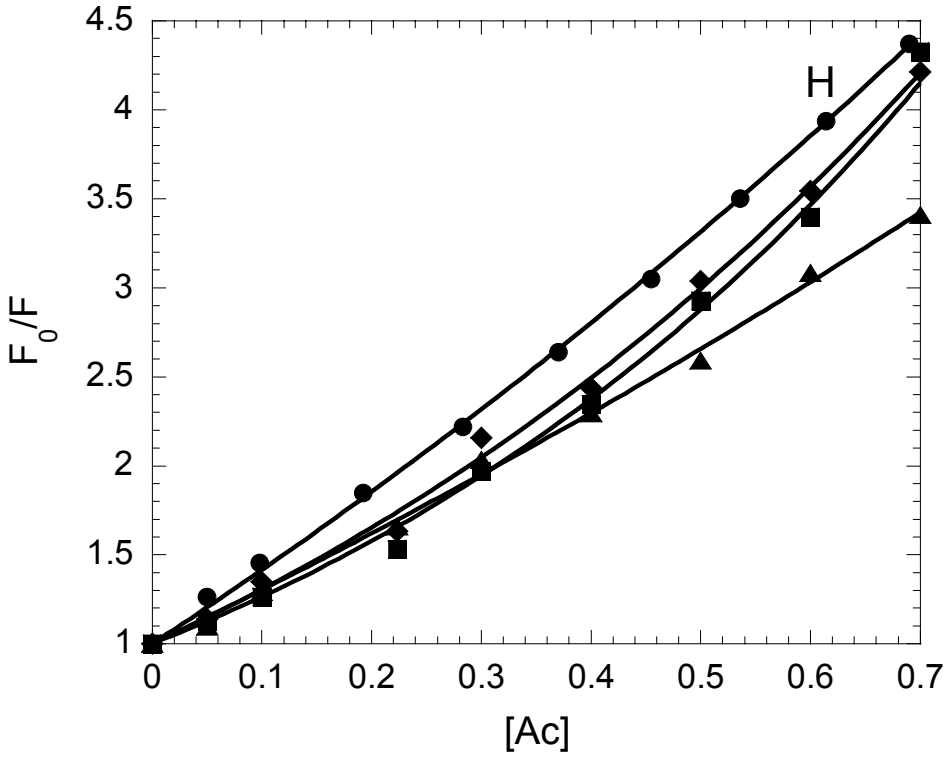

Figure 13. *Panel* H. Acrylamide quenching of procaspase-3(C163S) at pH 7 (●), pH 6 (■), pH 5 (▲) and pH 4 (◆). Data were fit to modified Stern-Volmer equation as described in the text.

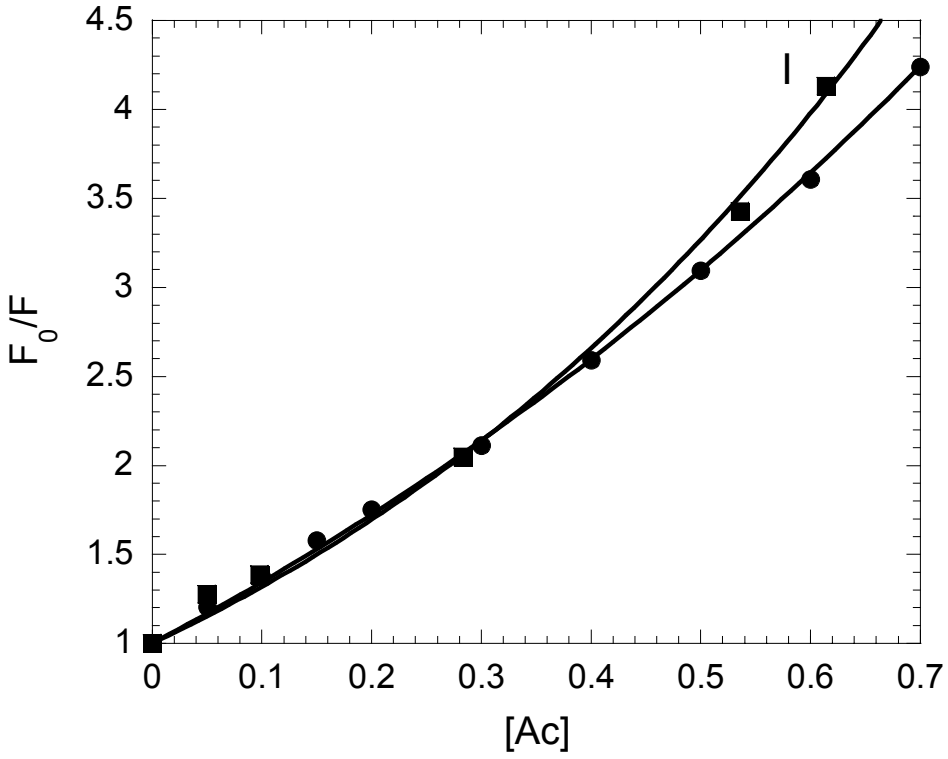

Figure 13. *Panel* I. Acrylamide quenching of mature caspase-3 at pH 7 (●) and pH 3 (■). Data were fit to modified Stern-Volmer equation as described in the text.

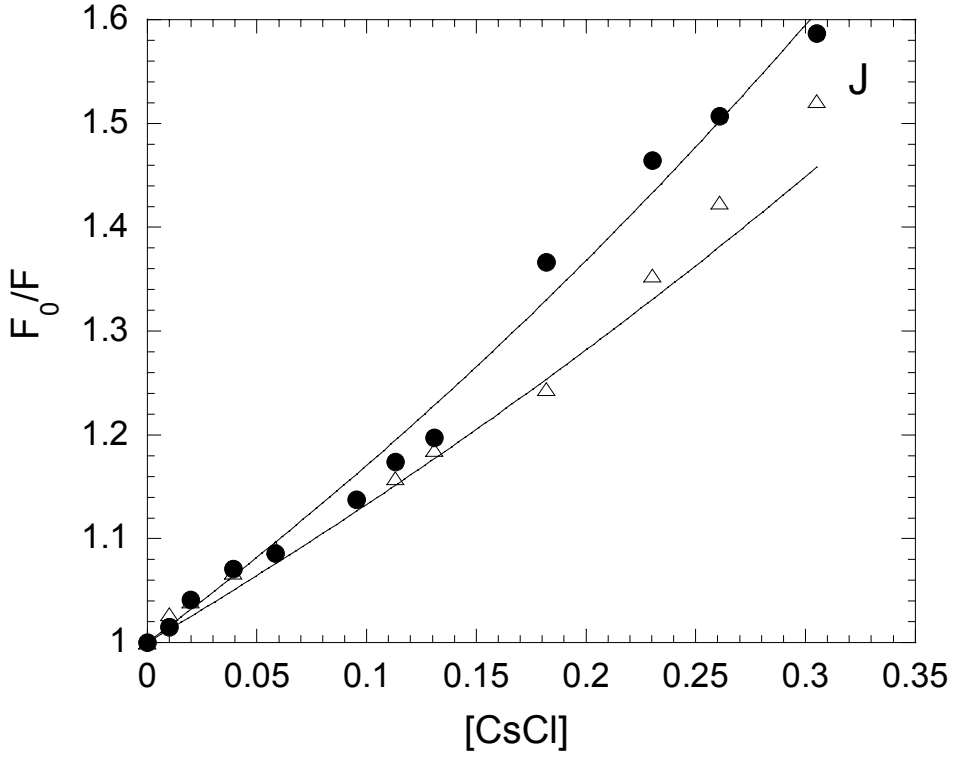

Figure 13. *Panel* J. Cesium chloride quenching of procaspase-3(C163S) at pH 7 (●) and pH 4 (Δ). Data were fit to modified Stern-Volmer equation as described in the text.

expression systems, caspase-3 activation is autocatalytic [60; 61; 62]. In order to prevent autoproteolysis, we substituted the active site cysteine with a serine residue (C163S) for our equilibrium unfolding studies. The C163S mutation prevents autolysis of the procaspase but is not structurally perturbing [26; 63; 64].

While there are no aromatic residues in the pro-domain, procaspase-3 has two tryptophan residues (W206 and W214), and both reside in the carboxy-terminal region of the polypeptide, that is, the region that becomes the small subunit of the mature caspase. In addition, there are ten tyrosine residues well distributed in the primary sequence. Based on these features, it is convenient to examine folding and unfolding of the tertiary structure by monitoring changes in fluorescence emission.

As shown in Figure 14, native procaspase-3(C163S) has a fluorescence emission maximum at 335 nm when excited at 280 nm (panel A) and 340 nm when excited at 295 nm (panel B), indicating that the tryptophans are more solvent exposed than the remaining aromatic residues. In the mature caspase-3 heterotetramer, the tryptophans are in or near the active site. Based on results from limited trypsin proteolysis of procaspase-3, the conformation of the procaspase-3 dimer appears to be similar to that of the heterotetramer. This suggests that in procaspase-3, the two tryptophan residues are in or near the active site and explains the red-shift in fluorescence emission (Figure 14, panel B) compared to the protein excited at 280 nm (Figure 14, panel A). In phosphate buffer containing 8 M urea, the fluorescence emission maximum is red-shifted to approximately 348 nm following excitation at either 280 nm (Figure 14, panel A) or 295 nm (Figure 14**,** panel B), indicating that the protein was largely unfolded under these solution conditions. In addition, the fluorescence intensity does not change dramatically. The far-UV circular

dichroism spectrum of procaspase-3(C163S) demonstrates a large β-sheet content, whereas the near-UV CD spectrum demonstrates a well defined packing of the aromatic side chains [22]. In 8 M urea-containing phosphate buffer, both near-UV and far-UV CD spectra show a large signal change due to loss of secondary and tertiary structure (data not shown).

At intermediate concentrations of urea (~3-5 M), the fluorescence emission spectra were blue-shifted compared to those for the native protein. Representative data are shown in Figure 14 (panels A and B) for protein in 4 M urea-containing phosphate buffer. Under these conditions, the emission maxima were either 337 nm **(**panel B**)** or 333 nm (panel A). These results suggested the presence of an equilibrium folding intermediate that is populated under these conditions (3-5 M urea).

Equilibrium unfolding of procaspase-3(C163S). We examined the equilibrium unfolding of procaspase-3(C163S) in phosphate buffer as a function of urea concentration (0 to 8 M), and the results are shown in Figure 15. In these experiments, we monitored changes in secondary structure by circular dichroism at 228 nm and changes in tertiary structure by fluorescence emission at 320 nm, following excitation at 280 nm or 295 nm.

The data show little to no change in signal between 0 and ~1.5 M urea, and this is followed by a cooperative decrease in signal from ~1.5 M urea to ~3 M urea. A second cooperative transition occurs between ~5 M and 7 M urea. While all three spectroscopic signals showed similar trends in the unfolding data, the relative signal in the plateau region (3-5 M urea) was significantly higher when the samples were excited at 295 nm

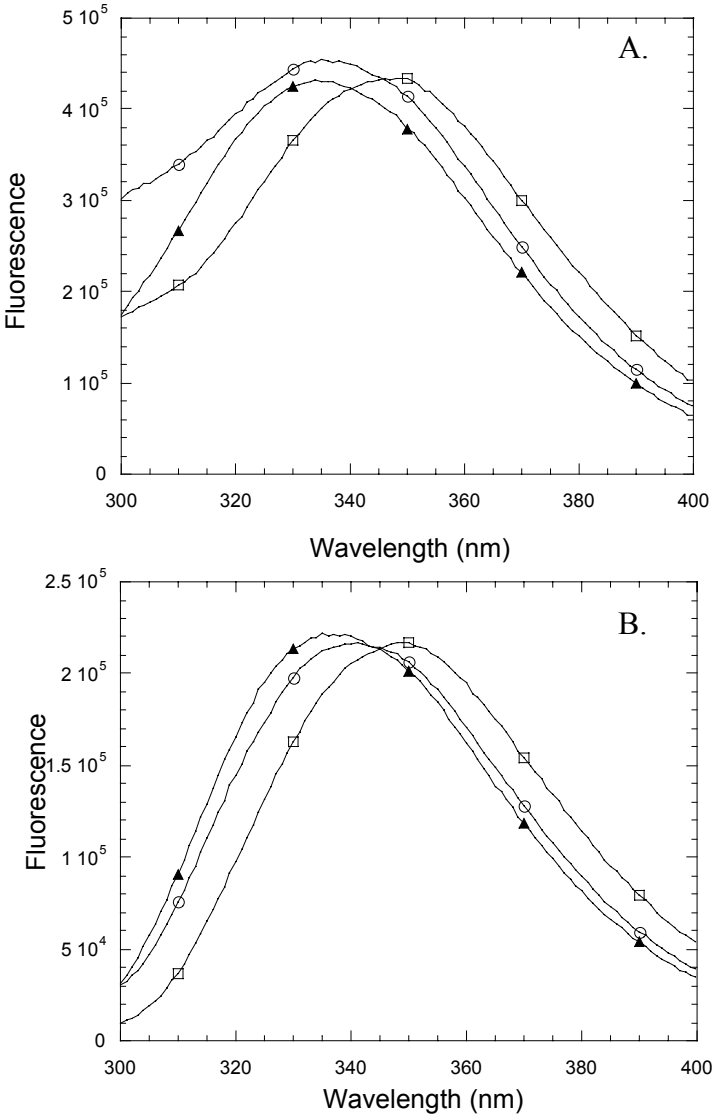

Figure 14. Fluorescence emission spectra of procaspase-3(C163S). *Panel* A, excitation at 280 nm. *Panel* B, excitation at 295 nm. Procaspase-3(C163S) (2 μM), was incubated for 24 hours, 25 °C in urea-containing phosphate buffer with the following urea concentrations: 0 M (○), 4 M (▲), 8 M (□).

(Figure 15, squares) compared to either the CD **(**diamonds**)** or fluorescence emission with excitation at 280 nm (circles). The error bars in Figure 15 represent the standard error obtained from four different experiments at 1 μM concentration of procaspase-3(C163S) performed on separate days, demonstrating the reproducibility of the experiments.

In order to examine reversibility, the protein was initially unfolded in phosphate buffer containing either 6 M or 8 M urea, and the samples were diluted into phosphate buffer so that the final protein concentration was 1 μM, and the final urea concentrations are shown in Figure 15 (solid circles). The data demonstrate the folding transitions are completely reversible.

Overall, the data shown in Figure 15 demonstrate at a minimum a three-state unfolding process in which a well populated folding intermediate is in equilibrium with the native and unfolded protein.

Protein concentration dependence on unfolding. Because procaspase-3 is a homodimer [22], we examined the effect of protein concentration on the equilibrium unfolding process. As shown in Figure 16, panels A-C, there was a shift in the midpoint of the second transition as the concentration of procaspase-3(C163S) was increased. Circular dichroism measurements at 228 nm (Figure 16, panel C) showed that the first transition was independent of the protein concentration.

The unusual feature of these data is that the relative amplitude of the plateau was dependent on the protein concentration. For example, as shown in Figure 16, panel A, the relative amplitude of the plateau decreased with a decrease in protein concentration, while the mid-point of the first transition was constant at ~2.4 M urea.

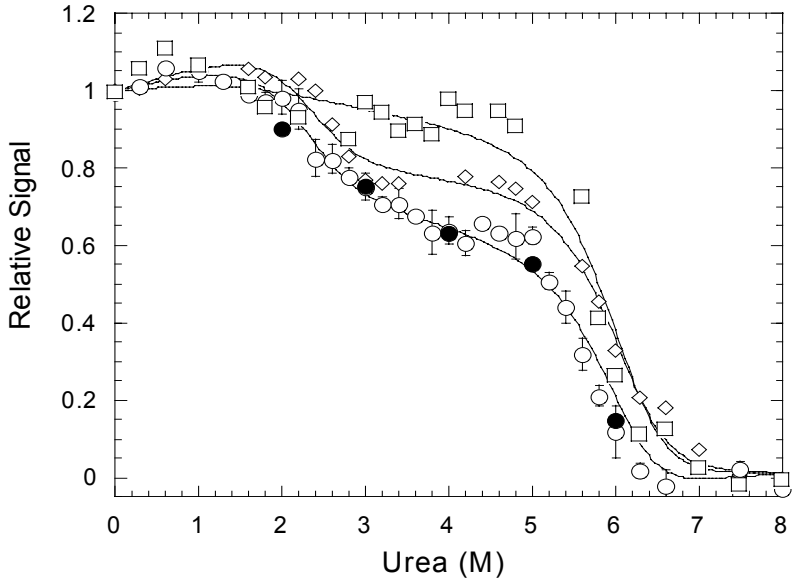

Figure 15. Equilibrium unfolding of procaspase-3(C163S). Unfolding was measured by CD at 228 nm (◇) and by fluorescence emission at 320 nm with excitation at either 280 nm (○) or at 295 nm (□). For all experiments the protein concentration was 1 μM. *Closed symbols* (●) represent refolded protein to show reversibility. *Error bars* show the standard error from four unfolding curves. For clarity, error bars and refolding data are not shown for all three data sets. The data were fit simultaneously (*solid lines*) as described under Materials and Methods using Igor Pro.

The results shown in Figure 16 suggest the four-state equilibrium model described in equation 1 in Materials and Methods. In this model, the dimeric native conformation, N_2, isomerizes to a dimeric intermediate, I_2, and the dimeric intermediate dissociates to a monomeric intermediate, I, which unfolds to U. The dissociation of I_2 to 2I leads to a change in the amplitude of the plateau.

Based on this model, we have determined the conformational free energy, ΔG^{H_2O}, and the cooperativity indices, or *m*-values, for each step in unfolding (see Materials and Methods). The solid lines in Figure 15 and Figure 16 are the results of fits of the model in equation 1 to the data. These results demonstrate that the data are well described by the four-state equilibrium model.

The free energy changes $\Delta G_1^{H_2O}$, $\Delta G_2^{H_2O}$, $\Delta G_3^{H_2O}$ and cooperativity indices m_1, m_2 and m_3, are shown in Table II. Overall, the data demonstrate that procaspase-3(C163S) is very stable, with total conformational free energy of 25.8 kcal/mol.

The plateau observed between 3 M and 5 M urea (Figure 16) is due to the dissociation of the dimeric intermediate, I_2, to the stable monomeric intermediate, I. As shown in Figure 16, this plateau is relatively flat. The fits of the data show that this is due to two factors. First, the cooperativity index, m_2, for this process is relatively small, 0.5 kcal/mol/M. Using equations 16 and 18 and the values determined for $\Delta G_2^{H_2O}$ and m_2, we calculate the equilibrium constant, K_2, at 4 M urea to be ~0.6 μM. This is consistent with the data shown in Figure 16, which demonstrate that dissociation occurs in the low micromolar range of protein concentration in the range of 3-5 M urea. Second, as described in Materials and Methods, the relative signals of I_2 and of I do not depend on the protein concentration, with I_2 having a larger relative signal than I. As the population

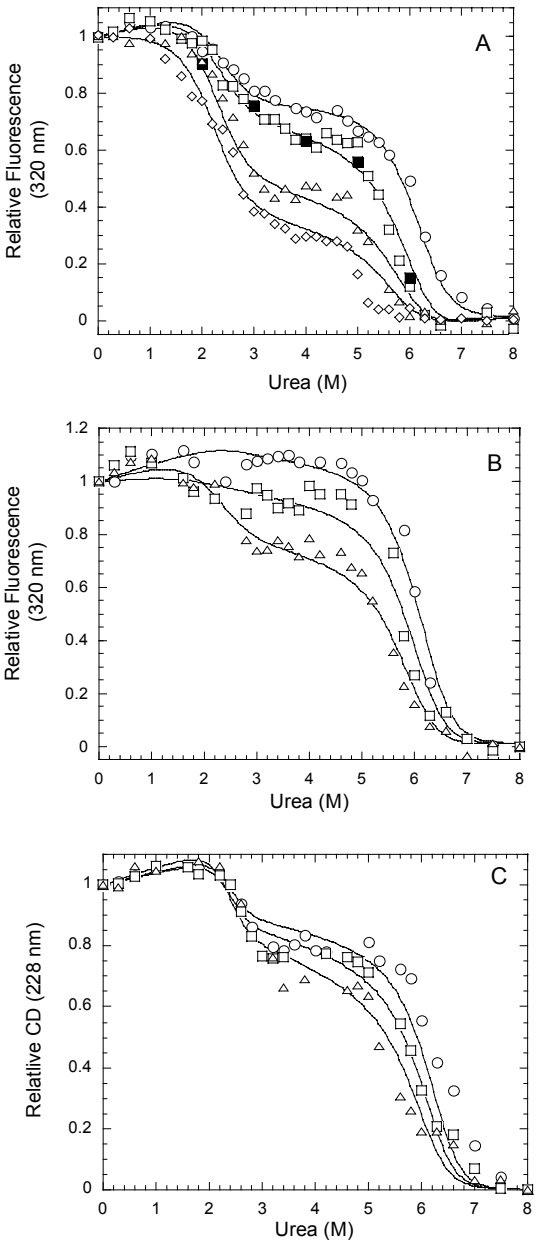

Figure 16. Concentration dependence of equilibrium unfolding of procaspase-3(C163S). For *panels* A and B, unfolding was monitored by fluorescence emission at 320 nm with excitation at 280 nm (*panel* A), or 295 nm (*panel* B), at protein concentrations of 0.25 μM (◇), 0.5 μM (△), 1 μM (□), 2 μM (○). *Closed symbols* (■) represent refolding of procaspase-3 (C163S) at 1 μM concentration. For *panel* C, unfolding was monitored by CD at 228 nm at protein concentrations of 0.5 μM (△), 1 μM (□), 2 μM (○). The data were fit simultaneously (*solid lines*) as described under Materials and Methods using Igor Pro.

of the monomeric intermediate is increased, due to dissociation of the dimeric intermediate at lower protein concentrations, the amplitude of the plateau is decreased.

By using the values from the experimental data for $\Delta G_1^{H_2O}$ (8.3 ± 1.3 kcal/mol), $\Delta G_2^{H_2O}$ (10.5 ± 1.0 kcal/mol), $\Delta G_3^{H_2O}$ (7.0 ± 0.5 kcal/mol), m_1 (2.8 ± 0.5 kcal/mol/M), m_2 (0.5 ± 0.1 kcal/mol/M) and m_3 (1.2 ± 0.1 kcal/mol/M), we calculated the equilibrium distribution of the four species, N_2, I_2, I and U, at each urea concentration. The results of these calculations are illustrated in Figure 17. In addition, the calculations were done at four protein concentrations (0.25 μM, 0.5 μM, 1 μM, and 2 μM). As shown in Figure 17, between 0 M and 3.5 M urea, there is a decrease in the population of native dimer and a concomitant increase in the population of the dimeric intermediate, I_2, as well as the monomeric intermediate, I. The mid-point of the transition is 2.4 M urea, consistent with the experimental results shown in Figure 16. Between 2 M and 7 M urea, there is a population of I_2 as well as a population of the monomeric intermediate, I. The relative populations of the dimeric and monomeric species are dependent on the protein concentration. The population of I_2 reaches a maximum at ~3.4 M urea, whereas the population of I reaches a maximum at ~5.5 M urea. The third transition, I to U, has a mid-point at ~6.1 M urea, although there remains a significant population of I_2 and I until ~6.8 M urea. This distribution of species explains both the change in amplitude between 3 M and 5 M urea as well as the protein concentration dependence between 5 M and 7 M urea (Figure 16).

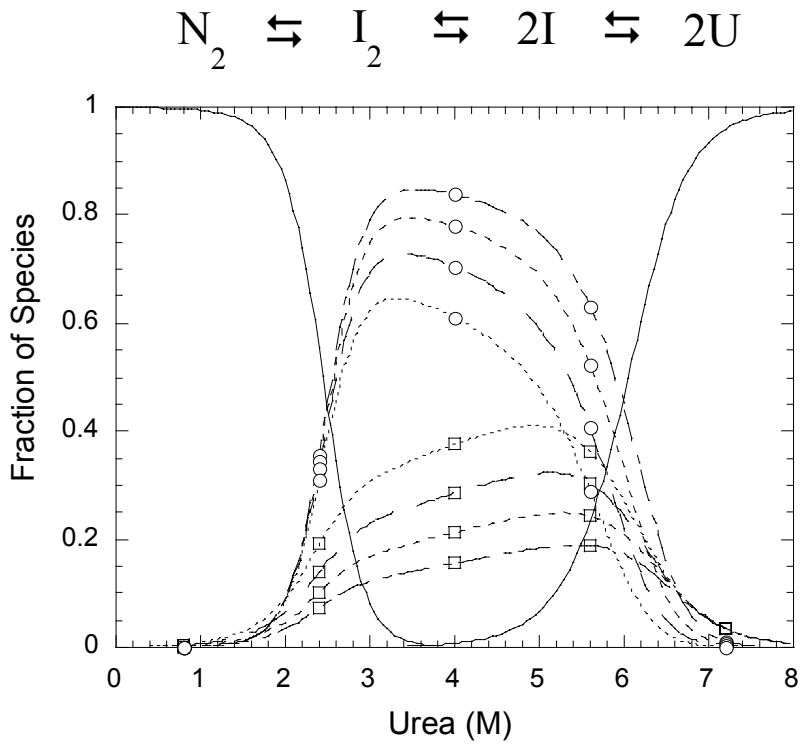

Figure 17. Fraction of species as a function of urea concentration. The fractions of native, dimeric intermediate, monomeric intermediate and the unfolded protein were calculated as a function of urea concentration. The protein concentrations were 0.25 μM (·····), 0.5 μM (— —), 1 μM (- - - -) and 2 μM (- —). 'N_2' refers to the native procaspase-3(C163S), 'I_2' and 'I' are the dimeric and monomeric intermediates respectively, and 'U' refers to the unfolded species. (○) fraction of I_2; (□) fraction of I.

Equilibrium unfolding of procaspase-3(C163S) at different pH. In order to look into the stability of the procaspase-3(C163S) versus pH as well as pH effects on procaspase conformational changes, we extended our equilibrium unfolding studies at different pH (from 8.5 and 4). 30 mM Tris-HCl was used as a buffer for experiments between pH 8.5 and 6.5 and 30 mM citrate buffer for experiments between pH 6 and 4. These, along with other studies were done to correlate physical properties to the functional changes in procaspase maturation and apoptosis.

Equilibrium unfolding of procaspase-3(C163S). We examined the equilibrium unfolding of procaspase-3(C163S) as a function of urea concentration (0-8 M) between pH 8.5 and 4. Sample preparation was done as described earlier. Average emission wavelength (AEW) calculation was done for data analysis (equation 22). This method of analysis is better than averaging the fluorescence emission at a particular wavelength as done previously, since it minimizes the noise and produces cleaner graphs. Representative data at pH 7.2 for 1 μM procaspase concentration is shown in Figure 18**.** The data for fluorescence emission for excitation at 280 nm, 295 nm and CD at 228 nm are shown in this figure to look into both tertiary and secondary structures respectively. Experiments using these different probes show similar unfolding pattern with a region of no signal change between 0 and 1.5 M urea, followed by a cooperative decrease in signal between 1.5 and 3 M urea. This is seen prominently in the CD data and matches very well with the previous unfolding data. The shoulder region is between 3 and 5 M urea and the second transition occurs between 5 and 7 M urea. The signal for the fluorescence study with excitation at 295 nm gives the highest signal as seen earlier. The unfolding pathway is reversible for all pH. The difference in the unfolding pattern between the

previous and this fluorescence data is due to the difference in the method of analysis although the interpretation, that it suggests at least a three–state unfolding process, is the same. Interestingly, the values of free energies as well as cooperativity indices for data at pH 7.2 derived by these two methods are comparable (Table II) suggesting reproducibility of the results.

***Equilibrium unfolding at pH 8.5*.** The unfolding data monitored by fluorescence (excitations 280 nm and 295 nm) and CD at 228 nm are shown in Figure 19. Overall, the data for three different probes show similar unfolding pattern with no change in signal between 0 to ~1.5 M urea, followed by a cooperative decrease in signal from 1.5 M to 3 M urea (increase in signal for excitation at 295 nm) and a shoulder region between 3 and 5 M urea. There is a second transition between 5 and 7 M urea. This is very well observed in the CD data. The protein shows concentration dependence and the amplitude of the shoulder region decreases as well as the mid-point of the second transition changes with decrease in protein concentration, suggesting a four-state unfolding model as described earlier. The protein is completely reversible at this pH and the refolding data are shown as solid triangles (▲) in the figure.

From the values of free energies (ΔG^{H_2O}) and cooperativity indices (*m*) obtained from the fits we calculated fraction of species at each urea concentration. The fractions were obtained at each of the four protein concentrations (0.25 μM, 0.5 μM, 1 μM and 2 μM). This is shown in Figure 19 panel D. There is a decrease in native protein between 0 and 3.7 M urea. At the same time an increase in the dimeric (I_2) as well as the monomeric intermediate (I) is seen. The midpoint of the first transition is ~2.3 M urea and this is consistent with the unfolding data as shown in Figure 19 A, B and C. We see a

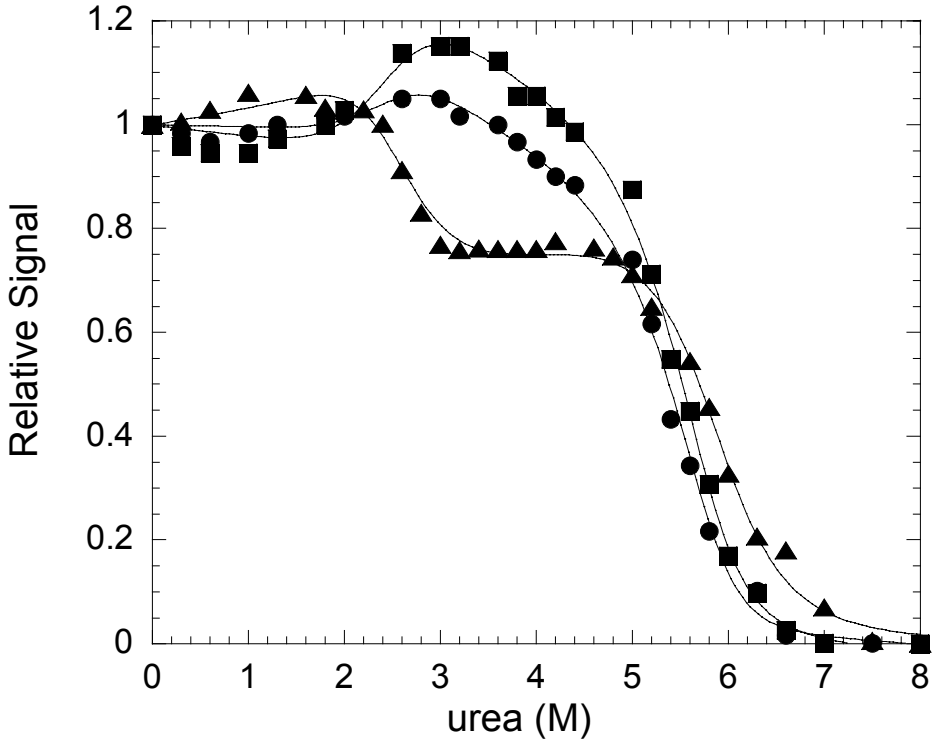

Figure 18. Equilibrium unfolding of procaspase-3(C163S) at pH 7.2. Unfolding was measured by CD at 228 nm (▲) and by fluorescence average emission wavelength with excitation at either 280 nm (●) or at 295 nm (■). For all experiments the protein concentration was 1 μM. The data were fit simultaneously (*solid lines*) as described under Materials and Methods using Igor Pro.

Table II. Comparison of the values of free energies and cooperative indices at pH 7.2 obtained from data analysis by fluorescence emission at 320 nm (method 1) and the other by calculating the average emission wavelength (AEW) (method 2). The CD is obtained at 228 nm for these two methods.

pH 7.2	$\Delta G_1^{H_2O}$ *kcal/mol*	$\Delta G_2^{H_2O}$ *kcal/mol*	$\Delta G_3^{H_2O}$ *kcal/mol*	$\Delta G_{tot}^{H_2O}$ *kcal/mol*	m_1 *kcal/mol /M*	m_2 *kcal/mol /M*	m_3 *kcal/mol /M*	m_{tot} *kcal/mol /M*
Method 1	8.3 ± 1.3	10.5 ± 1.0	7.0 ± 0.5	25.8 ± 0.0	2.8 ± 0.5	0.5 ± 0.1	1.2 ± 0.1	4.5 ± 0.0
Method 2	7.4 ± 0.1	12.6 ± 1.1	6.1 ± 0.9	26.1 ± 2.1	2.8 ± 0.0	0.6 ± 0.1	1.2 ± 0.15	4.6 ± 0.25

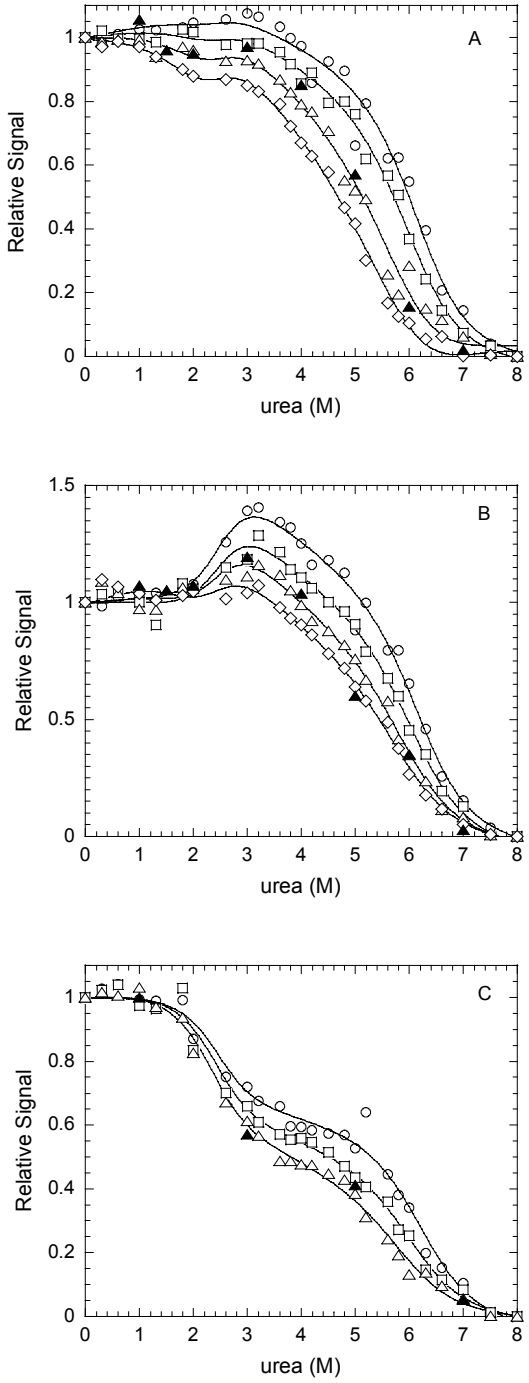

Figure 19. Equilibrium unfolding of procaspase-3(C163S) at different concentrations at pH 8.5. For *panels* A and B, unfolding was monitored by fluorescence with excitations at 280 nm (*panel* A) and 295 nm (*panel* B). *Panel* C represents CD data at 228 nm. The protein concentrations are as follows: 0.25 μM (◇), 0.5 μM (Δ), 1 μM (□) and 2 μM (○). (▲) represents refolding data at 0.5 μM protein concentration. The solid lines represent fits to the data as described under Materials and Methods.

population of I_2 as well as I between pH 2 and 7. The relative populations of the dimeric and the monomeric intermediate species are dependent on protein concentrations. The population of I_2 reaches a maximum at ~3.2 M urea, whereas the population of I reaches a maximum at ~5.1 M urea. The transition of I to the unfolded species (U) has a mid-point at ~6.2 M urea. There is still presence of I_2 and I till 6.4 M urea. The monomeric intermediate species I is still present at 8 M urea along with the unfolded species U. This figure explains both the concentration dependence and decrease in amplitude at the shoulder region between 3 and 5 M urea.

***Equilibrium unfolding at pH 8*.** The unfolding data are shown in Figure 20. Overall, the data for three different probes show similar unfolding pattern with no change in signal between 0 to ~1M urea, followed by a cooperative decrease in signal from 1M to 2.5 M urea (increase in signal for excitation at 295 nm) and a shoulder region between 2.5 and 4.5 M urea. There is a second transition between 4.5 and 7 M urea. This is very well observed in the CD data. The protein shows concentration dependence and the amplitude of the shoulder region decreases as well as the mid-point of the second transition changes with decrease in protein concentration, suggesting a four-state unfolding model as described earlier. The protein is completely reversible at this pH and the refolding data are shown as solid triangles (▲) in the figure.

The fractions of species at each urea concentration were obtained at each of the four protein concentrations (0.25 μM, 0.5 μM, 1 μM and 2 μM). This is shown in Figure 20, panel D. There is a decrease in native protein between 0 and 3.3 M urea. At the same time an increase in the dimeric (I_2) as well as the monomeric intermediate (I) is seen. The

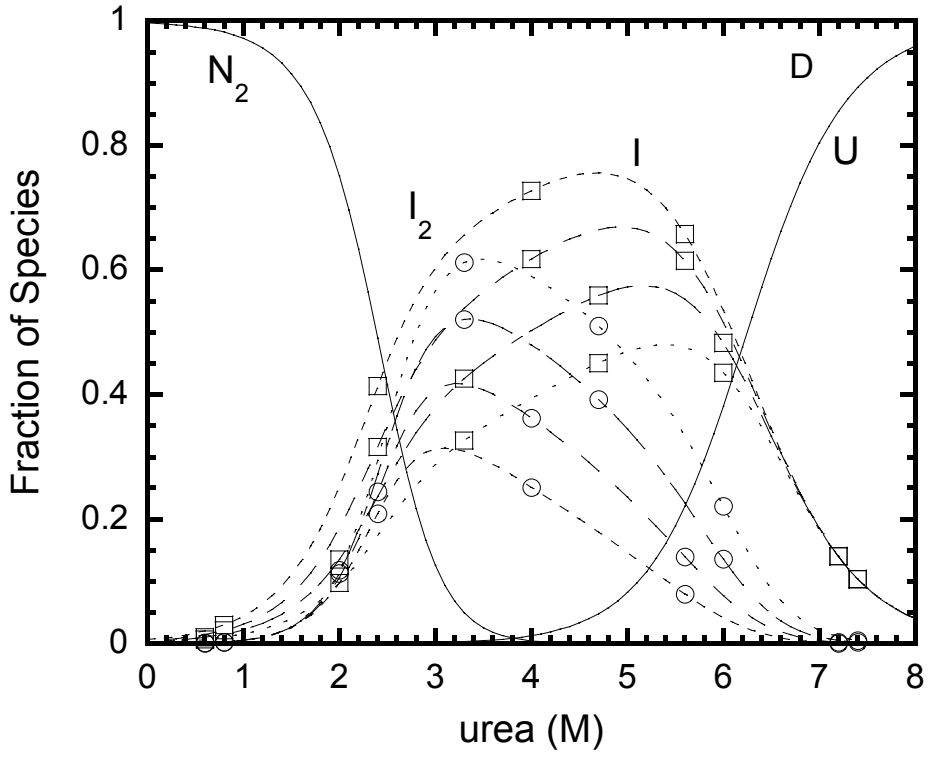

Figure 19. *Panel* D. Fraction of species as a function of urea concentration at pH 8.5. The fractions of native, dimeric intermediate, monomeric intermediate and the unfolded protein were calculated as a function of urea concentration. The protein concentrations were 0.25 μM (------), 0.5 μM (— —), 1 μM (- —) and 2 μM (·····). 'N_2' refers to the native procaspase-3(C163S), 'I_2' and 'I' are the dimeric and monomeric intermediates respectively, and 'U' refers to the unfolded species. (○) fraction of I_2; (□) fraction of I.

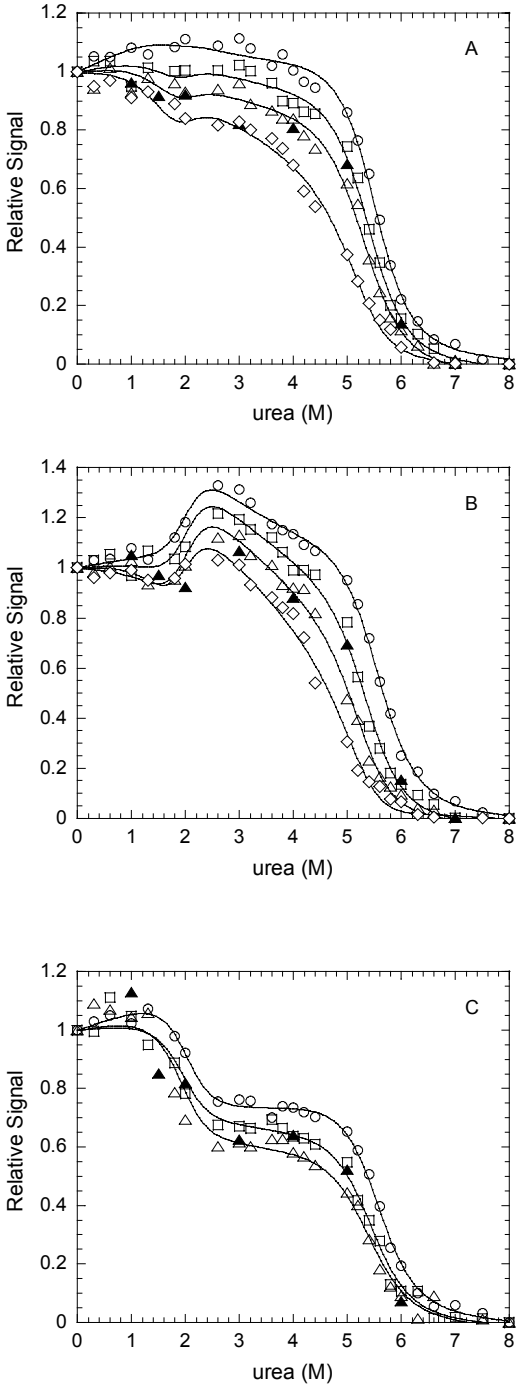

Figure 20. Equilibrium unfolding of procaspase-3(C163S) at different concentrations at pH 8. For *panels* A and B, unfolding was monitored by fluorescence with excitations at 280 nm (*panel* A) and 295 nm *(panel* B). *Panel* C represents CD data at 228 nm. The protein concentrations are as follows: 0.25 μM (◇), 0.5 μM (Δ), 1 μM (□) and 2 μM (○). (▲) represents refolding data at 0.5 μM protein concentration. The solid lines represent fits to the data as described under

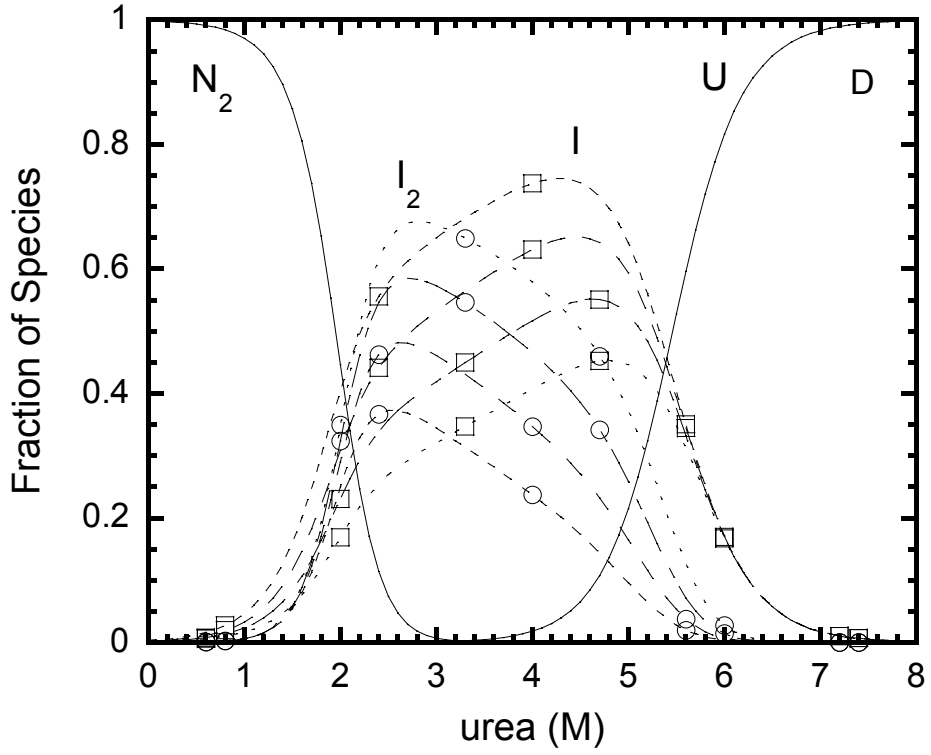

Figure 20. *Panel* D. Fraction of species as a function of urea concentration at pH 8. The fractions of native, dimeric intermediate, monomeric intermediate and the unfolded protein were calculated as a function of urea concentration. The protein concentrations were 0.25 μM (------), 0.5 μM (— —), 1 μM (- —) and 2 μM (·····). 'N_2' refers to the native procaspase-3(C163S), 'I_2' and 'I' are the dimeric and monomeric intermediates respectively, and 'U' refers to the unfolded species. (○) fraction of I_2; (□) fraction of I.

midpoint of the transition is ~1.9 M urea and this is consistent with the unfolding data as shown in Figure 20A, B and C. We see a population of I_2 as well as I between pH 2 and 7. The relative populations of the dimeric and the monomeric intermediate species are dependent on protein concentrations. The population of I_2 reaches a maximum at ~2.7 M urea, whereas the population of I reaches a maximum at ~4.5 M urea. The transition of I to the unfolded species (U) has a mid-point at ~5.5 M urea. There is still presence of I_2 and I till ~5.8 M urea. This figure explains both the concentration dependence and decrease in amplitude at the shoulder region.

***Equilibrium unfolding at pH 7.6*.** The unfolding data are shown in Figure 21**.** The data for three different probes (fluorescence excitations 280 nm, 295 nm and CD at 228 nm) show similar unfolding pattern with no change in signal between 0 to ~1.5M urea, followed by a cooperative decrease in signal from 1.5 M to 3 M urea (increase in signal for excitation at 295 nm) and a shoulder region between 3 and 5 M urea. There is a second transition between 5 and 7 M urea. This is very well observed in the CD data. The protein shows concentration dependence and the amplitude of the shoulder region decreases as well as the mid-point of the second transition changes with decrease in protein concentration, suggesting a four-state unfolding model as described earlier. The protein is completely reversible at this pH and the refolding data is shown as solid triangles (▲) in the figure.

The fractions of species at each urea concentration were obtained at each of the four protein concentrations (0.25 μM, 0.5 μM, 1 μM and 2 μM). This is shown in Figure 21, panel D. There is a decrease in native protein between 0 and 3.8 M urea. At the same time an increase in the dimeric (I_2) as well as the monomeric intermediate (I) is seen. The

midpoint of the transition is ~2.6 M urea and this is consistent with the unfolding data as shown in Figure 21A, B and C. We see a population of I_2 as well as I between pH 2 and 7. The relative populations of the dimeric and the monomeric intermediate species are dependent on protein concentrations. The population of I_2 reaches a maximum at ~3.4 M urea, whereas the population of I reaches a maximum at ~4.9 M urea. The transition of I to the unfolded species (U) has a mid-point at ~6 M urea. There is still presence of I_2 and I till ~6.1 M urea. This figure explains both the concentration dependence and decrease in amplitude at the shoulder region.

***Equilibrium unfolding at pH 7.2*.** The unfolding data are shown in Figure 22. The data for three different probes (fluorescence excitations 280 nm, 295 nm and CD at 228 nm) show similar unfolding pattern with no change in signal between 0 to ~1.5 M urea, followed by a cooperative decrease in signal from 1.5 M to 3 M urea (increase in signal for excitation at 295 nm) and a shoulder region between 3 and 5 M urea. There is a second transition between 5 and 7 M urea. This is very well observed in the CD data. The protein shows concentration dependence and the amplitude of the shoulder region decreases as well as the mid-point of the second transition changes with decrease in protein concentration, suggesting a four-state unfolding model as described earlier. The protein is completely reversible at this pH and the refolding data are shown as solid triangles (▲) in the figure.

The fractions of species at each urea concentration were obtained at each of the four protein concentrations (0.25 μM, 0.5 μM, 1 μM and 2 μM). This is shown in Figure 22

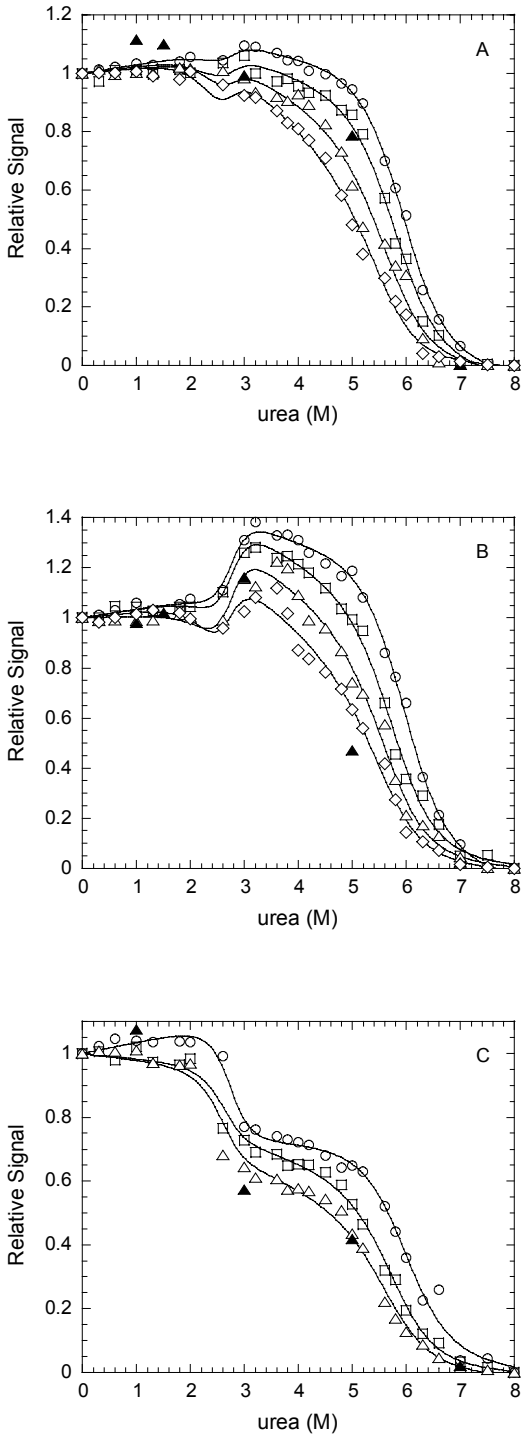

Figure 21. Equilibrium unfolding of procaspase-3(C163S) at different concentrations at pH 7.6. For *panels* A and B, unfolding was monitored by fluorescence with excitations at 280 nm (*panel* A) and 295 nm (*panel* B). *Panel* C represents CD data at 228 nm. The protein concentrations are as follows: 0.25 μM (◇), 0.5 μM (Δ), 1 μM (□) and 2 μM (○). (▲) represents refolding data at 0.5 μM protein concentration. The solid lines represent fits to the data as described under Materials and Methods.

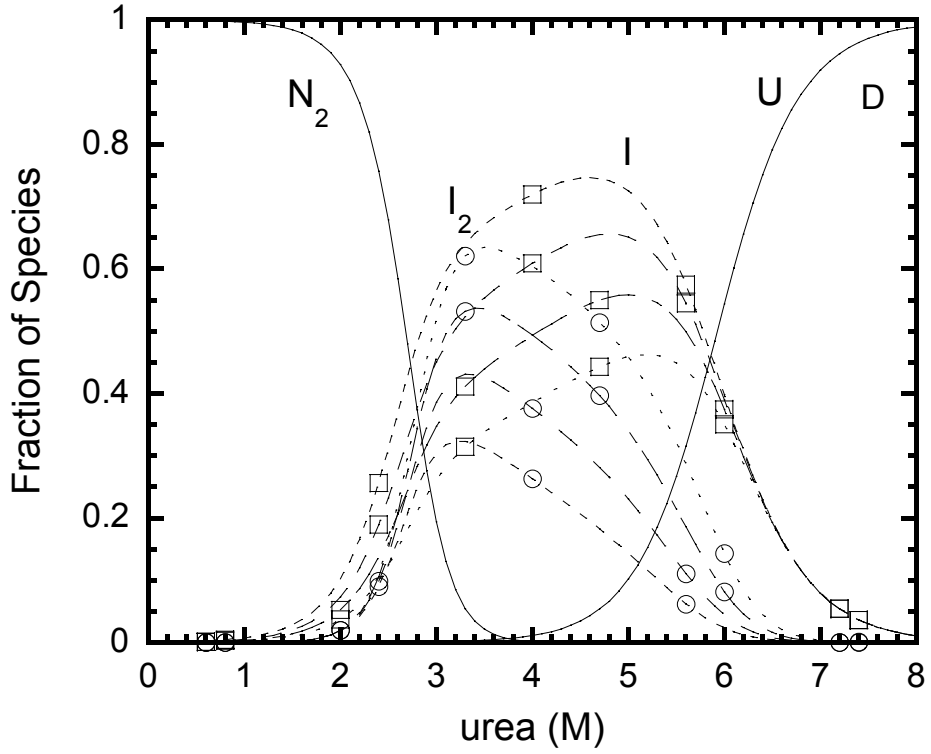

Figure 21. *Panel* D. Fraction of species as a function of urea concentration at pH 7.6. The fractions of native, dimeric intermediate, monomeric intermediate and the unfolded protein were calculated as a function of urea concentration. The protein concentrations were 0.25 μM (------), 0.5 μM (— —), 1 μM (- —) and 2 μM (·····). 'N_2' refers to the native procaspase-3(C163S), 'I_2' and 'I' are the dimeric and monomeric intermediates respectively, and 'U' refers to the unfolded species. (○) fraction of I_2; (□) fraction of I.

D. There is a decrease in native protein between 0 and 3.8 M urea. At the same time an increase in the dimeric (I_2) as well as the monomeric intermediate (I) is seen. The midpoint of the transition is ~2.6 M urea and this is consistent with the unfolding data as shown in Figure 22 A, B and C. We see a population of I_2 as well as I between pH 2 and 7. The relative populations of the dimeric and the monomeric intermediate species are dependent on protein concentrations. The population of I_2 reaches a maximum at ~3.3 M urea, whereas the population of I reaches a maximum at ~5.1 M urea. The transition of I to the unfolded species U has a mid-point at ~5.6 M urea. There is still presence of I_2 and I till ~6.3 M urea. This figure explains both the concentration dependence and decrease in amplitude at the shoulder region. There is a significant difference between the fraction of intermediate species at pH 7.2 compared to those at higher pH described above. Here, at pH 7.2, a significant fraction of I_2 (0.9) is seen compared to I (0.3), whereas, in pH 8.5, 8 and 7.6, the fractions are comparable, suggesting the dimeric intermediate state is more stable at pH 7.2.

***Equilibrium unfolding at pH 6.5*.** The unfolding data are shown in Figure 23. The data for three different probes (fluorescence excitations 280 nm, 295 nm and CD at 228 nm) show similar unfolding pattern with no change in signal between 0 to ~1.5M urea, followed by a cooperative decrease in signal from 1.5 M to 2.5 M urea (increase in fluorescence signal for excitations at 280 and 295 nm) and a shoulder region between 2.5 and 4.5 M urea. There is a second transition between 4.5 and 7 M urea. This is very well observed in the CD data. The protein shows concentration dependence and the amplitude of the shoulder region decreases as well as the mid-point of the second transition changes

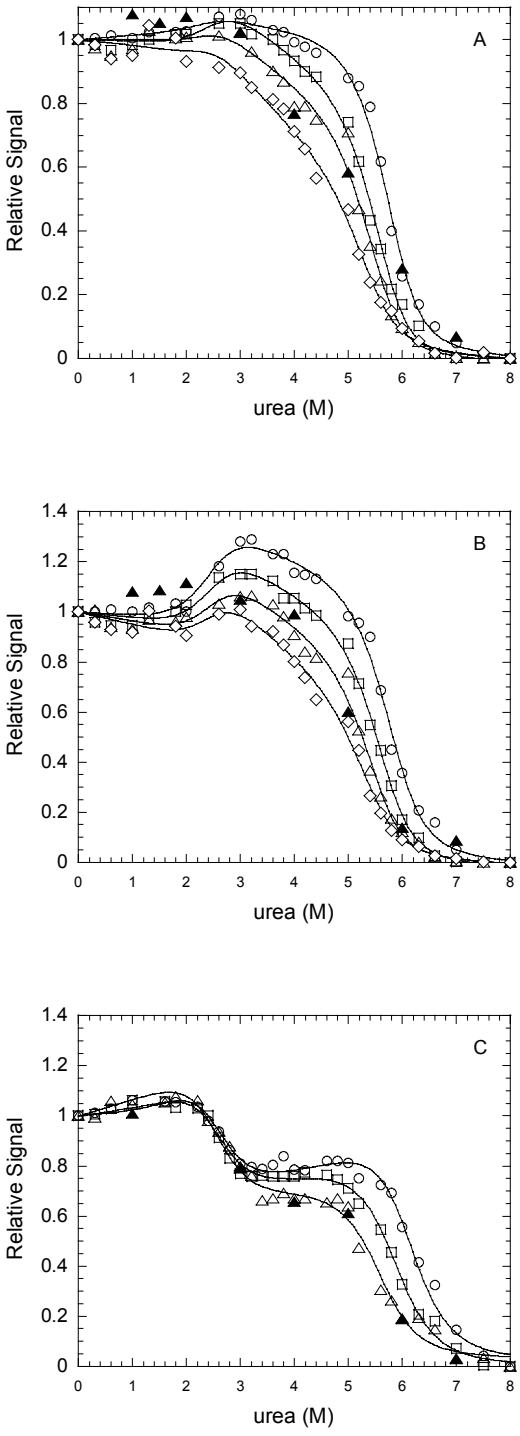

Figure 22. Equilibrium unfolding of procaspase-3(C163S) at different concentrations at pH 7.2. For *panels* A and B, unfolding was monitored by fluorescence with excitations at 280 nm (*panel* A) and 295 nm (*panel* B). *Panel* C represents CD data at 228 nm. The protein concentrations are as follows: 0.25 μM (◇), 0.5 μM (Δ), 1 μM (□) and 2 μM (○). (▲) represents refolding data at 0.5 μM protein concentration. The solid lines represent fits to the data as described under Materials and Methods.

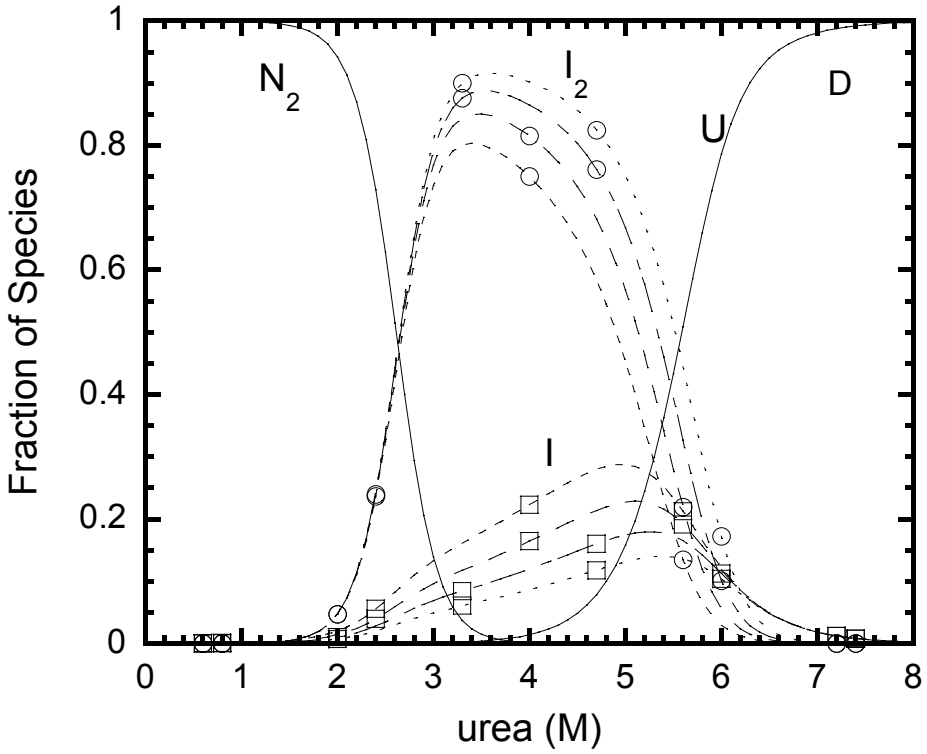

Figure 22. *Panel* D. Fraction of species as a function of urea concentration at pH 7.2. The fractions of native, dimeric intermediate, monomeric intermediate and the unfolded protein were calculated as a function of urea concentration. The protein concentrations were 0.25 μM (------), 0.5 μM (— —), 1 μM (- —) and 2 μM (·····). 'N_2' refers to the native procaspase-3(C163S), 'I_2' and 'I' are the dimeric and monomeric intermediates respectively, and 'U' refers to the unfolded species. (○) fraction of I_2; (□) fraction of I.

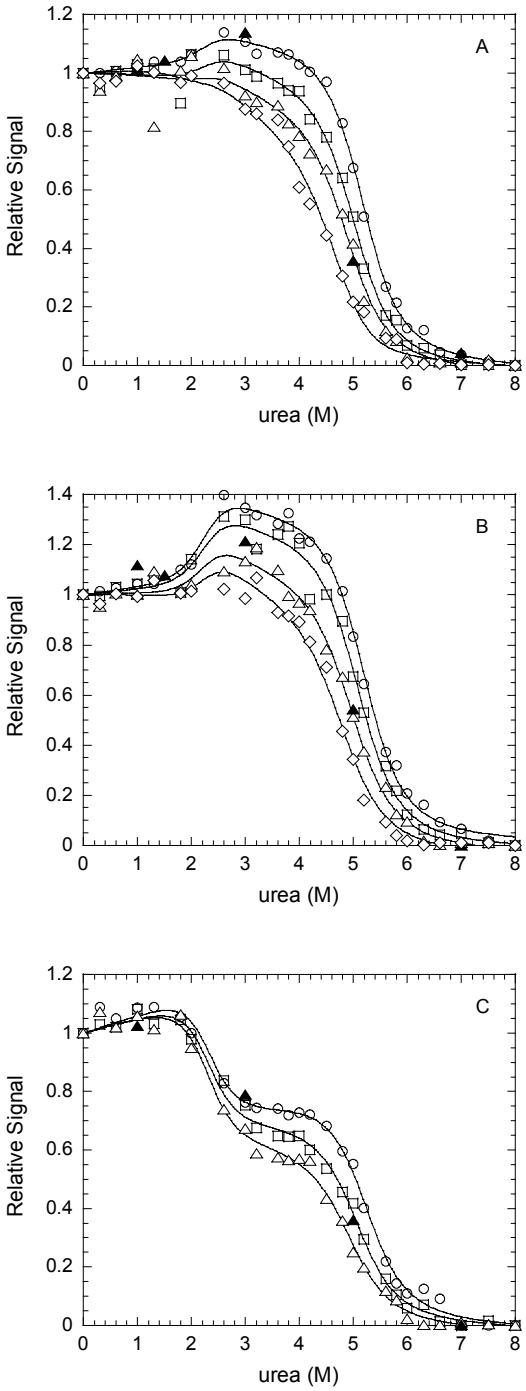

Figure 23. Equilibrium unfolding of procaspase-3(C163S) at different concentrations at pH 6.5. For *panels* A and B, unfolding was monitored by fluorescence with excitations at 280 nm (*panel* A) and 295 nm (*panel* B). *Panel* C represents CD data at 228 nm. The protein concentrations are as follows: 0.25 μM (◇), 0.5 μM (Δ), 1 μM (□) and 2 μM (○). (▲) represents refolding data at 0.5 μM protein concentration. The solid lines represent fits to the data as described under Materials and Methods.

with decrease in protein concentration, suggesting a four-state unfolding model as described earlier. The protein is completely reversible at this pH and the refolding data are shown as solid triangles (▲) in the figure.

The fractions of species at each urea concentration were obtained at each of the four protein concentrations (0.25 μM, 0.5 μM, 1 μM and 2 μM). This is shown in Figure 23 D. There is a decrease in native protein between 0 and 3.2 M urea. At the same time an increase in the dimeric (I_2) as well as the monomeric intermediate (I) is seen. The midpoint of the transition is ~2.2 M urea and this is consistent with the unfolding data as shown in Figure 23 A, B and C. We see a population of I_2 as well as I between pH 2 and 7. The relative populations of the dimeric and the monomeric intermediate species are dependent on protein concentrations. The population of I_2 reaches a maximum at ~3 M urea, whereas the population of I reaches a maximum at ~4.3 M urea. The transition of I to the unfolded species U has a mid-point at ~5 M urea. There is still presence of I_2 and I till ~5.5 M urea. This figure explains both the concentration dependence and decrease in amplitude at the shoulder region.

***Equilibrium unfolding at pH 6*.** The unfolding data is shown in Figure 24. The data for three different probes (fluorescence excitations 280 nm, 295 nm and CD at 228 nm) show similar unfolding pattern with no change in signal between 0 to ~1.4 M urea, followed by a cooperative decrease in signal from 1.4 M to 1.9 M urea (increase in fluorescence signal for excitations at 280 and 295 nm), a shoulder region between 1.9 and 4.1 M urea. There is a second transition between 4.1 and 7 M urea. This is very well observed in the CD data. The protein shows concentration dependence and the amplitude

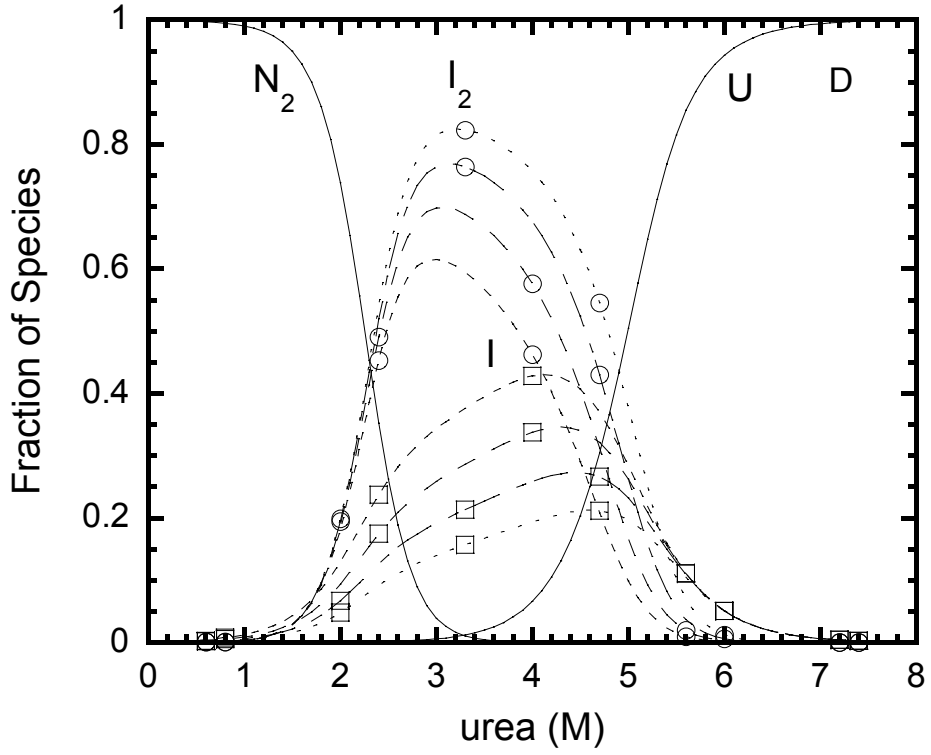

Figure 23. *Panel* D. Fraction of species as a function of urea concentration at pH 6.5. The fractions of native, dimeric intermediate, monomeric intermediate and the unfolded protein were calculated as a function of urea concentration. The protein concentrations were 0.25 μM (------), 0.5 μM (— —), 1 μM (- —) and 2 μM (·····). 'N_2' refers to the native procaspase-3(C163S), 'I_2' and 'I' are the dimeric and monomeric intermediates respectively, and 'U' refers to the unfolded species. (○) fraction of I_2; (□) fraction of I.

of the shoulder region decreases as well as the mid-point of the second transition changes with decrease in protein concentration, suggesting a four-state unfolding model as described earlier.

The fractions of species at each urea concentration were obtained at each of the four protein concentrations (0.25 μM, 0.5 μM, 1 μM and 2 μM). This is shown in Figure 24 D. The protein is completely reversible at this pH and the refolding data are shown as solid triangles (▲) in the figure. There is a decrease in native protein between 0 and 2.9 M urea. At the same time an increase in the dimeric (I_2) as well as the monomeric intermediate (I) is seen. The midpoint of the transition is ~1.8 M urea and this is consistent with the unfolding data as shown in Figure 24 A, B and C. We see a population of I_2 as well as I between pH 2 and 7. The relative populations of the dimeric and the monomeric intermediate species are dependent on protein concentrations. The population of I_2 reaches a maximum at ~2.5 M urea, whereas the population of I reaches a maximum at ~4 M urea. The transition of I to the unfolded species U has a mid-point at ~4.8 M urea. There is still presence of I_2 and I till ~5.3 M urea. This figure explains both the concentration dependence and decrease in amplitude at the shoulder region.

***Equilibrium unfolding at pH 5.5*.** The unfolding data are shown in Figure 25. The data for three different probes (fluorescence excitations 280 nm, 295 nm and CD at 228 nm) show similar unfolding pattern with no change in signal between 0 to ~1 M urea, followed by a cooperative decrease in signal from 1M to 1.9 M urea (increase in fluorescence signal for excitations at 280 and 295 nm), a shoulder region between ~1.9 and ~4.1 M urea. There is a second transition between 4.1 and 7 M urea. This is very well

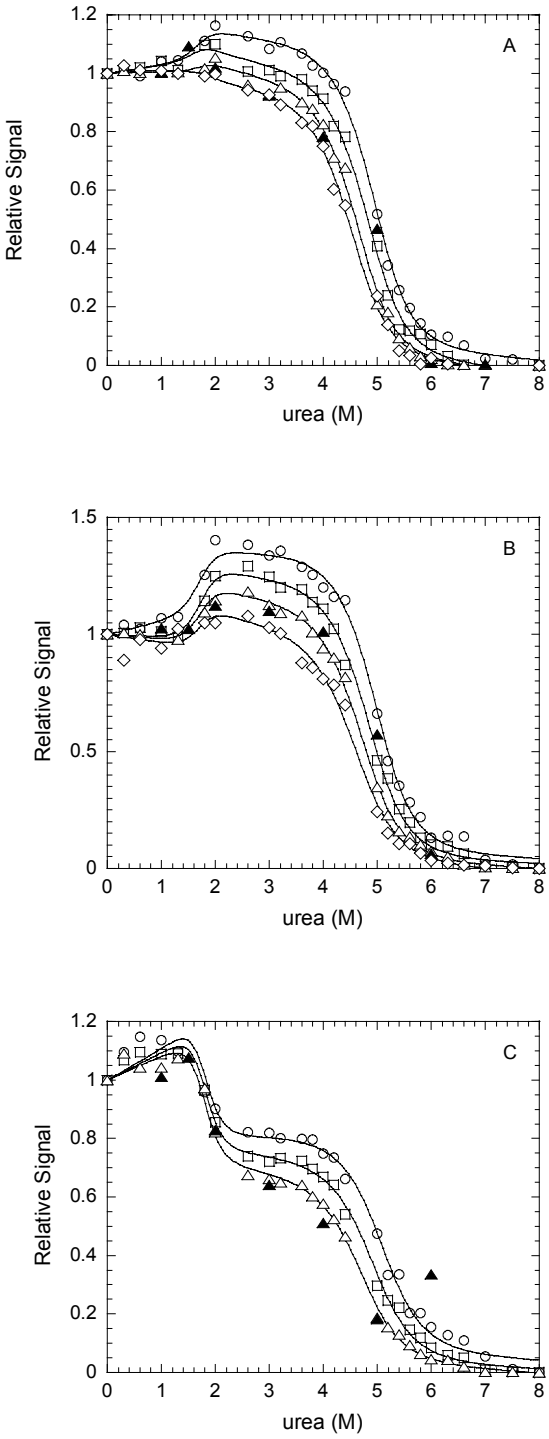

Figure 24. Equilibrium unfolding of procaspase-3(C163S) at different concentrations at pH 6. For *panels* A and B, unfolding was monitored by fluorescence with excitations at 280 nm (*panel* A) and 295 nm (*panel* B). *Panel* C represents CD data at 228 nm. The protein concentrations are as follows: 0.25 μM (◇), 0.5 μM (Δ), 1 μM (□) and 2 μM (○). (▲) represents refolding data at 0.5 μM protein concentration. The solid lines represent fits to the data as described under Materials and Methods.

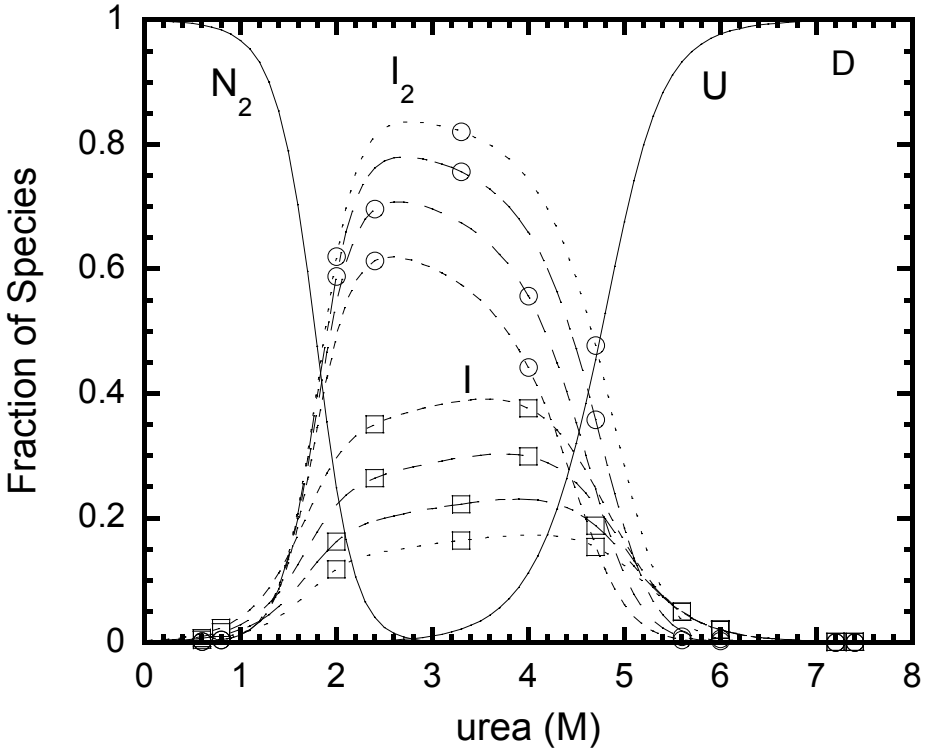

Figure 24. *Panel* D. Fraction of species as a function of urea concentration at pH 6. The fractions of native, dimeric intermediate, monomeric intermediate and the unfolded protein were calculated as a function of urea concentration. The protein concentrations were 0.25 μM (------), 0.5 μM (— —), 1 μM (- —) and 2 μM (·····). 'N_2' refers to the native procaspase-3(C163S), 'I_2' and 'I' are the dimeric and monomeric intermediates respectively, and 'U' refers to the unfolded species. (○) fraction of I_2; (□) fraction of I.

observed in CD data. The protein shows concentration dependence and the amplitude of the shoulder region decreases as well as the mid-point of the second transition changes with decrease in protein concentration, suggesting a four-state unfolding model as described earlier. The protein is completely reversible at this pH and the refolding data are shown as solid triangles (▲) in the figure.

The fractions of species at each urea concentration were obtained at each of the four protein concentrations (0.25 μM, 0.5 μM, 1 μM and 2 μM). This is shown in Figure 25 D. There is a decrease in native protein between 0 and 2 M urea. At the same time an increase in the dimeric (I_2) as well as the monomeric intermediate (I) is seen. The midpoint of the transition is ~1.1 M urea and this is consistent with the unfolding data as shown in Figure 25 A, B and C. We see a population of I_2 as well as I between pH 2 and 7. The relative populations of the dimeric and the monomeric intermediate species are dependent on protein concentrations. The population of I_2 reaches a maximum at ~1.8 M urea, whereas the population of I reaches a maximum at ~4 M urea. The transition of I to the unfolded species U has a mid-point at ~4.3 M urea. There is still presence of I_2 and I till ~5.3 M urea. This figure explains both the concentration dependence and decrease in amplitude at the shoulder region.

***Equilibrium unfolding at pH 5*.** The unfolding data are shown in Figure 26. The data for three different probes (fluorescence excitations 280 nm, 295 nm and CD at 228 nm) show similar unfolding pattern with no change in signal between 0 to ~0.9 M urea,

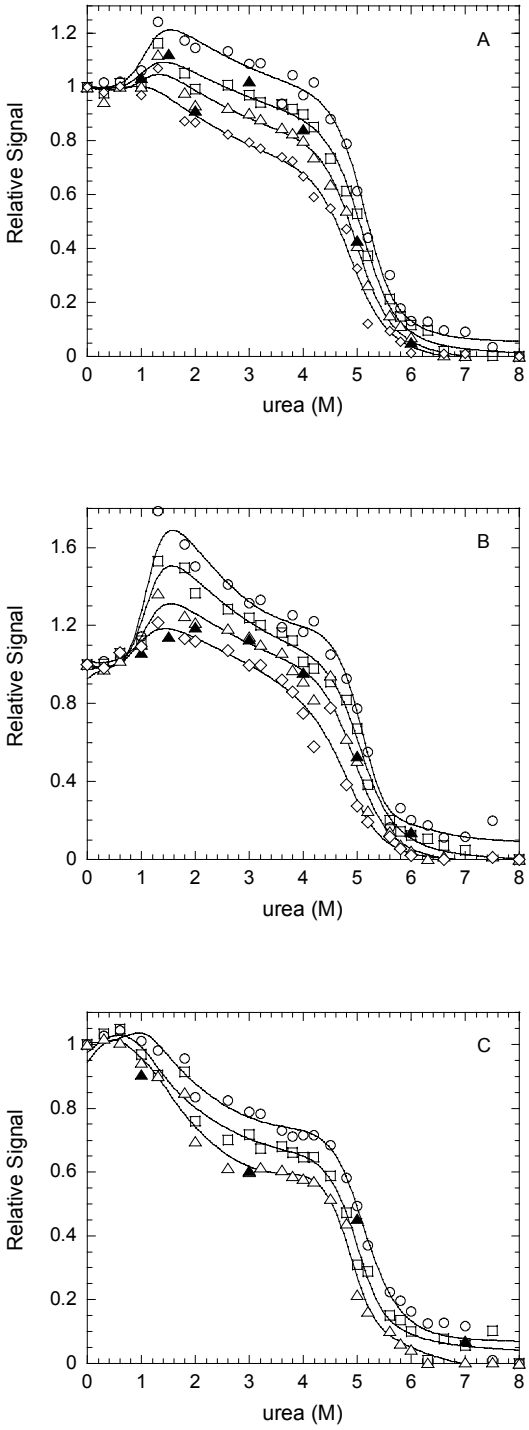

Figure 25. Equilibrium unfolding of procaspase-3(C163S) at different concentrations at pH 5.5. For *panels* A and B, unfolding was monitored by fluorescence with excitations at 280 nm (*panel* A) and 295 nm (*panel* B). *Panel* C represents CD data at 228 nm. The protein concentrations are as follows: 0.25 μM (◇), 0.5 μM (Δ), 1 μM (□) and 2 μM (○). (▲) represents refolding data at 0.5 μM protein concentration. The solid lines represent fits to the data as described under Materials and Methods.

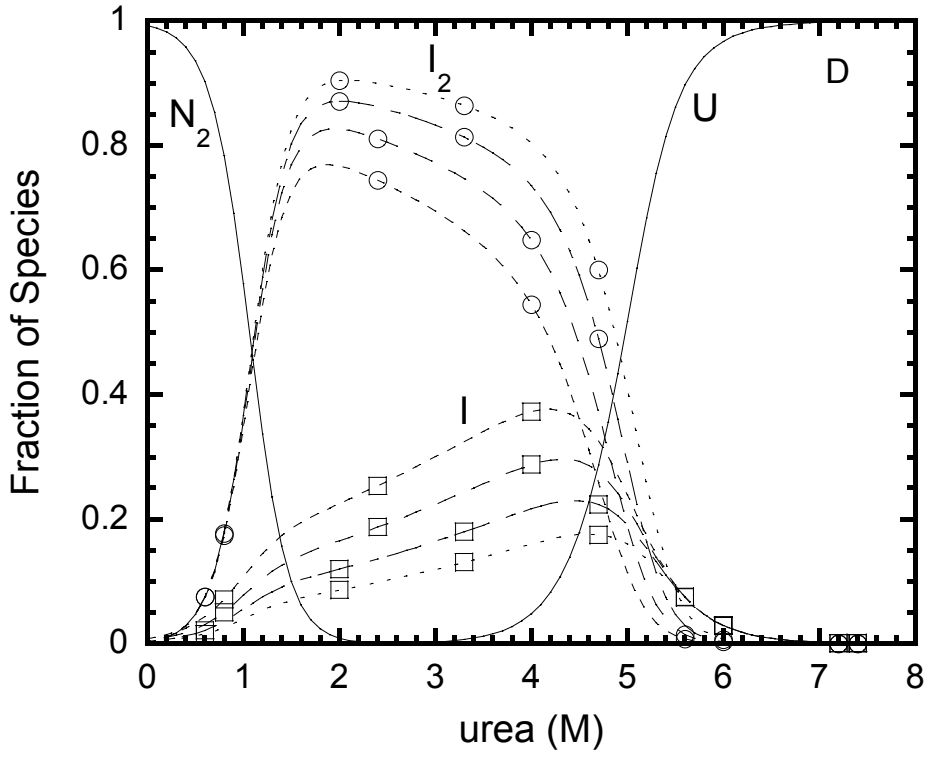

Figure 25. *Panel* D. Fraction of species as a function of urea concentration at pH 5.5. The fractions of native, dimeric intermediate, monomeric intermediate and the unfolded protein were calculated as a function of urea concentration. The protein concentrations were 0.25 μM (------), 0.5 μM (— —), 1 μM (- —) and 2 μM (·····). 'N_2' refers to the native procaspase-3(C163S), 'I_2' and 'I' are the dimeric and monomeric intermediates respectively, and 'U' refers to the unfolded species. (○) fraction of I_2; (□) fraction of I.

followed by a cooperative decrease in signal from 0.9 M to 1.9 M urea (increase in fluorescence signal for excitations at 280 and 295 nm), a shoulder region between ~1.9 and ~3.9 M urea. There is a second transition between 3.9 and 7 M urea. This is very well observed in CD data. The protein shows concentration dependence and the amplitude of the shoulder region decreases as well as the mid-point of the second transition changes with decrease in protein concentration, suggesting a four-state unfolding model as described earlier. The protein is completely reversible at this pH and the refolding data are shown as solid triangles (▲) in the figure.

The fractions of species at each urea concentration were obtained at each of the four protein concentrations (0.25 μM, 0.5 μM, 1 μM and 2 μM). This is shown in Figure 26 D. There is a decrease in native protein between 0 and 2 M urea. At the same time an increase in the dimeric (I_2) as well as the monomeric intermediate (I) is seen. The midpoint of the transition is ~1.2 M urea and this is consistent with the unfolding data as shown in Figure 26 A, B and C. We see a population of I_2 as well as I between pH 2 and 7. The relative populations of the dimeric and the monomeric intermediate species are dependent on protein concentrations. The population of I_2 reaches a maximum at ~2.1 M urea, whereas the population of I reaches a maximum at ~4 M urea. The transition of I to the unfolded species U has a mid-point at ~4.7 M urea. There is still presence of I_2 and I till ~5.3 M urea. This explains both the concentration dependence and decrease in amplitude at the shoulder region.

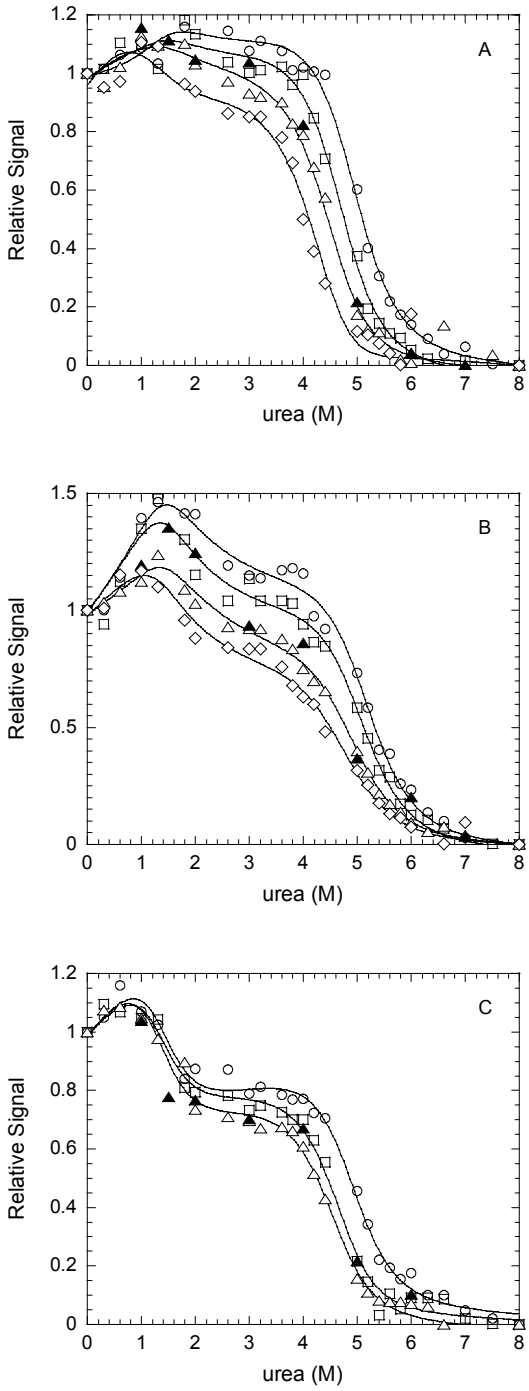

Figure 26. Equilibrium unfolding of procaspase-3(C163S) at different concentrations at pH 5. For *panels* A and B, unfolding was monitored by fluorescence with excitations at 280 nm (*panel* A) and 295 nm (*panel* B). *Panel* C represents CD data at 228 nm. The protein concentrations are as follows: 0.25 μM (◇), 0.5 μM (Δ), 1 μM (□) and 2 μM (○). (▲) represents refolding data at 0.5 μM protein concentration. The solid lines represent fits to the data as described under Materials and Methods.

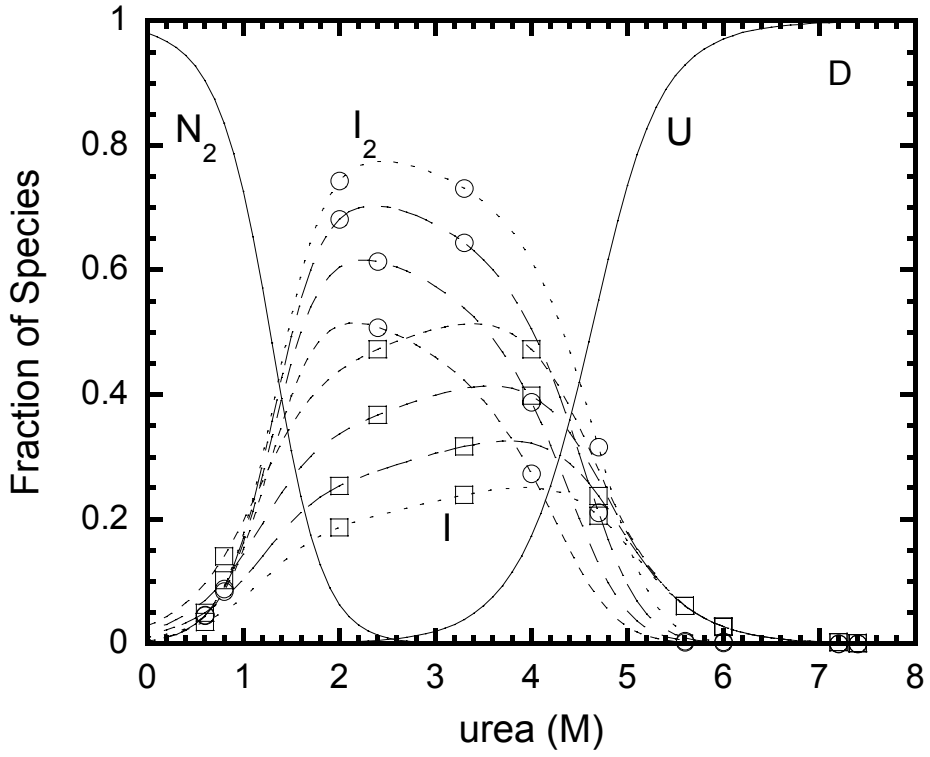

Figure 26. *Panel* D. Fraction of species as a function of urea concentration at pH 5. The fractions of native, dimeric intermediate, monomeric intermediate and the unfolded protein were calculated as a function of urea concentration. The protein concentrations were 0.25 μM (------), 0.5 μM (— —), 1 μM (- —) and 2 μM (·····). 'N_2' refers to the native procaspase-3(C163S), 'I_2' and 'I' are the dimeric and monomeric intermediates respectively, and 'U' refers to the unfolded species. (○) fraction of I_2; (□) fraction of I.

***Equilibrium unfolding at pH 4.75*.** The unfolding data are shown in Figure 27. The data for three different probes (fluorescence excitations 280 nm, 295 nm and CD at 228 nm) show similar unfolding pattern with no change in signal between 0 to ~0.6 M urea, followed by a cooperative decrease in signal from 0.9 M to 1.9 M urea (increase in fluorescence signal for excitations at 280 and 295 nm) and a shoulder region between ~1.9 and ~3.5 M urea. There is a second transition between 3.5 and 7 M urea. This is very well observed in the CD data. The protein shows concentration dependence (less prominent as compared with the ones at higher pH) and the amplitude of the shoulder region decreases as well as the mid-point of the second transition changes with decrease in protein concentration, suggesting a four-state unfolding model as described earlier. The protein is completely reversible at this pH and the refolding data are shown as solid triangles (▲) in the figure.

The fractions of species at each urea concentration were obtained at each of the four protein concentrations (0.25 μM, 0.5 μM, 1 μM and 2 μM). This is shown in Figure 27 D. At 0 M urea, native protein as well as I_2 and I are present. There is a decrease in native protein between 0 and ~1.2 M urea. At the same time an increase in the dimeric (I_2) as well as the monomeric intermediate (I) is seen. We see a population of I_2 between 0 and 4 M urea , whereas I between pH 0 and 7. The relative populations of the dimeric and the monomeric intermediate species are dependent on protein concentrations. The population of I_2 reaches a maximum at ~0.6 M urea, whereas the population of I reaches a maximum at ~2.7 M urea. The transition of I to the unfolded species U has a mid-point at ~4.4 M urea. This figure explains both the concentration dependence and decrease in amplitude at the shoulder region.

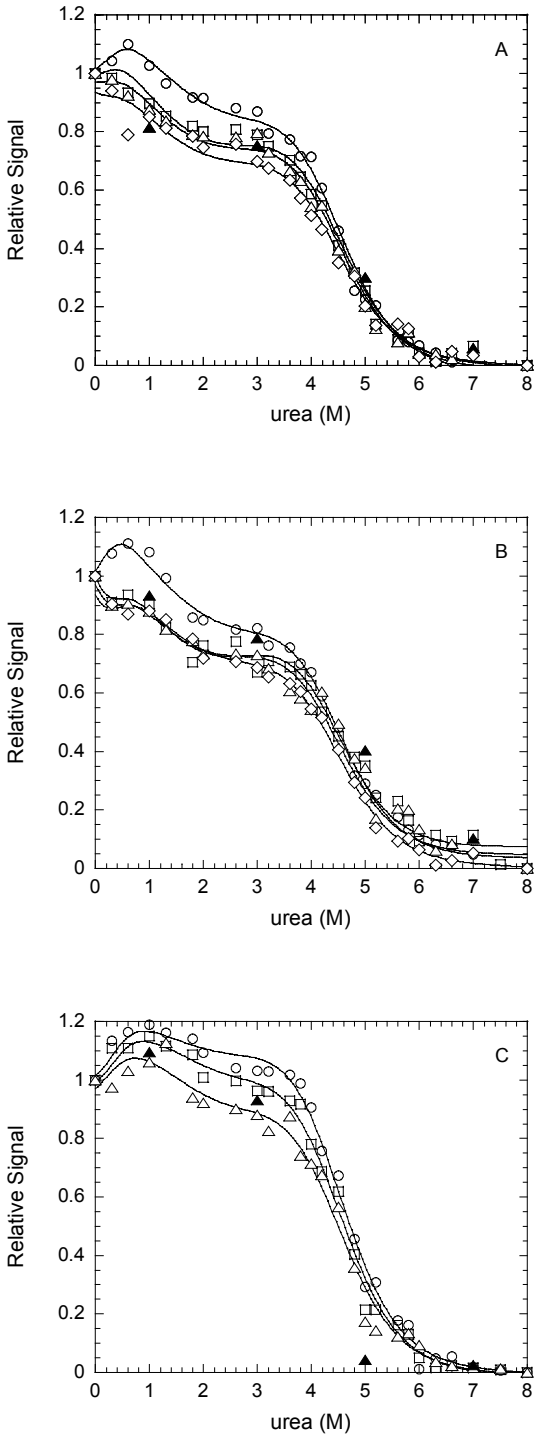

Figure 27. Equilibrium unfolding of procaspase-3(C163S) at different concentrations at pH 4.75. For *panels* A and B, unfolding was monitored by fluorescence with excitations at 280 nm (*panel* A) and 295 nm (*panel* B). *Panel* C represents CD data at 228 nm. The protein concentrations are as follows: 0.25 μM (◇), 0.5 μM (Δ), 1 μM (□) and 2 μM (○). (▲) represents refolding data at 0.5 μM protein concentration. The solid lines represent fits to the data as described under Materials and Methods.

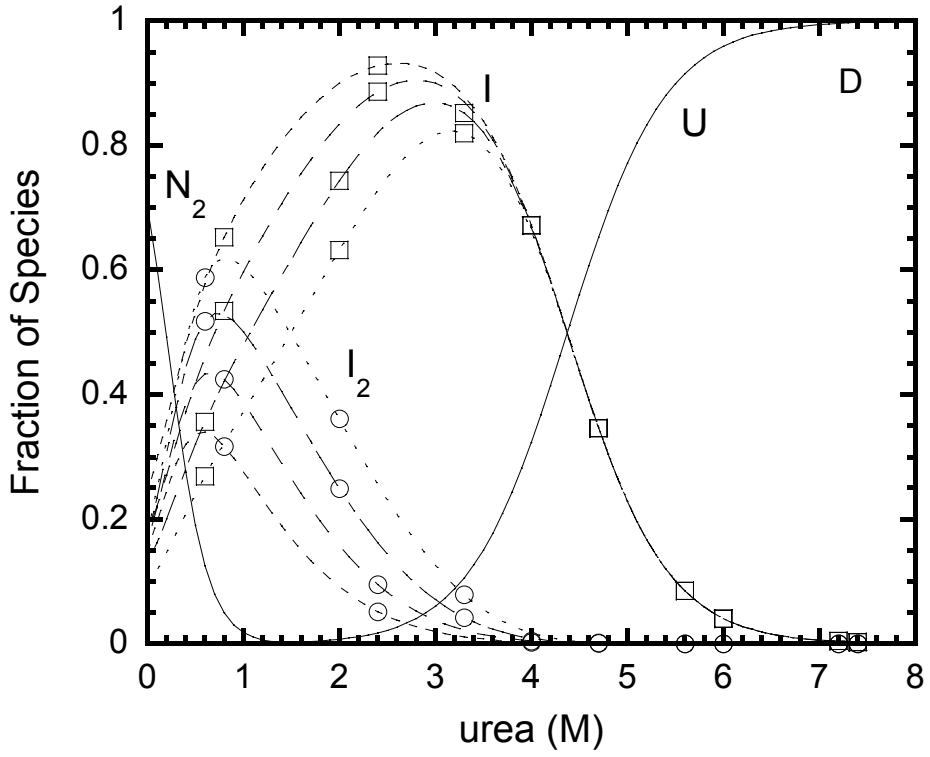

Figure 27. *Panel* D. Fraction of species as a function of urea concentration at pH 4.75. The fractions of native, dimeric intermediate, monomeric intermediate and the unfolded protein were calculated as a function of urea concentration. The protein concentrations were 0.25 μM (------), 0.5 μM (— —), 1 μM (- —) and2 μM (·····). 'N_2' refers to the native procaspase-3(C163S), 'I_2' and 'I' are the dimeric and monomeric intermediates respectively, and 'U' refers to the unfolded species. (○) fraction of I_2; (□) fraction of I.

***Equilibrium unfolding at pH 4.5*.** The unfolding data are shown in Figure 28. The data for three different probes (fluorescence excitations 280 nm, 295 nm and CD at 228 nm) show similar unfolding pattern with a cooperative transition from ~0 M to ~1 M urea (not observed in CD data), a shoulder region between ~1 M and ~3.3 M urea. There is a second transition between 3.3 M and 7 M urea. The protein shows no concentration dependence for fluorescence data (Figure 28 A and B) and little concentration dependence for CD data (Figure 28 C). The data was therefore fit to a three-state monomer model as described under Materials and Methods. The protein is completely reversible at this pH and the refolding data are shown as solid triangles (▲) in the figure.

The fractions of species at each urea concentration were obtained. This is shown in Figure 28 D. At 0 M urea, monomeric native state N, (at this pH) as well as intermediate state I are present. There is a decrease in native protein between 0 and ~2 M urea. At the same time an increase in the monomeric intermediate (I) is seen. We see a population of I between 0 and 7 M urea. The population of I reaches a maximum at ~2 M urea. The transition of I to the unfolded species U has a mid-point at ~4.3 M urea. This figure explains the loss of concentration dependence at this pH.

***Equilibrium unfolding at pH 4.2*.** The unfolding data are shown in Figure 29. The data for three different probes (fluorescence excitations 280 nm, 295 nm and CD at 228 nm) show similar unfolding pattern with a cooperative transition from ~0 M to ~0.8 M urea (not observed in the CD data) and a shoulder region between ~0.8 M and ~2.1 M urea. There is a second transition between 2.1 M and 7 M urea. The protein shows no concentration dependence for fluorescence data (Figure 29 A and B) and little

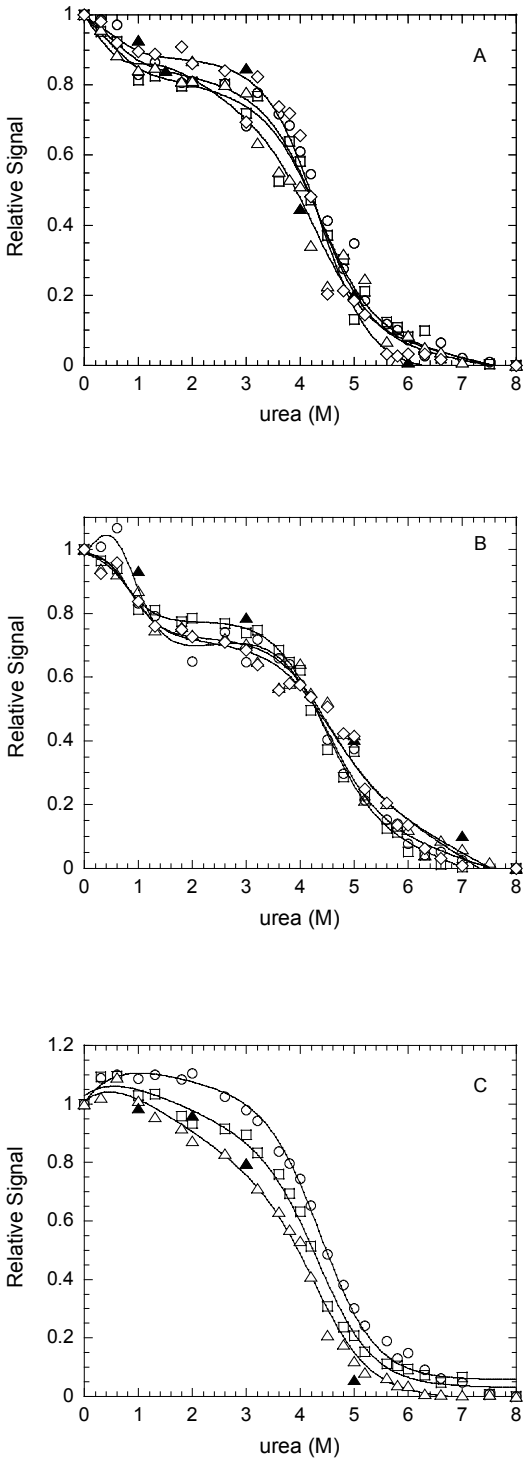

Figure 28. Equilibrium unfolding of procaspase-3(C163S) at different concentrations at pH 4.5. For *panels* A and B, unfolding was monitored by fluorescence with excitations at 280 nm (*panel* A) and 295 nm (*panel* B). *Panel* C represents CD data at 228 nm. The protein concentrations are as follows: 0.25 μM (◇), 0.5 μM (Δ), 1 μM (□) and 2 μM (○). (▲) represents refolding data at 0.5 μM protein concentration. The solid lines represent fits to the data as described under Materials and Methods.

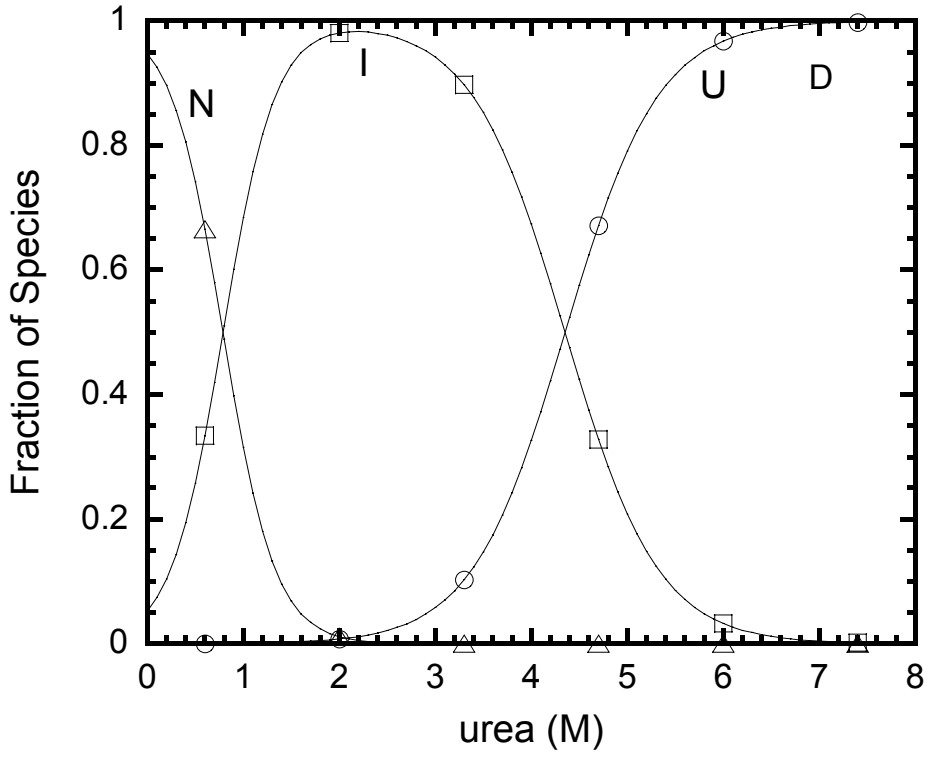

Figure 28. *Panel* D. Fraction of species as a function of urea concentration at pH 4.5. The fractions of native, monomeric intermediate and the unfolded protein were calculated and plotted against urea concentration. 'N' refers to the native procaspase-3(C163S), 'I', the monomeric intermediate and 'U' refers to the unfolded species. The native species is shown as (△), intermediate as (□) and the unfolded species as (○). The points are joined by solid lines.

concentration dependence for CD data (Figure 29 C). The data was therefore fit to a three-state monomer model as described under Materials and Methods. The protein is completely reversible at this pH and the refolding data are shown as solid triangles (▲) in the figure.

The fractions of species at each urea concentration were obtained. This is shown in Figure 29 D. At 0 M urea, monomeric native state N (at this pH), as well as intermediate state I are present. There is a decrease in native protein between 0 and ~2.8 M urea. At the same time an increase in the monomeric intermediate (I) is seen. We see a population of I between 0 and 7 M urea. The population of I reaches a maximum at ~2.1 M urea. The transition of I to the unfolded species U has a mid-point at ~3.9 M urea. This figure is consistent with the equilibrium unfolding data and explains the loss of concentration dependence at this pH.

***Equilibrium unfolding at pH 4*.** The unfolding data are shown in Figure 30. The data for three different probes (fluorescence excitations 280 nm, 295 nm and CD at 228 nm) show similar unfolding pattern with a shoulder region from ~0 M to ~1.4 M urea followed by a transition between 1.4 M and 7 M urea. The protein shows no concentration dependence for fluorescence data (Figure 30 A and B) as well as for CD data (Figure 30 C). The data was therefore fit to a two-state monomer model as described under Materials and Methods. The protein is completely reversible at this pH and the refolding data are shown as solid triangles (▲) in the figure.

The fractions of species at each urea concentration were obtained. This is shown in Figure 30 D. The native protein decreases with increase in urea concentration with a concomitant increase in the unfolded protein. The midpoint of the transition is at ~3.2 M

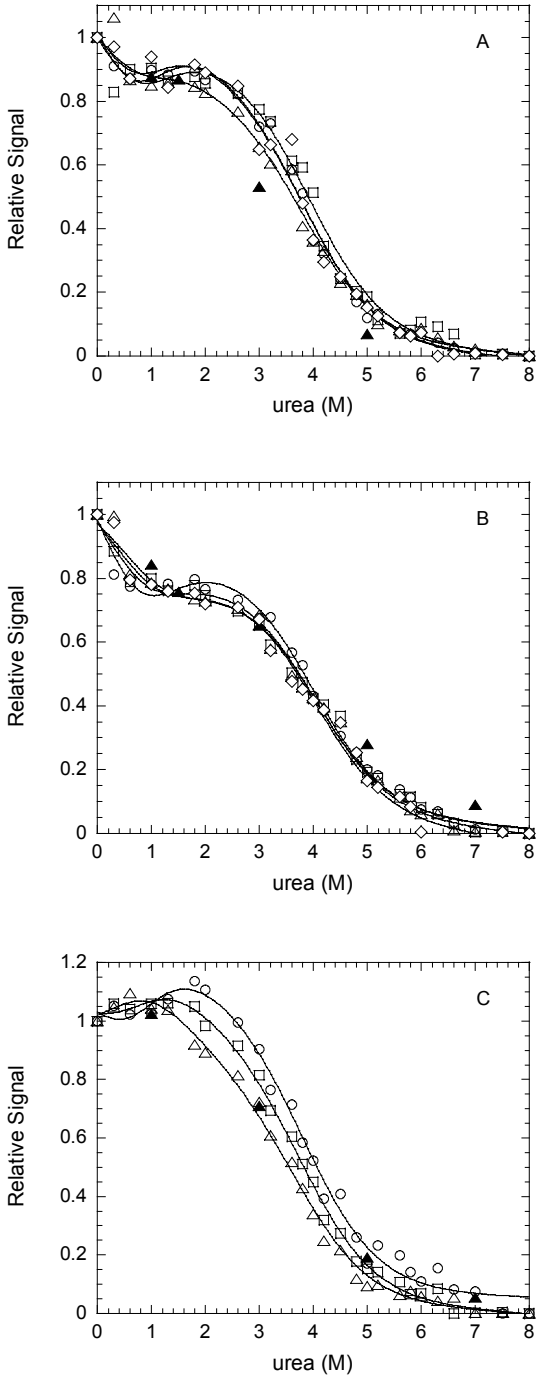

Figure 29. Equilibrium unfolding of procaspase-3(C163S) at different concentrations at pH 4.2. For *panels* A and B, unfolding was monitored by fluorescence with excitations at 280 nm (*panel* A) and 295 nm (*panel* B). *Panel* C represents CD data at 228 nm. The protein concentrations are as follows: 0.25 μM (◇), 0.5 μM (Δ), 1 μM (□) and 2 μM (○). (▲) represents refolding data at 0.5 μM protein concentration. The solid lines represent fits to the data as described under Materials and Methods.

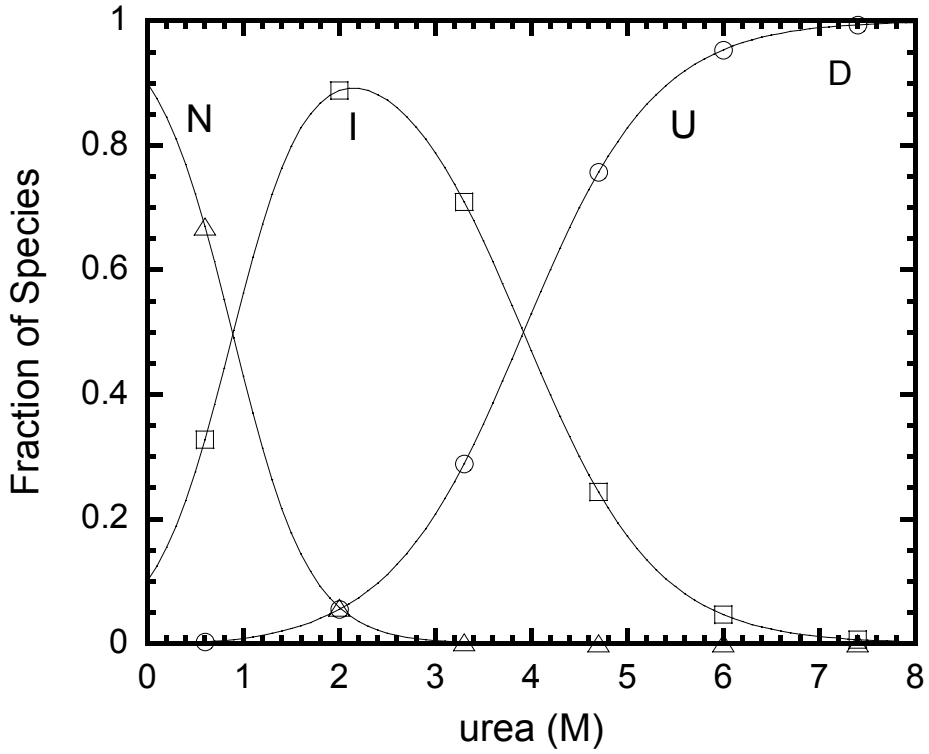

Figure 29. *Panel* D. Fraction of species as a function of urea concentration at pH 4.2. The fractions of native, monomeric intermediate and the unfolded protein were calculated and plotted against urea concentration. 'N' refers to the native procaspase-3(C163S), 'I', the monomeric intermediate and 'U' refers to the unfolded species. The native species is shown as (△), intermediate as (□) and the unfolded species as (○). The points are joined by solid lines.

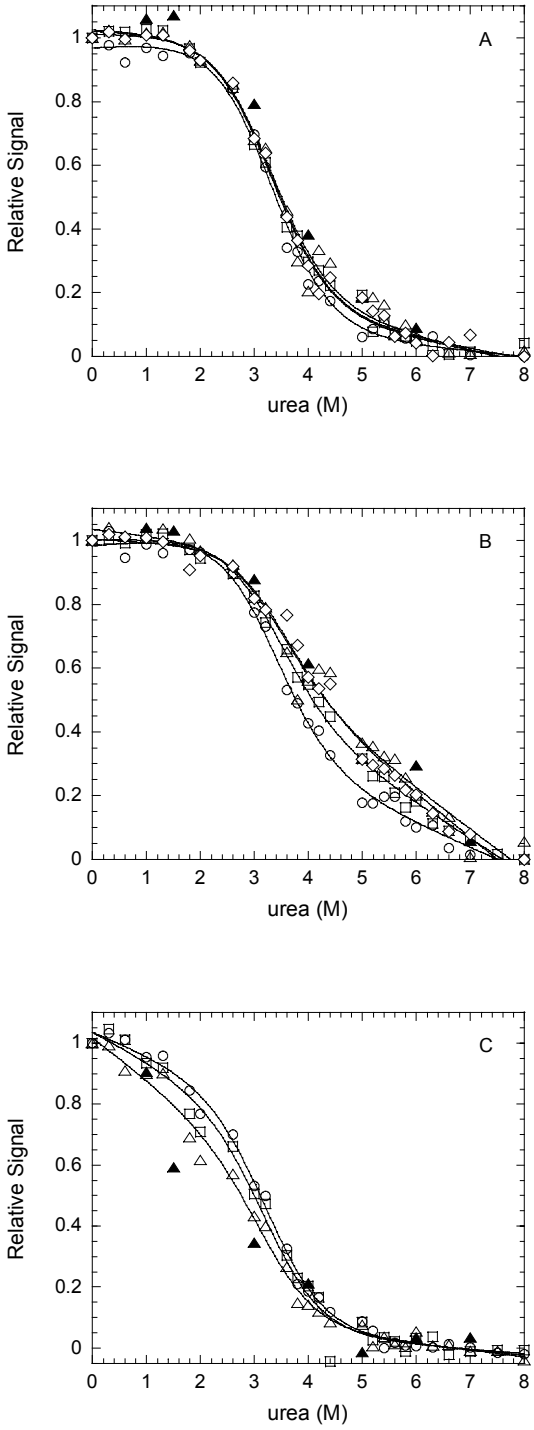

Figure 30. Equilibrium unfolding of procaspase-3(C163S) at different concentrations at pH 4. For *panels* A and B, unfolding was monitored by fluorescence with excitations at 280 nm (*panel* A) and 295 nm (*panel* B). *Panel* C represents CD data at 228 nm. The protein concentrations are as follows: 0.25 μM (◇), 0.5 μM (Δ), 1 μM (□) and 2 μM (○). (▲) represents refolding data at 0.5 μM protein concentration. The solid lines represent fits to the data as described under Materials and Methods.

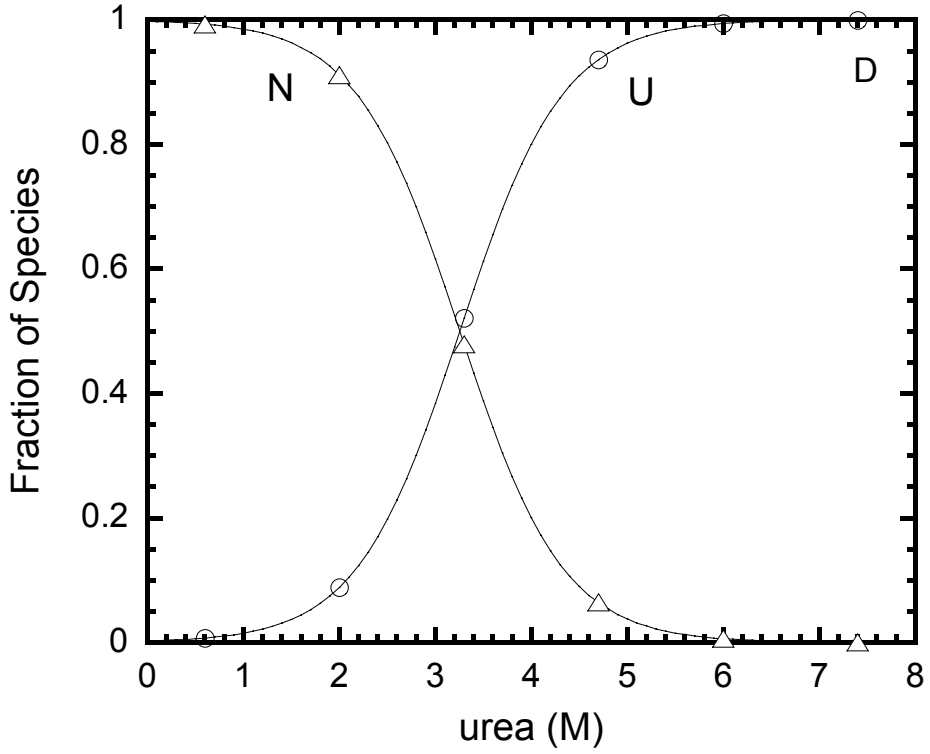

Figure 30. *Panel* D. Fraction of species as a function of urea concentration at pH 4. The fractions of native and the unfolded protein were calculated and plotted against urea concentration. 'N' refers to the native procaspase-3(C163S), and 'U' refers to the unfolded species. The native species is shown as (△) and the unfolded species as (○). The points are joined by solid lines.

urea. This figure is consistent with the equilibrium unfolding data and explains the loss of concentration dependence at this pH.

***Effect of concentration dependence*.** Because procaspase-3 is a homodimer at pH 7.2, we examined the effect of protein concentration on equilibrium unfolding process. The data were fit to a 4-state model, where the native dimer isomerizes to an intermediate dimer that dissociates to give another intermediate monomer, which unfolds to the unfolded monomeric species as shown in equation 1 under Materials and Methods. This effect was examined as a function of pH. The experiments were done with protein concentrations 2 μM, 1 μM, 0.5 μM and 0.25 μM. For experiments at pH 8.5, 8, 7.6, 7.2, 6.5, 6, 5.5, 5 and 4.75, the data fit very well to the four-state model as described earlier. The fluorescence data for pH 4.5 and pH 4.2 showed very little, while, the CD data showed some concentration dependence. The data did not fit to a four-state model. The data were fit to a three-state model where a dimeric species unfolds into two monomeric intermediates and consequently to two unfolded monomers. The fraction of species calculated from this analysis did not give dimeric species. The unfolding data fit well to a three-state monomer model where a native monomer unfolds to an intermediate species that subsequently unfolds. These observations suggest that the first species includes some dimer and the first ΔG is underestimated. The data at pH 4, show a two-state transition and no concentration dependence. Hence, the data were fit to a two-state monomer model as described under Materials and Methods.

***Effect of pH*.** The unfolding curves for the protein between pH 8.5 and pH 4.75 show concentration dependence with two transitions and a shoulder region. The amplitude of the shoulder decreases with decrease in concentration and also the midpoint of the second

transition changes with change in concentration, suggesting a four-state unfolding model as described earlier. There is a shift in the shoulder region towards higher urea concentration with decrease in pH between pH 8.5 and 7.2 and then towards lower urea concentration with decrease in pH up to pH 4.75. This suggest that the native state becomes less stable with decrease in pH and is most stable ~pH 7.2. The intermediate states observed at higher pH are absent or become less prominent with decrease in pH suggesting that the protein undergoes a pH-dependent conformational change. The protein below pH 4.75 is fit to a three-state monomer suggesting the protein dissociates at that point. The conformation still changes between pH 4.2 and pH 4, where, at pH 4, the protein undergoes a two-step unfolding process. There is no concentration dependence observed from pH 4.5 to pH 4 and that is consistent with the three-state and two-state monomer models. The change in unfolding pattern versus pH is very well illustrated in Figure 31 (panels A-L) for CD data at 1 μM protein concentration.

Stability versus pH. Free energies for three different transitions were plotted versus pH and the data are represented in Figure 32 A. The free energies $\triangle G_1^{H_2O}$, $\triangle G_2^{H_2O}$ and $\triangle G_3^{H_2O}$ show similar trend, i.e. a bell-shaped curve. $\triangle G_1^{H_2O}$ shows maximum stability ~ pH 7.6 and a slow decrease in stability with decrease in pH until pH 4.75. $\triangle G_2^{H_2O}$ shows maximum stability at pH 7.2 and a significant drop in stability is observed between pH 5 and 4.75. $\triangle G_3^{H_2O}$ is constant (within error) for all pH. Figure 32 B shows the plot of total free energy ($\triangle G^{H_2O}$) versus pH and represents a bell-shaped curve showing the protein is most stable at pH 7.2 (26 kcal/mol). The stability decreases slowly with pH and suddenly drops from pH 5 (14.9 kcal/mol) to pH 4 (3.6 kcal/mol). This is consistent with major conformational change between pH 5 and 4 as observed by V8 protease studies and

fluorescent quenching studies described later. The decrease in free energy also accounts for absence of one or two states as observed in higher pH (Figure 32 A). Figure 32 C shows the plot of cooperativity indices m_1, m_2 and m_3 versus pH. All three plots show that the '*m*' values are constant within experimental error. This suggests that no major unfolding of the protein occurs with decrease in pH that might result in a significant change in △ASA. Figure 32 D illustrates the total cooperativity index versus pH. The '*m*' value is constant between pH 8 and 5 within experimental error, suggesting similar unfolding pattern within that pH range. The '*m*' values drop suddenly from pH 4.75 to pH 4.2 as observed in Figure 32 D. This is consistent with conformational change and dimer dissociation between pH 5 and pH 4. The values of free energies as well as the cooperativity indices for all transitions are shown in Table III.

III. Role of the short pro-domain in procaspase-3

The pro-domain of procaspase-3 is 28 amino acids long with no known function. Fluorescence anisotropy experiments from our laboratory [22] show that the pro-domain binds the protease domain in trans. In order to see whether the pro-domain plays a role in the folding and maturation of the protein, we examined the urea-dependent equilibrium folding of the pro-less variant of procaspase-3(C163S) (Figure 33) in presence and absence of the pro-domain. The fluorescence emission was monitored at 320 nm following excitation at 280 nm. Although the number of data points is limited in these studies, the unfolding data are similar to those described for procaspase-3(C163S).

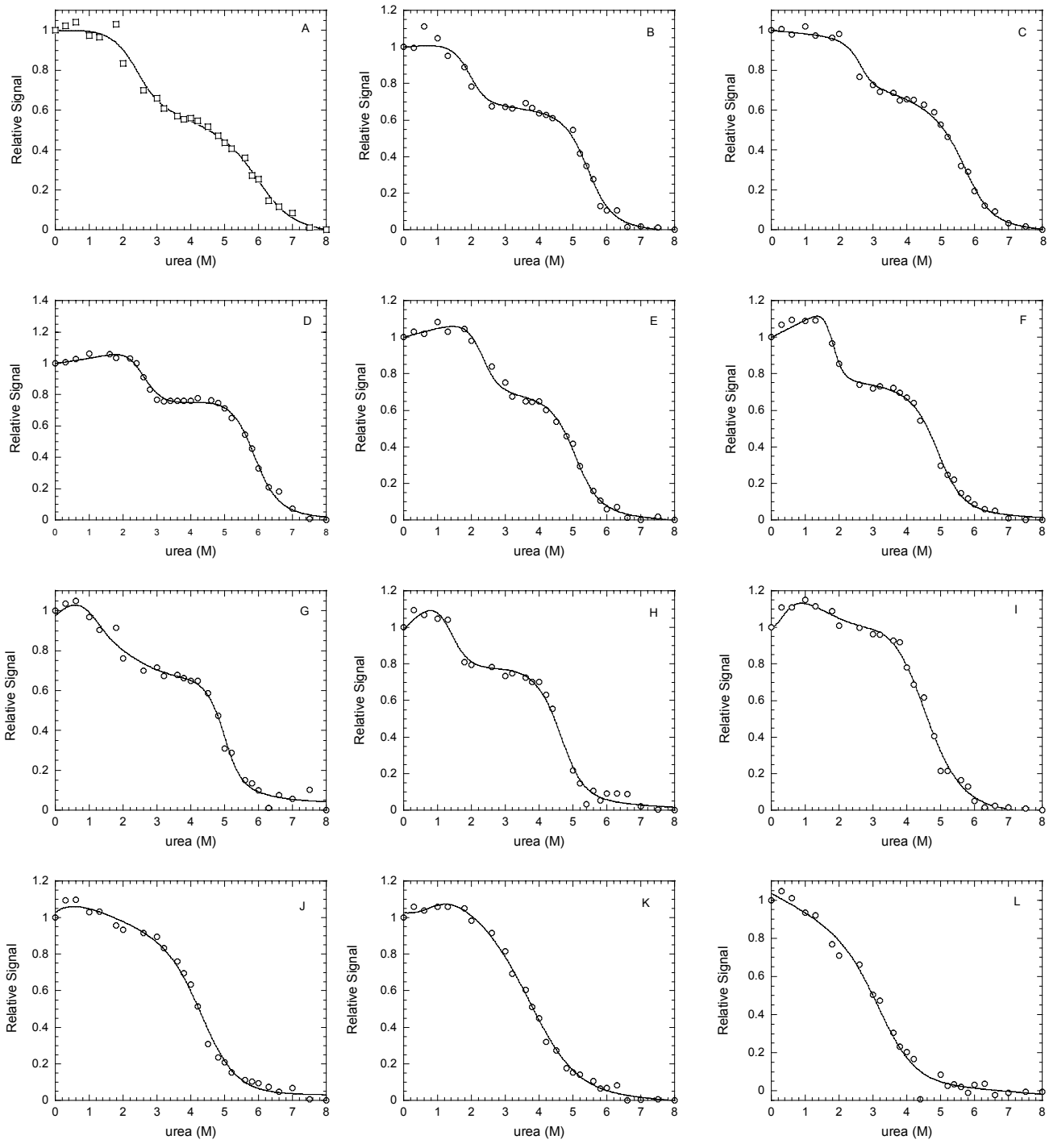
A
B
C
D
E
F
G
H
I
J
K
L
Relative Signal
urea (M)

Figure 31. Equilibrium unfolding of procaspase-3(C163S) at different pH. Panels A-L represent unfolding data measured by CD at 228 nm at 1 μM protein concentration for pH 8.5, 8, 7.6, 7.2, 6.5, 6, 5.5, 5, 4.75, 4.5, 4.2 and 4 respectively. The data are represented by (○). The data were fit (*solid lines*) as described under Materials and Methods using Igor Pro.

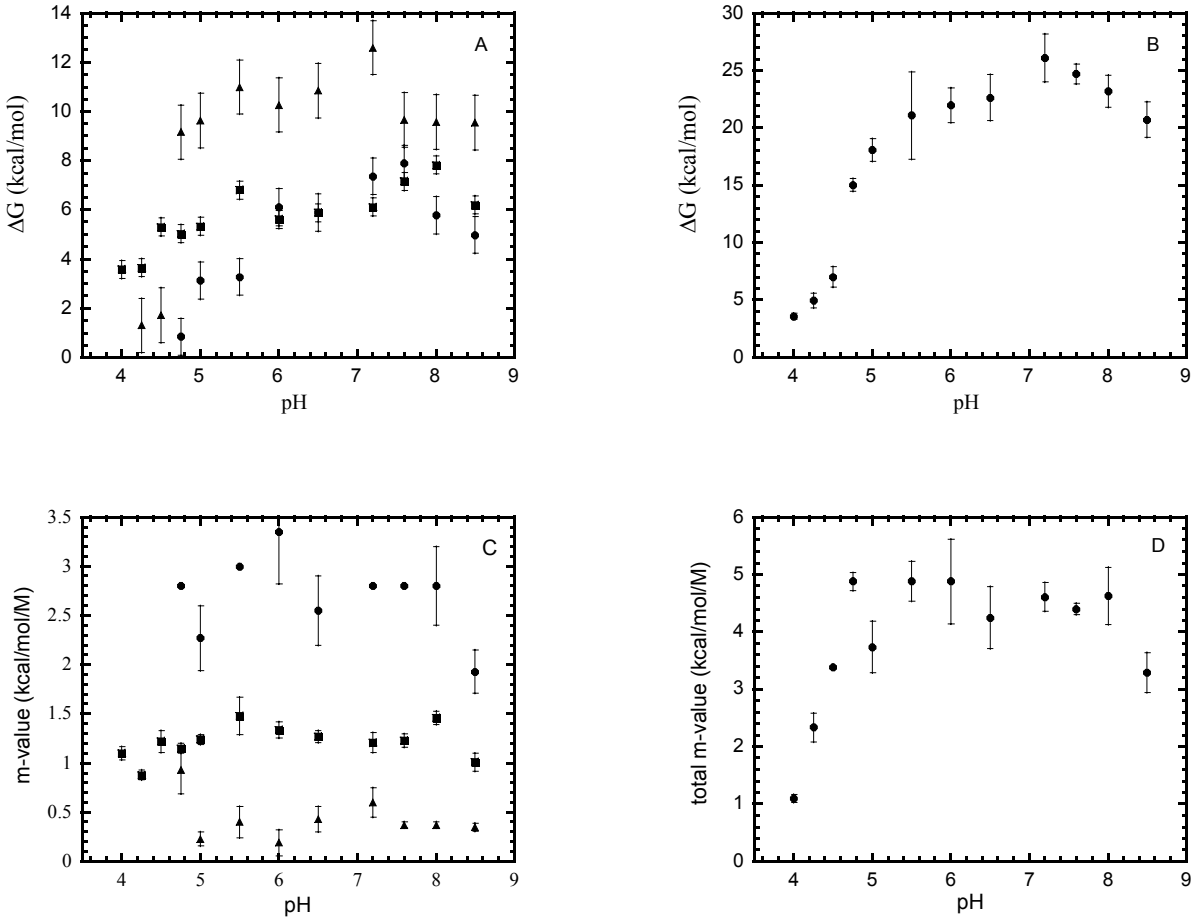

Figure 32. *Panel* A. Plot of free energies $\triangle G_1^{H_2O}$, $\triangle G_2^{H_2O}$, and $\triangle G_3^{H_2O}$ for procaspase-3(C163S) versus pH. (●) represents $\triangle G_1^{H_2O}$, (▲) represents $\triangle G_2^{H_2O}$ and (■) represents $\triangle G_3^{H_2O}$. *Panel* B. Plot of total free energy ($\triangle G^{H_2O}$) versus pH. *Panel* C. Plot of cooperative indices m_1, m_2 and m_3 versus pH. (●) represents m_1, (▲) represents m_2 and (■) represents m_3. *Panel* D. Plot of total cooperative index (m) versus pH. Error bars show standard error from 11 unfolding curves (four each from two sets of fluorescence data and three from CD data).

Table III. Table depicting free energies and cooperativity indices for the unfolding process of procaspase-3(C163S) at different pH.

pH	$\Delta G_1^{H_2O}$ *(kcal/mol)*	$\Delta G_2^{H_2O}$ *(kcal/mol)*	$\Delta G_3^{H_2O}$ *(kcal/mol)*	$\Delta G_{tot}^{H_2O}$ *(kcal/mol)*	m_1 *(kcal/mol /M)*	m_2 *(kcal/mol /M)*	m_3 *(kcal/mol /M)*	m_{tot} *(kcal/mol /M)*
8.5	4.9 ± 0.6	9.6 ±0.3	6.2 ± 0.6	20.7 ± 1.5	1.93 ± 0.22	0.35 ± 0.04	1.01 ± 0.09	3.29 ± 0.35
8.0	5.8 ± 0.8	9.6 ± 0.2	7.8 ± 0.4	23.2 ± 1.4	2.8 ± 0.4	0.37 ± 0.03	1.46 ± 0.07	4.63 ± 0.5
7.6	7.9 ± 0.1	9.7 ±0.3	7.2 ± 0.5	24.7 ± 0.9	2.8 ± 0.0	0.37 ± 0.03	1.23 ± 0.07	4.40 ± 0.1
7.2	7.4 ± 0.1	12.6 ± 1.1	6.1 ± 0.9	26.1 ± 2.1	2.8 ± 0.0	0.6 ± 0.15	1.21 ± 0.1	4.61 ± 0.25
6.5	5.9 ± 0.8	10.7 ± 0.6	5.9 ± 0.6	22.6 ± 2.0	2.55 ± 0.35	0.43 ± 0.13	1.27 ± 0.06	4.25 ± 0.54
6.0	6.1 ± 1.0	10.3 ± 0.3	5.6 ± 0.2	22.0 ± 1.5	3.35 ± 0.53	0.19 ± 0.13	1.34 ± 0.08	4.88 ± 0.74
5.5	3.3 ± 0.1	11.0 ± 1.9	6.8 ± 1.8	21.1 ± 3.8	3.0 ± 0.0	0.40 ± 0.16	1.48 ± 0.19	4.88 ± 0.35
5.0	3.1 ± 0.6	9.6 ± 0.2	5.3 ± 0.3	18.1 ± 1.0	2.27 ± 0.33	0.23 ± 0.07	1.24 ± 0.05	3.74 ± 0.45
4.75	0.8 ± 0.2	9.2 ± 0.1	5.0 ± 0.2	15.0 ± 0.5	2.8 ± 0.0	0.93 ± 0.24	1.15 ± 0.05	4.88 ± 0.29
4.5	-	1.7 ± 0.6	5.3 ± 0.5	7.0 ± 1.1	-	2.17 ± 0.39	1.22 ± 0.11	3.39 ± 0.5
4.2	-	1.3 ± 0.3	3.7 ± 0.3	5.0 ± 0.6	-	1.46 ± 0.2	0.88 ±0.05	2.34 ± 0.25
4.0	-	-	3. 8 ± 0.2	3.8 ± 0.2	-	-	1.10 ± 0.07	1.10 ± 0.07

Equilibrium unfolding studies of the pro-less variant in presence of 8 M urea is shown in Figure 33, panel A. The solid circle (●) represents unfolding curve, whereas the open square (□) represents the refolding data. The fluorescence signal for the unfolding data is higher than the refolding data suggesting the protein does not fold reversibly. Since the refolding signal is very low compared to the unfolding data, the protein looks like it does not unfold in Figure 33 A. Figure 33, panel B shows equilibrium unfolding of the pro-less variant with the pro-peptide at (0.1 : 1) ratio. The refolding signals for 7, 6 and 4 M urea are close to the unfolding data suggesting refolding to some extent up to 4 M. Below 4 M urea, the signals of the refolding data drop suggesting that the protein does not refold at that point. Therefore, the protein starts refolding with the addition of the pro-domain but still does fold completely. Figure 33, panel C shows equilibrium unfolding of the pro-less variant with the pro-peptide at (0.5 : 1) ratio. The refolding signals for 7, 6 and 4 M urea overlap with the unfolding data suggesting that the protein refolds till 4 M urea. Below 4 M urea, the signals of the refolding data drop suggesting that the protein does not refold at that point. Therefore, the protein refolds more than with the addition of 0.1 M pro-peptide concentration but still does not refold completely. Figure 33, panel D shows equilibrium unfolding of the pro-less variant with the pro-peptide at (1: 1) ratio. The refolding signals at all urea concentrations overlap with the unfolding signals suggesting complete refolding of the protein. These results suggest that the protein does not fold reversibly until 1:1 pro-peptide to protein concentration. Moreover, with higher pro-peptide concentration (2.5:1) as shown in Figure 33, panel E, the folding is not completely reversible, since a higher refolding

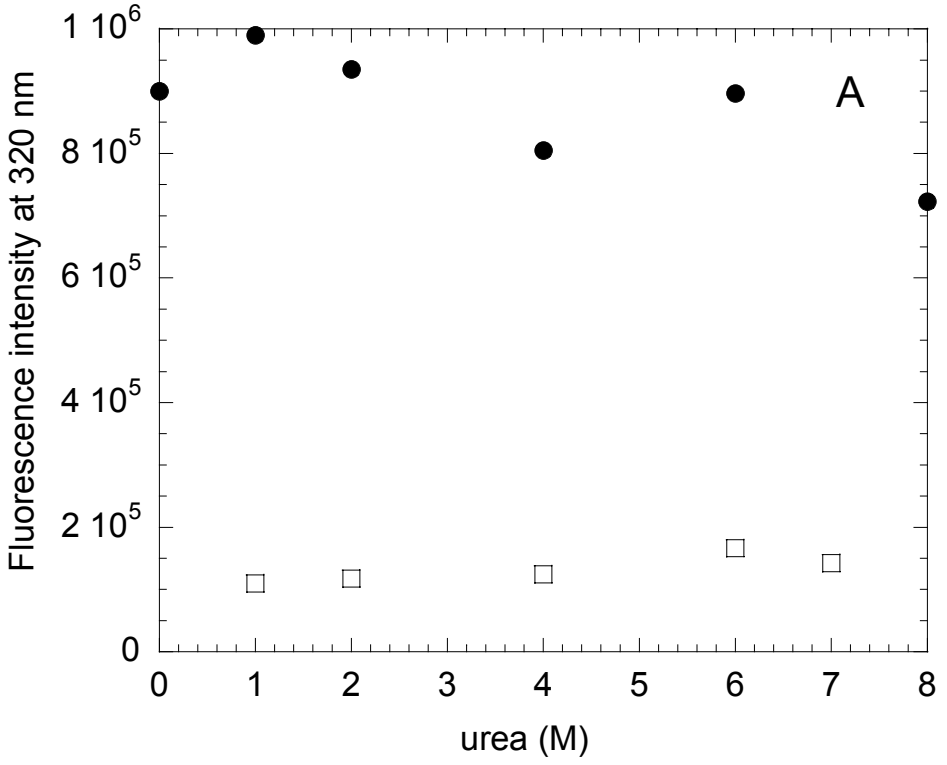

Figure 33. *Panel* A. Equilibrium unfolding of pro-less variant of procaspase-3(C163S) in presence of different urea concentrations. The fluorescence excitation was at 280 nm and fluorescence emission scans were taken between 305-400 nm. The fluorescence intensity at 320 nm was plotted vs. urea concentration. (●) represents unfolding data whereas, (□) represents the refolding curve.

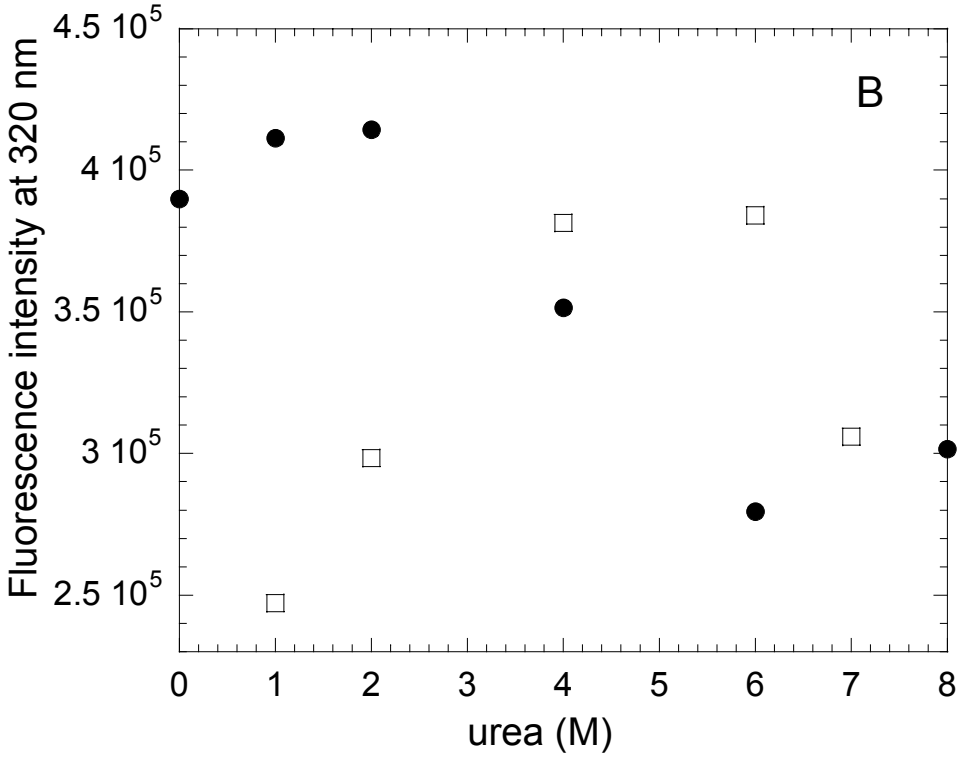

Figure 33. *Panel* B. Equilibrium unfolding of pro-less variant of procaspase-3(C163S) in presence of the pro-domain in *trans*. The ratio between the pro-domain and the pro-less variant is 0.1 : 1. The fluorescence excitation was at 280 nm and fluorescence emission scans were taken between 305-400 nm. The fluorescence intensity at 320 nm was plotted vs. urea concentration. (●) represents unfolding data whereas, (□) represents the refolding curve.

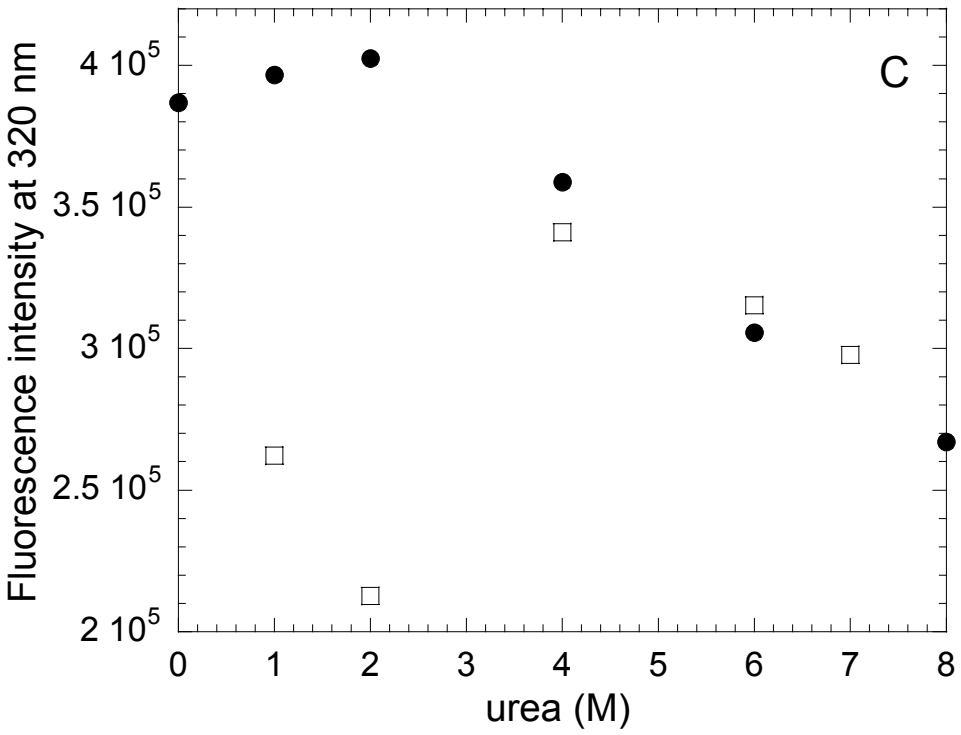

Figure 33. *Panel* C. Equilibrium unfolding of pro-less variant of procaspase-3(C163S) in presence of the pro-domain in *trans*. The ratio between the pro-domain and the pro-less variant is 0.5 : 1. The fluorescence excitation was at 280 nm and fluorescence emission scans were taken between 305-400 nm. The fluorescence intensity at 320 nm was plotted vs. urea concentration. (●) represents unfolding data whereas, (□) represents the refolding curve.

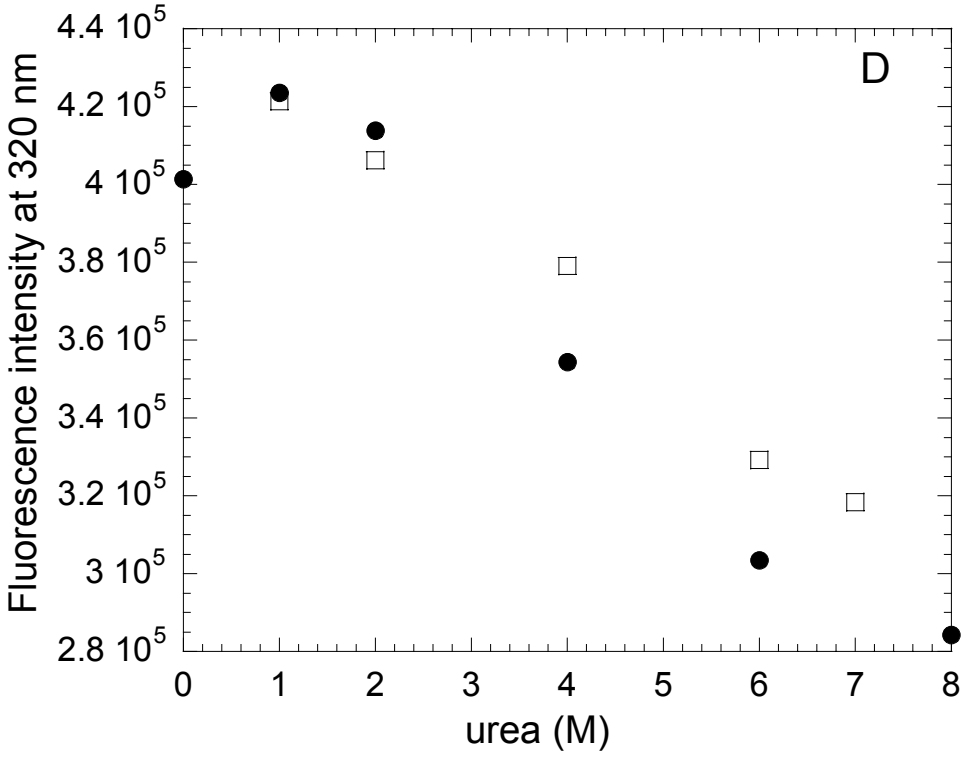

Figure 33. *Panel* D. Equilibrium unfolding of pro-less variant of procaspase-3(C163S) in presence of the pro-domain in *trans*. The ratio between the pro-domain and the pro-less variant is 1 : 1. The fluorescence excitation was at 280 nm and fluorescence emission scans were taken between 305-400 nm. The fluorescence intensity at 320 nm was plotted vs. urea concentration. (●) represents unfolding data whereas, (□) represents the refolding curve.

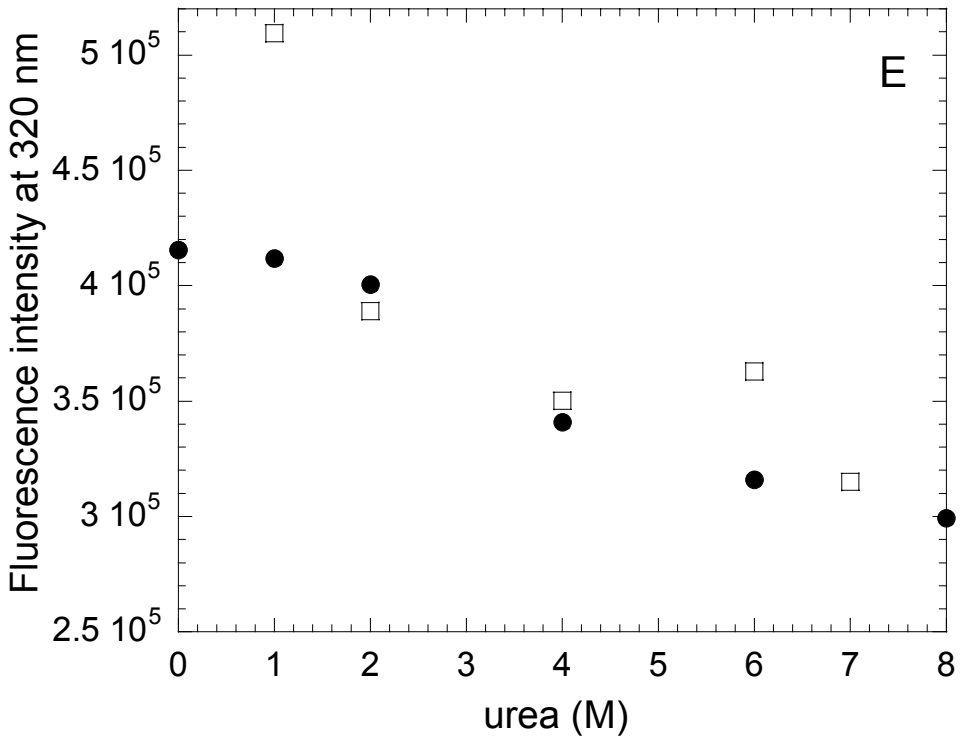

Figure 33. *Panel* E. Equilibrium unfolding of pro-less variant of procaspase-3(C163S) in presence of the pro-domain in *trans*. The ratio between the pro-domain and the pro-less variant is 2.5 : 1. The fluorescence excitation was at 280 nm and fluorescence emission scans were taken between 305-400 nm. The fluorescence intensity at 320 nm was plotted vs. urea concentration. (●) represents unfolding data whereas, (□) represents the refolding curve.

signal at 1 M urea concentration is observed.

In order to see whether the interaction with the pro-peptide is non-specific we repeated the experiments with the pro-peptide of procaspase-1. Procaspase-1 has a long prodomain (119 amino acids). Interestingly after removal of the CARD domain (92 amino acids), the remaining 27 amino acids have no known function. It is similar in length to the procaspase-3 pro-domain although the sequence is very low (Figure 34). Figure 35, panel A shows the equilibrium unfolding of the pro-less variant in presence of procaspase-1 pro-domain in the ratio of 0.1 : 1 (pro-domain to pro-less variant). The data show refolding up to 4 M urea and the protein does not refold beyond that point. Figure 35, panel B shows the equilibrium unfolding of the pro-less variant in presence of procaspase-1 pro-domain in the ratio of 0.5 : 1 (pro-domain to pro-less variant). The data show refolding up to 4 M urea and the protein does not refold at lower urea concentrations. Figure 35, panel C shows the equilibrium unfolding of the pro-less variant in presence of procaspase-1 pro-domain in the ratio of 1 : 1 (pro-domain to pro-less variant). Interestingly the signal for the refolding data does not overlap with the unfolding data at any urea concentration suggesting the protein does not refold even at 1 : 1 protein to pro-peptide concentration. Figure 35, panel D shows the equilibrium unfolding of the pro-less variant in presence of procaspase-1 pro-domain in the ratio of 2 : 1 (pro-domain to pro-less variant). The protein does not refold till 2 M urea concentration but shows a signal at 1 M urea concentration that overlaps with the unfolding species. Since it is not possible for the protein to regain its original conformation at 1 M urea, it can be said that the protein adopts a different conformation

Pro-1 ^{93}QTSGNYL**NMQD**SQGVLSSFPAPQ**AVQD**^{120}

Pro-3 ^{1}MENTE**NSVD**SKSIKNLEPKIIHGS**ESMD**^{28}

Figure 34. Comparison of pro-domain sequences of procaspase-1 (partial) and procaspase-3. The amino acids that are in bold and underlined represent the processing sites. The cleavage occurs after the aspartate residues (in bold, underlined).

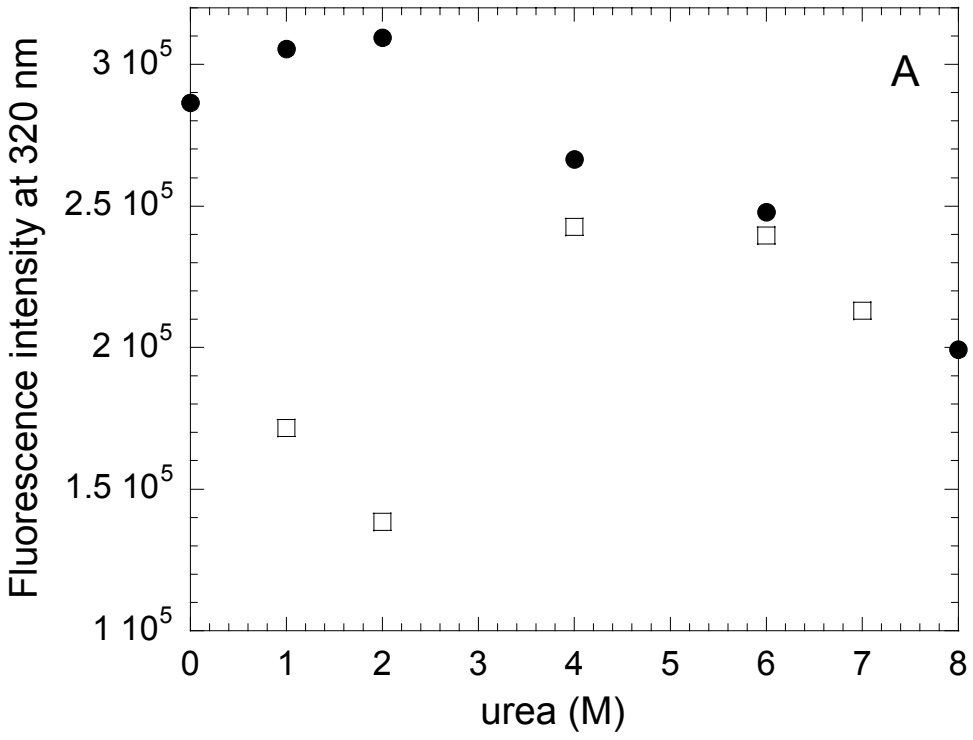

Figure 35. *Panel* A. Equilibrium unfolding of pro-less variant of procaspase-3(C163S) in presence of pro-domain of procaspase-1 in *trans*. The ratio between the pro-domain and the pro-less variant is 0.1 : 1. The fluorescence excitation was at 280 nm and fluorescence emission scans were taken between 305-400 nm. The fluorescence intensity at 320 nm was plotted vs. urea concentration. (●) represents unfolding data whereas, (□) represents the refolding curve.

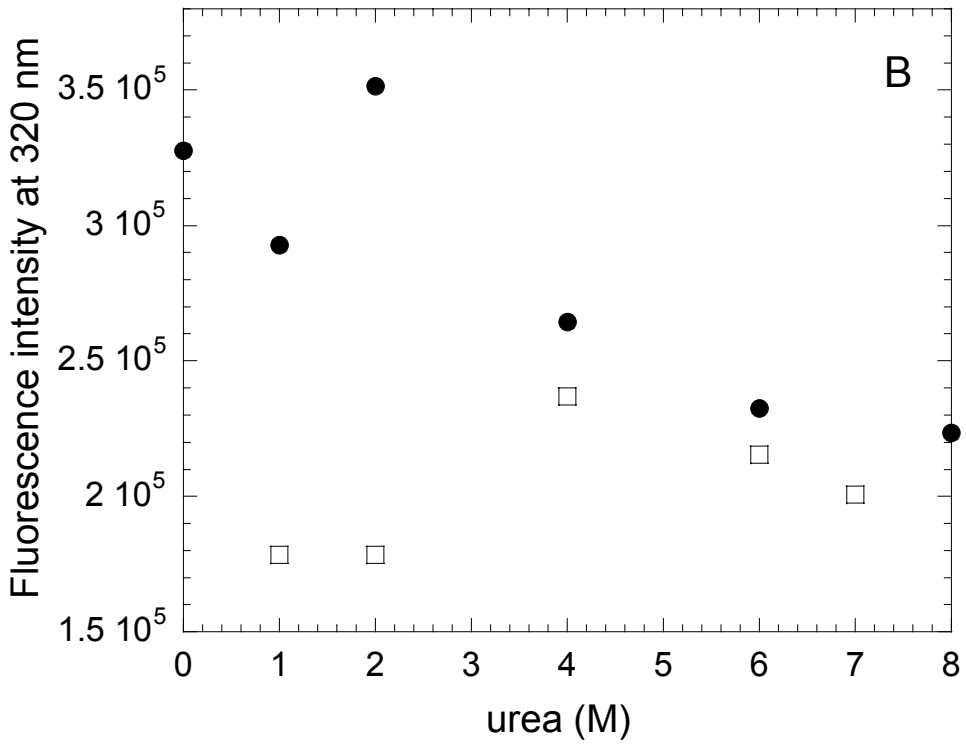

Figure 35. *Panel* B. Equilibrium unfolding of pro-less variant of procaspase-3(C163S) in presence of the pro-domain of procaspase-1 in *trans*. The ratio between the pro-domain and the pro-less variant is 0.5 : 1. The fluorescence excitation was at 280 nm and fluorescence emission scans were taken between 305-400 nm. The fluorescence intensity at 320 nm was plotted vs. urea concentration. (●) represents unfolding data whereas, (□) represents the refolding curve.

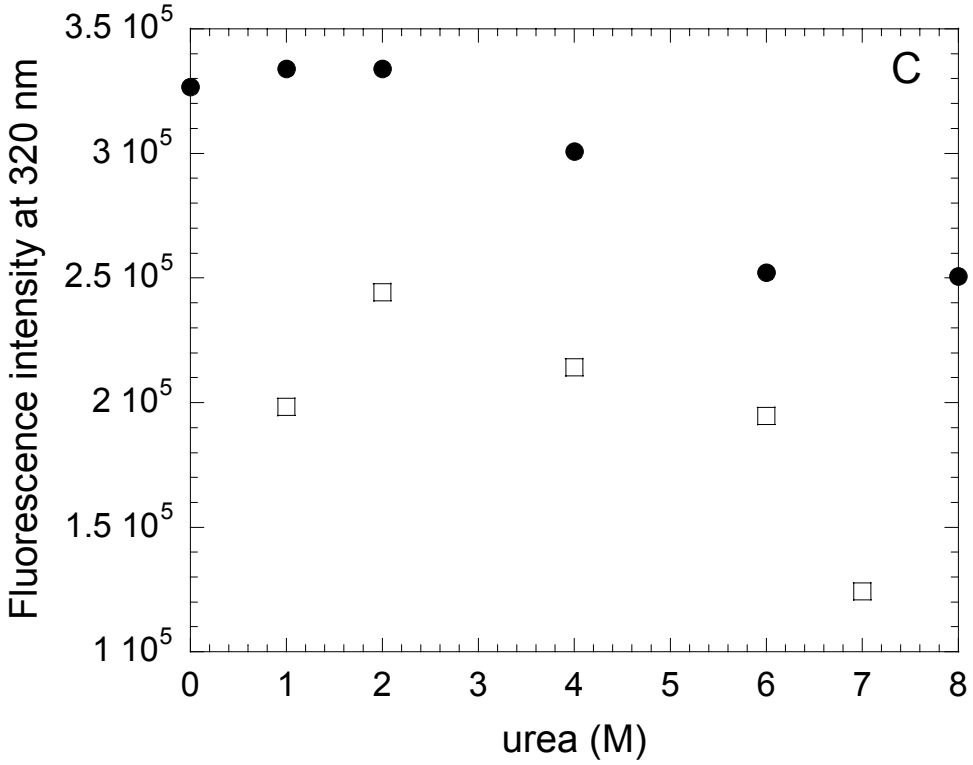

Figure 35. *Panel* C. Equilibrium unfolding of pro-less variant of procaspase-3(C163S) in presence of the pro-domain of procaspase-1 in *trans*. The ratio between the pro-domain and the pro-less variant is 1: 1. The fluorescence excitation was at 280 nm and fluorescence emission scans were taken between 305-400 nm. The fluorescence intensity at 320 nm was plotted vs. urea concentration. (●) represents unfolding data whereas, (□) represents the refolding curve.

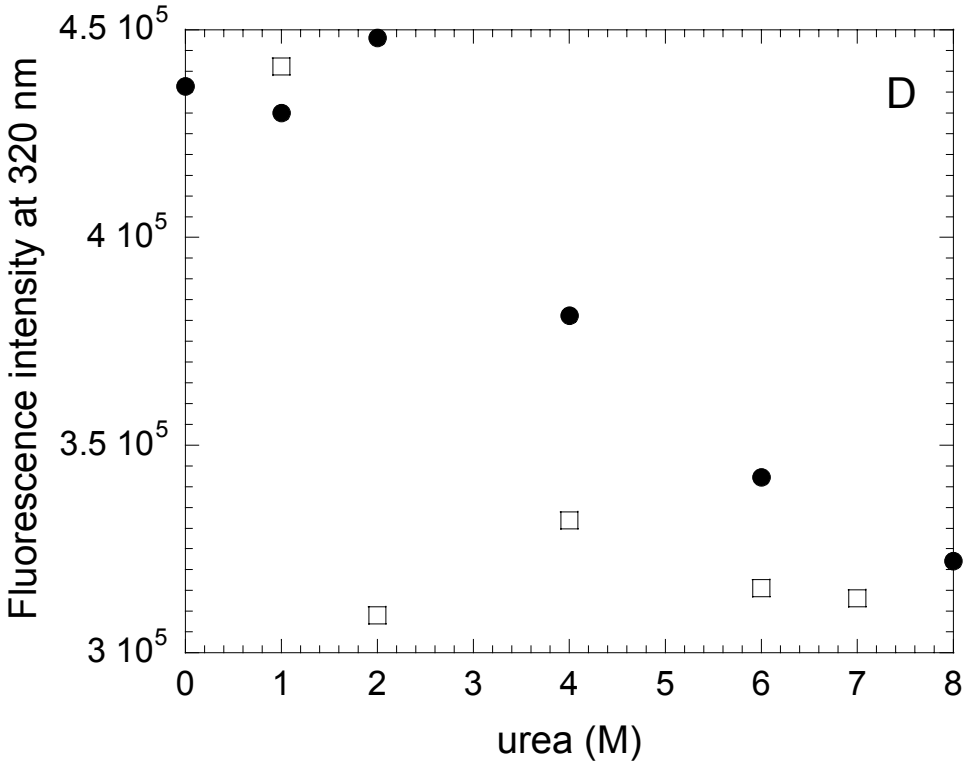

Figure 35. *Panel* D. Equilibrium unfolding of pro-less variant of procaspase-3(C163S) in presence of the pro-domain of procaspase-1 in *trans*. The ratio between the pro-domain and the pro-less variant is 2 : 1. The fluorescence excitation was at 280 nm and fluorescence emission scans were taken between 305-400 nm. The fluorescence intensity at 320 nm was plotted vs. urea concentration. (●) represents unfolding data whereas, (□) represents the refolding curve.

at that urea concentration the fluorescence of which matches the unfolding data at 1 M urea. These observations suggest that the protein does not fold reversibly in presence of any amount of pro-peptide of procaspase-1. Thus, the interaction with the procaspase-3 pro-domain is specific.

The ratio of refolding to unfolding of pro-less variant in presence of its own pro-peptide as well as procaspase-1 pro-peptide are shown in Figure 36 panels A and B respectively. A histogram is plotted with the fluorescence intensities of the refolded versus unfolded protein or protein and pro-peptide mixture at 1 M urea concentration. In Figure 36, panel A, the ratio is very low for the pro-less variant without the pro-peptide (0.13) and either lower or higher with pro-peptide concentrations other than 1 (0.6, 0.66, 1.25 for ratios 0.1, 0.5 and 2.5 respectively). At 1:1 protein to pro-peptide ratio, the refolding to unfolding ratio is 1 suggesting the protein is fully reversible. This result suggests that the folding is not reversible without the pro-peptide and is partially reversible at lower pro-peptide concentrations. The protein folds reversibly only after addition of the pro-peptide in 1:1 ratio. Figure 36, panel B represents the histogram depicting refolding to unfolding ratio of the pro-less variant with different concentrations of the pro-peptide of procaspase-1. The refolding is similar for 0.1:1, 0.5:1 and 1:1 pro-peptide to protein ratio (~0.6) suggesting that the interaction between the pro-less variant and procaspase-3 pro-peptide is specific. The higher refolding value at pro-peptide to protein ratio was 2 : 1 due to higher refolding signal at 1 M urea concentration.

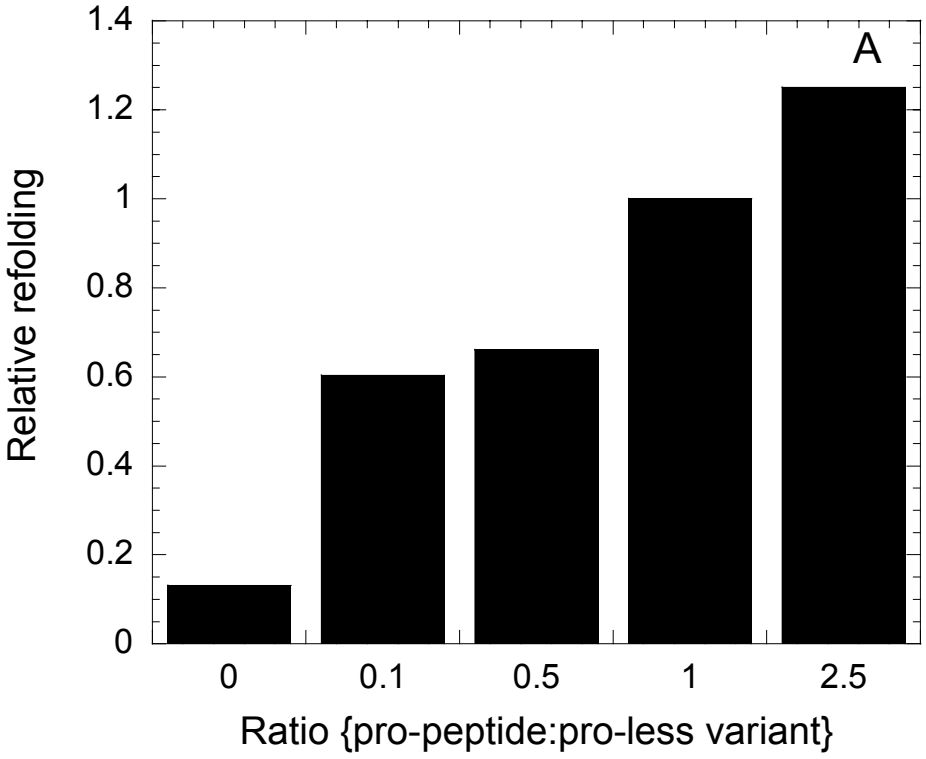

Figure 36. *Panel* A. Effect of pro-peptide on folding. Yield of native protein versus procaspase-3 pro-peptide concentration.

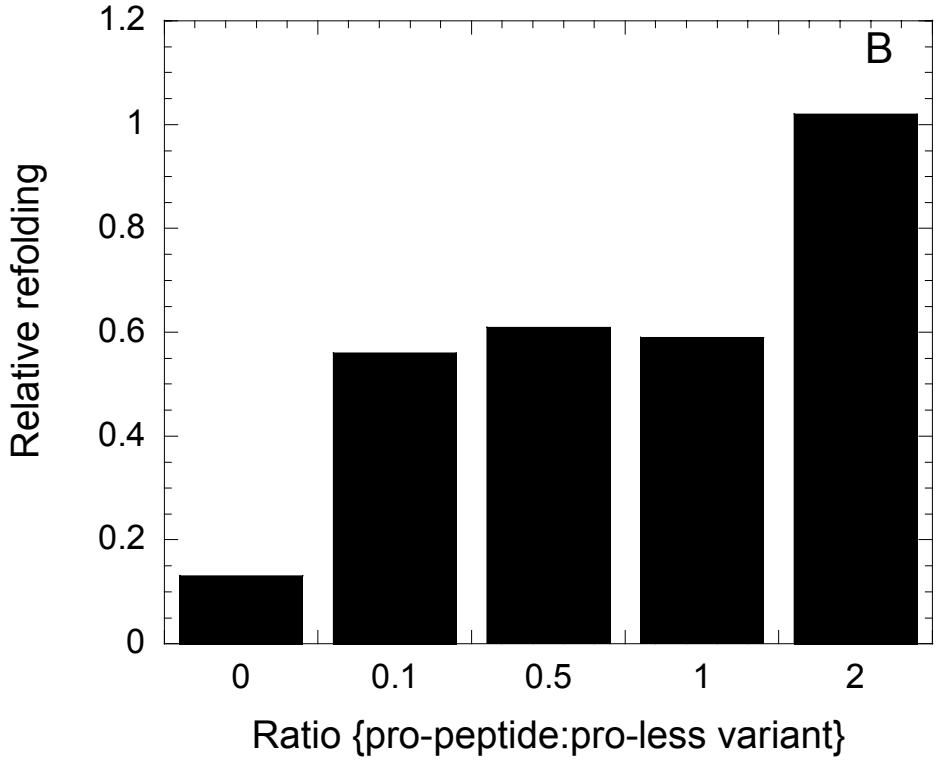

Figure 36. *Panel* B. Effect of pro-peptide of procaspase-1 on folding. Yield of native protein versus pro-peptide concentration

DISCUSSION

Studies of protein folding have had a major impact on the understanding of protein function and the control of human disease [65; 66; 67; 68]. Caspases are the key mediators in apoptosis, a process that is absolutely necessary to maintain homeostasis in eumetazoans. While dysregulation of apoptosis is a common factor in a number of autoimmune diseases, neurodegenerative disorders and cancers [2], learning to selectively manipulate the level of apoptosis through the activation or inhibition of caspases may well lead to therapeutic strategies for these diseases.

Another underlying question in the studies of caspases is why the procaspases are not active in the cell. It is thought that the upstream caspases are stored as inactive monomers until apoptotic signals facilitate their dimerization and subsequent auto-activation. Less clear is why the downstream, executioner procaspases are inactive because they are known to be homodimers in the cell [69]. Moreover, the rate of autolysis for the procaspases increases at lower pH and the role of the short pro-domain in the folding and assembly of the executioner caspases is still unclear. Therefore, study of the folding, stability and active site conformation of procaspase-3 will provide insight into dimerization, maturation, and inhibition of the executioner caspases [3; 8; 9; 10; 11].

I. Characterization of active site conformation of procaspase-3

The recent structures of procaspase-7 [18; 28] suggest mechanisms for the procaspase dormancy. The C-terminal region of the intersubunit linker, called the blocking segment

(K186-V189), occupies the central cavity and prevents insertion of the elbow loop region of loop L3 from the opposite monomer. As a consequence, loop L3 is unraveled and solvent exposed. In addition, the covalent connectivity between the subunits prevents formation of the loop bundle between loops L4, L2 and L2'. Thus, the contacts that stabilize these loops in the active caspase have not formed in the procaspase. Upon cleavage at D175, loops L3 and L4 move to positions similar to those found in the active caspase, but loop L2' remains in the closed conformation, that is, bound in the central cavity. Upon binding of substrate/inhibitor, loop L2' flips 180° to contact loops L2 and L4, forming the loop bundle. Overall, the procaspase-7 structures show that the incomplete formation of the S1, S2, and S4 subsites are incompatible with the binding of peptide substrates.

Nicholson and coworkers showed that procaspase-3 is catalytically competent [30], although the steady-state parameters were not described. Using a triple mutant in which the three processing sites were removed (D9A,D28A,D175A), our co-workers show that the activity of procaspase-3 is about 200-fold lower than that of the mature caspase-3 and the decrease in activity has been attributed to decrease in its catalytic efficiency but not to its substrate binding ability (data not shown). Other uncleavable procaspases have been described as catalytically competent as well [30].

We note here that experiments performed on the triple mutant are only suggestive of the wild-type protein since point mutations may have effects on local secondary structures. However, we also note that with the exception of the activity measurements, procaspase-3(D_3A) and procaspase-3(C163S) are interchangeable in the biochemical and biophysical studies described here. The inactive procaspase-3(C163S), which is similar to

the C163A mutation used in the structural studies [18; 28], contains the three processing sites. Our results indicate that replacing the three aspartates with alanine has minimal effects on the protein structure, but the conclusions are tempered by our work on a mutant rather than the wild-type protein.

Our suggestion of a structural model in which loop L3 is inserted into the active site, with consequential formation of the substrate-binding pocket, is supported by the following observations. First, trypsin cleaves R207, in loop L3, much more slowly than K57/R64, in loop L1, with a factor of >40 in $t_{½}$ values ($t_{½}$ < 2 minutes versus ~75 minutes). In addition, R207 is protected from cleavage upon binding of inhibitor. Second, fluorescence emission studies showed that W206, on loop L3, is not solvent exposed but rather appears to be close to W214 in the active site. This was shown by a blue-shift in the fluorescence emission wavelength maximum of the two tryptophan mutants, W206Y and W214V. If W206 were exposed to solvent in the procaspase, then one would expect a red-shifted fluorescence emission in the W214V mutant. In addition, there was no change in the tryptophan fluorescence emission of the procaspase upon binding of inhibitor, again suggesting that W206 is close to W214 in the procaspase. Third, fluorescence emission and quenching studies showed that, at pH >7, the tryptophans are less solvent accessible in the procaspase compared to the mature caspase. This is observed as a red-shift in tryptophan fluorescence emission upon maturation, consistent with an opening of the active site. A more open active site is shown also by the increase in the accessibility of R207 to cleavage by trypsin in the mature caspase. This is consistent with a decrease in the pKa's of the two catalytic groups upon maturation. The accessibility of the negatively charged iodide quencher was low at pH>7 and increased at lower pH, with

two transitions observed. While it is not yet clear what these titrations represent in terms of conformational changes in the protein, the protonations leading to the conformational change appear to affect the electrostatic environment of the tryptophanyl residues by making it more electropositive rather than facilitating the unraveling of loop L3. This is supported by the observations that there was no effect of pH on the accessibility of either acrylamide or cesium in the fluorescence quenching studies.

Results from limited proteolysis by V8 protease are consistent with other conformational changes that occur upon maturation, as observed in the structural studies. In particular, D190, near the blocking segment (K186-V189), is cleaved by V8 protease in the procaspase, but it is protected in the mature caspase. In caspase-3, D190 may form a salt-bridge with K137, on helix 3. The distance between the two side-chains decreases about 4 Å upon maturation, and these movements may be related also to the salt bridge that forms between E106 and R86 upon maturation. If this is true, then the movements in loop L2' may somehow facilitate movements in helices-2 and -3, on the surface of the large subunit. In addition to these movements, the C-terminus of the small subunit, particularly E272, becomes more accessible to the protease upon maturation. In the quaternary structure, E272 is in the same face of the protein as D190, although the two are separated by ~20 Å. Overall, our results are consistent with movements in loop L2' upon maturation, as observed in the structural studies.

Nicholson and coworkers showed that a tri-aspartate "safety-catch" in the intersubunit linker (D179-D181) affects procaspase dormancy in a pH-dependent manner [30]. The loop containing the tri-peptide may adopt a pH-sensitive conformation that renders the IETD175 cleavage site inaccessible. We also observe a pH-dependent conformational

change in the pro-peptide and in loop L4 in the V8 protease assays. First, the pro-peptide appears to dissociate from the protein at pH 5. This is observed as a rapid removal of the pro-peptide by V8 protease at lower pH. Second, the accessibility of E248/D253 in loop L4 is much greater at pH 5 than at pH 7, suggesting that loop L4 undergoes a conformational change that results in faster cleavage by the protease. Between pH 7 and 5, there is little change in the fluorescence emission of the procaspase, although at lower pH there is a blue-shift in the emission wavelength maximum. Thus, in addition to the intersubunit linker tri-aspartate "safety-catch" described by Nicholson and coworkers, the pro-peptide and loop L4 also undergo pH-dependent conformational changes.

The presence of a well-formed active site has been observed in the zymogens of other proteases, although the precise mechanisms of their activation differ [70]. In lysosomal cathepsins, the active site is fully formed, but the pro-domain interacts with the active site and prevents maturation [71]. The activation is triggered by a drop in pH that substantially weakens the interaction between the pro-peptide and the catalytic domain, resulting in widening the active site cleft [72]. In the trypsin family of serine proteases, the dislocated catalytic machinery of trypsinogen undergoes re-orientation after proteolysis at R15 [72]. Here, we suggest that the procaspase-3 dimer has an intact substrate-binding pocket, like caspase-3, and the active site in caspase-3 adopts an open conformation after cleavage of the intersubunit linker. Cleavage at D175 allows the linker to move away from the catalytic groove and form the loop bundle.

We suggest that formation of the loop bundle is critical in opening and stabilizing the active site. The contacts formed between loops L2, L4, and L2' may move loop L4 away from the catalytic groove, further opening the active site. Loop L4 has four phenylalanine

residues in close proximity to the tryptophans. Positioning the phenylalanines close to the tryptophans could account for the blue-shifted fluorescence emission observed for the procaspase. Upon maturation, conformational changes in loops L4 and L2 may open the active site, consistent with the structural studies. These movements allow the C163 side-chain to rotate toward the S1 sub-site and hence form the oxyanion hole.

This mechanism stresses the importance of dimerization on active site formation. Indeed, it is generally accepted that caspase monomers are inactive. The best evidence for this is observed in caspase-9 [73], although it also has been shown in caspase-1 [64]. Under normal physiological conditions caspase-9 is a monomer, and activity is associated with the formation of transient dimers [73]. In the absence of the dimeric structure, the loop bundle cannot form.

It is worth noting that the recognition sequence in the executioner subfamily is not optimized for auto-activation. The caspases in this subfamily prefer the sequence DEXD [6], whereas the sequence in the intersubunit linker is IXXD. The (I/V/L)EXD sequence is preferred by caspases-6, -8, -9 and -10 [6]. In contrast, procaspases in the caspase-1 subfamily are activated following cleavage at WXXD in the intersubunit linker. The WEXD sequence is preferred by the caspase-1 subfamily [6] and is in keeping with the general idea of a scaffold-mediated auto-activation. This may add another level of control to attenuate the auto-activation of the executioner procaspases.

II. Folding and stability of procaspase-3

We have described conditions for the equilibrium unfolding of procaspase-3 in urea-containing phosphate buffer, as monitored by both fluorescence emission and circular

dichroism measurements. The folding is completely reversible, and the data demonstrated biphasic transitions, suggesting an apparent three-state unfolding process. There was a blue shift in the fluorescence emission spectrum when the protein was incubated in 4 M urea-containing buffer, suggesting that the tryptophanyl residues remain mostly buried in the equilibrium intermediate. Above 5 M urea, there was both a decrease in intensity and a red shift in the fluorescence emission spectrum, demonstrating the unfolding of the protein. When we examined unfolding at several concentrations of procaspase-3 (C163S), we observed that the mid-point for the first transition was constant, whereas the mid-point for the second transition was dependent on the protein concentration. This suggested that the second transition represents the dissociation of the dimer and that the intermediate populated between 3 M and 5 M urea was a dimer. Interestingly, however, the amplitude of the plateau was also dependent on the protein concentration. While these results cannot be explained by a three-state unfolding process, they are well described by a four-state model. In this model, the native dimer isomerizes to a dimeric intermediate, and the dimeric intermediate dissociates to a monomeric intermediate, which then unfolds. The decrease in the amplitude of the plateau is a result of the dissociation of the dimeric intermediate to the monomeric intermediate. Based on this model, we have determined the conformational free energies and *m*-values for the three steps in equilibrium unfolding. The data show that the protein is very stable, with a conformational free energy of 25.8 kcal/mol, and that unfolding is a highly cooperative process.

These results show two important points. First, dimerization of procaspase-3 occurs as a result of the association of two monomeric folding intermediates. Therefore, we

consider procaspase-3 dimerization to be a folding event. Second, the stability of the dimer contributes significantly to the conformational free energy of the protein (approximately 18.8 kcal/mol). These results are consistent with our previous conclusions based on the solution properties of the dimer [22], and we predict that the protein is also a dimer *in vivo*.

According to Schellman [74] and Alonso and Dill [75], the *m*-value should be proportional to the surface area of the protein exposed to solvent upon unfolding, ΔASA. Scholtz and coworkers [76] have described empirical relationships that correlate ΔASA with experimental *m*-values, as shown in equation 27.

$$m = 368 + 0.11*(\Delta ASA) \qquad \text{(Eq. 27)}$$

Using this equation and the value determined for m_2, one can calculate the ΔASA for the transition of $I_2 \rightleftharpoons 2I$ to be 1,200 Å^2. Based on the crystal structure of caspase-3 [19], the dimer interface between the two small subunits comprises 2000 Å^2. Given the experimental error in determining the value of m_2 (± 0.1 kcal/mol/M), our results suggest that the dimer interface may be largely intact in the dimeric intermediate, I_2. It is interesting to note that the equilibrium unfolding of procaspase-3 is unique as it represents a complex four-state model, where dissociation of the dimer and unfolding of the monomeric species do not occur simultaneously as usually observed with other oligomeric proteins [51; 77].

Procaspase-3(C163S) unfolds at lower urea concentrations with decrease in pH as shown in Figure 37 A and B. Figure 37 A shows the fraction of native species versus urea

concentration. The fraction is similar between pH 8.5 and 6.5 and decreases slowly up to pH 5. The fraction of native species is less than unity below pH 5 suggesting presence of intermediate species even at 0 M urea. Figure 37 B represents the fraction of unfolded species versus urea concentration. It shows that the protein unfolds at lower urea concentration with decrease in pH. Thus, the protein slowly loses its stability up to pH 5 and then dramatically between pH 5 and 4. This is suggestive of a conformational change within that pH range and is consistent with the values of the total free energy involved in this unfolding process as shown in Figure 32, panel B. The shoulder region is shifted to lower urea concentration with decrease in pH below pH 6.5. Thus, the native state isomerizes to the dimeric intermediate faster at lower pH and therefore the native state loses stability with decrease in pH. This can be seen from the $\Delta G_1^{H_2O}$ values in Table III (i.e. 7.4 ± 0.1 kcal/mol at pH 7.2 and 0.84 ± 0.2 kcal/mol at pH 4.75). At pH 4.75, a considerable amount of dimeric and monomeric intermediates are seen at 0 M urea, which suggests that the protein starts unfolding at that pH even without addition of urea. Further decrease in pH from 4.75 to 4.5 shows loss of concentration dependence suggesting the protein dissociates at that point. Between pH 4.2 and 4, the protein further changes its conformation and loses its intermediate monomeric state. The native monomer unfolds to an unfolded monomer. This change in protein conformation between pH 5 and 4 is also observed in V8 protease studies. This change is attributed to the conformational change in the protein except in the loop L4 region. Moreover, there is a slow conformational change between pH 7 and 5 as observed in the V8 protease studies. This is due to the pro-domain being more solvent-exposed and unbound at lower pH as well as a conformational change in the loop L4 region.

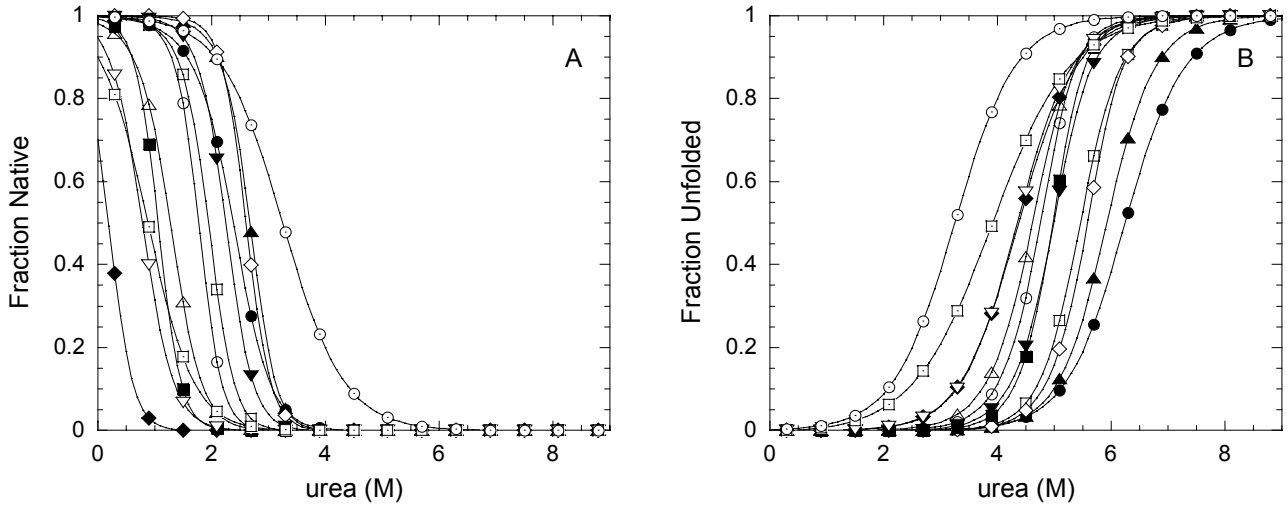

Figure 37. *Panel* A. Fraction of native species of procaspase-3(C163S) at different pH. *Panel* B. Fraction of unfolded species of procaspase-3(C163S) at different pH. (●) represents data at pH 8.5, (□) represents data at pH 8, (▲) represents data at pH 7.6, (◇) represents data at pH 7.2, (▼) represents data at pH 6.5, (○) represents data at pH 6, (■) represents data at pH 5.5, (Δ) represents data at pH 5, (◆) represents data at pH 4.75, (▽) represents data at pH 4.5, (⊡) represents data at pH 4.2, (⊙) represents data at pH 4.

It is interesting to note that the protein unfolds via different mechanisms at different pH, i.e. the mechanism moves from a four-state dimer to a three-state monomer and then to a two-state monomer. The total free energies (Table III) show that the protein is most stable at pH 7.2 and its stability decreases with decrease in pH. Data from our lab shows a blue-shift in the tryptophan fluorescence for procaspase-3(C163S) between pH 5 and 4 with a pKa of ~ 4.7 suggesting titration of one or more acidic groups in that region. Although the specific groups have not been identified, it suggests that one or more salt-bridges might affect the dimer stability in procaspase-3.

According to Dill [78], proteins with homologous native conformations can fold via different structural intermediates, or pathways, in order to reach the homologous conformation. Although the structures of the procaspases are not known, they are likely to be similar, with the noted exceptions of the pro-domains. The non-native conformations that occur during the folding of the procaspases, however, are not necessarily conserved, and thus may represent specific targets for inhibition. For example, we have found that a thermodynamically stable dimeric intermediate is present during the folding of procaspase-3. In the caspase-3 dimer, and by analogy the procaspase-3 dimer, the dominant forces linking the two monomers are hydrogen bonding interactions between the two antiparallel β-strands of the small subunits and hydrophobic interactions between Val^{266} and $Val^{266\#}$ at the two-fold symmetry axis. In contrast, the dimer interface of procaspase-1 is very different. While the interface is also comprised of two antiparallel β-strands, it consists of four charged residues that form two salt bridges. It is not yet known whether the folding intermediate observed for procaspase-3 also exists for procaspase-1, but our data suggest that the intermediate may

be very different. Thus, while the native structures are conserved, the folding pathways may differ.

III. Role of the short pro-domain in procaspase-3

We examined the mutant of procaspase-3(C163S) that lacks the pro-domain (pro-less variant). We have shown that the pro-less variant does not fold reversibly in *vitro* unless the pro-peptide is present in *trans* at equimolar concentrations to the pro-less variant. The yield of the native pro-less variant is ~10% in the absence of the pro-peptide; however, the yield increases to ~100% at ratios of 1:1 (pro-peptide : pro-less variant) or greater. These data suggest that the pro-peptide of procaspase-3 functions as an intra-molecular chaperone or IMC. The interesting paradox shown by our data is that the pro-less variant is a dimer when produced and purified from the *E.coli* expression system. However, the *in vitro* refolding experiments demonstrate that the folding is not reversible in the absence of the pro-peptide. We suggest that this is due to the difference in protein concentrations found in the two experimental conditions that is, the protein expression was high in the recombinant system. Whereas, in our *in vitro* refolding experiments, the protein concentration was in low micromolar range. Our hypothesis is that the pro-peptide of procaspase-3 assists in the folding process by facilitating dimerization. Further experiments are required to confirm this.

CONCLUSIONS

The overall conclusions from these studies are:

1. Procaspase-3(C163S) has both the active sites active as its mature counterpart.
2. Limited proteolysis with trypsin, fluorescence quenching and pH titration studies show that loop L3 is not unraveled and solvent exposed in the zymogen, even at lower pH.
3. V8 protease studies are consistent with movements in loops L2', L2 and L4 during maturation. These movements are observed in the crystal structures.
4. Therefore, procaspase-3 has an intact substrate-binding pocket with loop L3 inserted into the active site pocket.
5. Zymogen processing leads to a more solvent accessible conformation of the active site facilitating catalysis.
6. Procaspase-3(C163S) unfolds via a four-state unfolding process at pH 7.2. Folding contributes significantly to the stability of the protein.
7. Dimerization is a folding process in procaspase-3(C163S).
8. The protein moves from a four-state dimeric unfolding model (pH 8.5 to pH 4.75) to a three-state monomer (pH 4.5 to 4.2) and finally to a two-state monomer model (pH 4). This is consistent with conformational change and dissociation of the dimer between pH 5 and 4.
9. Stability of procaspase-3 is maximum at pH 7.2 and decreases with decrease in pH.
10. One or more salt-bridges might affect the stability of the dimer.

11. The pro-peptide moves away from the protease domain and is solvent-exposed at lower pH.
12. The pro-peptide might act as an intra-molecular chaperone during protein folding.

FUTURE STUDIES

These experiments will help develop further studies that will answer several intriguing questions as well as confirm some of our preliminary results.

1. Characterization of folding and assembly of procaspase-1.

This will tell us whether the procaspases fold and assemble via similar mechanisms. Established biophysical probes will be employed to determine whether procaspase-1 is a monomer or dimer, determine the equilibrium folding mechanism of procaspase-1 and characterize the kinetics of folding. Results from these experiments will determine whether the folding mechanisms are conserved and will test the paradigm of caspase-1 assembly.

2. Determination of how the pro-domains of procaspase-1 and –3 function as intramolecular chaperones (IMC) during folding.

Evidence is presented that the pro-peptide of procaspase-3 functions as an IMC. Experiments will be performed to look at the role of the pro-domain of procaspase-1. Using a combination of mutational and biophysical studies, the kinetic folding step(s) that is altered by the pro-peptide will be studied. Also it will be seen whether the action is specific to each procaspase and what is the mechanism of action. These results will describe precise mechanism of action and will determine whether the action is specific to each procaspase.

REFERENCES

1. Kerr, J., Wyllie, A. & Currie, A. (1972). Apoptosis: A basic biological phenomenon with wide-ranging implications in tissue kinetics. *British Journal of Cancer* 26, 239-257.
2. Kumar, S. (1999). Regulation of caspase activation in apoptosis: implications in pathogenesis and treatment of disease. Clinical and experimental pharmacology and physiology. *Clin Expl Pharmacol Physiol* 26, 295-303.
3. Earnshaw, W. C., Martins, L. M. & Kaufmann, S. H. (1999). Mammalian caspases: structure, activation, substrates, and functions during apoptosis. *Annu Rev Biochem* 68, 383-424.
4. Salvesen, G. & Dixit, V. (1999). Caspase activation: the induced-proximity model. *Proc Natl Acad Sci U S A* 96, 10964-10967.
5. Liu, X., Kim, C., Yang, J., Jemmerson, R. & Wang, X. (1996). Induction of apoptotic program in cell-free extracts: requirement for dATP and cytochrome c. *Cell* 86, 147-157.
6. Grutter, M. (2000). Caspases: key players in programmed cell death. *Curr Opin Struct Biol* 10, 649-655.
7. Thornberry, N., Bull, H., Calaycay, J., Chapman, K., Howard, A., Kostura, M., Miller, D., Molineaux, S., Weidner, J., Aunins, J., Elliston, K., Ayala, J., Casano, F., Chin, J., Ding, G.-F., Egger, L., Gaffney, E., Limjuco, G., Palyha, O., Raju, S., Rolando, A., Salley, J., Yamin, T.-T., Lee, T., Shively, J., MacCross, M., Mumford, R., Schimdt, J. & Tocci, M. (1992). A novel heterodimeric cysteine

protease required for interleukin-1ß-processing in monocytes. *Nature* 356, 768-774.

8. Budihardjo, I., Oliver, H., Lutter, M, Luo, X. & Wang, X. (1999). Biochemical pathways of caspase activation during apoptosis. *Annu Rev Cell Dev Biol* 15, 269-290.

9. Thornberry, N. A., Rano, T. A., Peterson, E. P., Rasper, D. M., Timkey, T., Carcia-Calvo, M., Hotzager, V. M., Nordstrom, P. A., Roy, S., Vaillancourt, J. P., Chapman, K. T., and Nicholson, D. W. (1997). A combinatorial approach defines specificities of members of the caspase family and granzyme B. *J Biol Chem* 272, 17907-17911.

10. Stennicke, H. & Salvesen, G. (1997). Biochemical characteristics of caspases-3, -6, -7, and -8. *J Biol Chem* 272, 25719-25723.

11. Garcia-Calvo, M., Peterson, E. P., Rasper, D. M., Vaillancourt, J. P., Zamboni, R., Nicholson, D. W., and Thornberry, N. A. (1999). Purification and catalytic properties of human caspase family members. *Cell Death Differ* 6, 362-369.

12. Alnemri, E. (1997). Mammalian cell death proteases: a family of highly conserved aspartate specific cysteine protease*s. J Cell Biol* 64, 33-42.

13. Rotonda, E., Rasper, D., Ruel R, V., JP, Thornberry, N., Becker, J., Rotonda, J., Nicholson, D., Fazil, K., Gallant, M., Gareau, Y. & Labelle, M. (1996). The three-dimensional structure of apopain/CPP32, a key mediator of apoptosis. *Nat Struct Biol* 7, 619-625.

14. Walker, N. P. C., Talanian, R.V., Brady, K.D., Dang, L.C., Bump, N.J., Ferenz, C.R., Franklin, S., Ghayur, T., Hackett, M.C. and Hammill, L.D. (1994). Crystal

structure of the cysteine protease interleukin-1beta-converting enzyme: A (p20/p10)2 homodimer. *Cell* 78, 343-352.

15. Wilson, K. P., Black, J.A., Thomson, J.A., Kim, E.E., Griffith, J.P., Navia, M.A., Murcko, M.A., Chambers, S.P., Aldape, R.A., Raybuck, S.A. and Livingston, D.J. (1994). Structure and mechanism of interleukin-1 beta converting enzyme. *Nature* 370, 270-275.

16. Watt, W., Koeplinger, K.A., Mildner, A.M., Heinrikson, R.L., Tomasselli, G. Watenpaugh, K.D. (1999). The atomic resolution structure of human caspase-8, a key activator of apoptosis. *Structure* 27, 1135-1143.

17. Wei, Y., Fox, T., Chambers, S.P., Sintchak, J., Coll, J.T., Golec, J.M., Swenson, L., Wilson, K.P ., Charifson, P.S. (2000). The structures of caspases-1, -3, -7 and -8 reveal the basis for substrate and inhibitor selectivity. *Chem Biol* 7, 423-432.

18. Chai, J., Shiozaki, E., Srinivasula, S., Wu, Q., Data, P., Alnemri, E. & Shi, Y. (2001). Structural Basis of Caspase-7 Inhibition by XIAP. *Cell* 104, 769-780.

19. Mittl, P., Di Marco, S., Krebs, J., Bai, X., Karanewsky, D., Priestle, J., Tomaselli, K. & Grutter, M. (1997). Structure of recombinant human CPP32 in complex with the tetrapeptide Acetyl-Asp-Val-Ala-Asp fluoromethyl ketone. *J Biol Chem* 272, 6539-6547.

20. Tewari, M., Quan, L., O'Rouke, K., Desnoyers, S., Zeng, Z., Beidler, D., Poirier, G., Salvesen, G. & Dixit, V. (1995). Yama/CPP32 beta, a mammalian homolog of CED-3, is a CrmA-inhibitable protease that cleaves the death substrate poly(ADP-ribose) polymerase. *Cell* 81, 801-809.

21. Kuida, K., Zheng, T., Na, S., Kuan, C.-Y., Yang, D., Karasuyama, H., Rakic, P. & Flavell, R. (1996). Decreased apoptosis in the brain and premature lethality in CPP32-deficient mice. *Nature* 384, 368-372.

22. Pop, C., Chen, Y., Smith, B., Bose, K., Bobay, B., Tripathy, A., Franzen, S. & Clark, A. (2001). Removal of the pro-domain does not affect the conformation of the procaspase-3 dimer. *Biochemistry* 40, 14224-14235.

23. Shi, Y. (2002). Mechanisms of caspase activation and inhibition during apoptosis. *Mol Cell* 9, 459-470.

24. Stennicke, H., Jurgensmeier, J., Shin, H., Deveraux, Q., Wolf, B., Yang, X., Zhou, Q., Ellerby, H., Ellerby, L., Bredesen, D., Green, D., Reed, J., Froelich, C. & Salvesen, G. (1998). Pro-caspase-3 is a major physiologic target of caspase-8. *J Biol Chem* 273, 27084-27090.

25. Stennicke, H. & Salvesen, G. (1998). Properties of the caspases. *Biochim Biophys Acta* 1387, 17-31.

26. Gu, Y., Wu, J., Faucheu, C., Lalanne, J.-L., Diu, A., Livingston, D. J. & Su, M. S.-S. (1995). Interleukin-1 beta converting enzyme requires oligomerization for activity of processed forms in vivo. *EMBO J* 14, 1923-1931.

27. Chai, J., Wu, Q., Shiozaki, E., Srinivasula, S., Alnemri, E. & Shi, Y. (2001). Crystal structure of a procaspase-7 zymogen: mechanisms of activation and substrate binding. *Cell* 107, 399-407.

28. Riedl, S., Fuentes-Prior, P., Renatus, M., Kairies, N., Krapp, S., Huber, R., Salvesen, G. & Bode, W. (2001). Structural basis for the activation of human procaspase-7. *Proc Natl Acad Sci U S A* 98, 14790-14795.

29. Saunders, P., Cooper, J., Roodell, M., Schroeder, D., Borchert, C., Isaacson, A., Schendel, M., Godfrey, K., Cahill, D., Walz, A., Loegering, R., Gaylord, H., Woyno, I., Kaluyzhny, A., Krzyzek, R., Mortari, F., Tsang, M. & Roff, C. (2000). Quantification of active caspase 3 in apoptotic cells. *Anal Biochem* 284, 114-124.

30. Roy, S., Bayly, C., Gareau, Y., Houtzager, V., Kargman, S., Keen, S., Rowland, K., Seiden, I., Thornberry, N. & Nicholson, D. (2001). Maintenance of caspase-3 proenzyme dormancy by an intrinsic "safety catch" regulatory tripeptide. *Proc Natl Acad Sci U S A* 98, 6132-6137.

31. Muzio, M., Stockwell, B., Stennicke, H., Salvesen, G. & Dixit, V. (1998). An induced proximity model for caspase-8 activati*on. J Biol Chem.* 273, 2926-2930.

32. Stennicke, H. & Salvesen, G. (1999). Caspases: Preparation and Characterization. *Methods* 17, 313-319.

33. Anfinsen, C. B. (1973). Principles that govern the folding of protein chains. *Science* 181, 223-230.

34. Baker, D. (2000). A surprising simplicity to protein folding. *Nature* 405, 39-42.

35. Grantcharova, V., Alm, E., Baker, D. & Horwich, A. (2001). Mechanisms of protein folding. *Curr Opin Struct Biol* 11, 70-82.

36. Jackson, S. (1998). How do small single domain proteins fold? *Fold Des* 3, 81-91.

37. Mirny, L. & Sakhnovich, E. (1999). Universally conserved positions in protein folds: reading evolutionary signals about stability, folding kinetics and function. *J Mol Biol* 291, 177-196.

38. Allaire, M., Chernaia, M., Malcolm, B. & James, M. (1994). Picornaviral 3C cysteine proteinases have a fold similar to chymotrypsin-like serine proteinases. *Nature* 369, 72-76.

39. Kourie, J. (2002). Prion channel proteins and their role in vacuolation and neurodegenerative diseases. *Eur Biophys J.* 31, 409-416.

40. Shinde, U., Fu, X. & Inouye, M. (1999). A pathway for conformational diversity in proteins mediated by intramolecular chaperones. *J Biol Chem* 274, 15615-15621.

41. Baker, D., Sohl, J. & Agard, D. A protein-folding reaction under kinetic control. *Nature* 356, 194-195.

42. Baker, D., Silen, J. & Agard, D. (1992). Protease pro region required for folding is a potent inhibitor of the mature enzyme. *Proteins* 12, 339-344.

43. Anfinsen, C. & Scheraga, H. (1975). Experimental and theoretical aspects of protein folding. *Adv Prot Chem* 29, 205-300.

44. Wang, Z., Mottonen, J. & Goldsmith, E. (1996). Kinetically controlled folding of the serpin plasminogen activator inhibitor 1. *Biochemistry* 35, 16443-16448.

45. Sauter, N., Mau, T., Rader, S. & Agard, D. (1998). Structure of alpha-lytic protease complexed with its pro region. *Nat Struct Biol* 5, 945-950.

46. Shinde, U. & Inouye, M. (1995). Folding pathway mediated by an intramolecular chaperone: characterization of the structural changes in pro-subtilisin E coincident with autoprocessing. *J Mol Biol* 252, 25-30.

47. Fernandez-Alnemri, T., Litwack, G. & Alnemri, E. (1995). Mch2, a new member of the apoptotic Ced-3/Ice cysteine protease gene family. *Cancer Research* 55, 2737-2742.

48. Clark, A., Ramanathan, R. & Frieden, C. (1998). Purification of GroEL with low fluorescence background. *Methods in Enzymology* 290, 100-118.

49. Edelhoch, H. (1967). Spectroscopic determination of tryptophan and tyrosine in proteins. *Biochemistry* 6, 1948-1954.

50. Pace, C., Shirley, B. & Thompson, J. (1989). *Protein Structure, A Practical Approach* (ed.), C. T., Ed.), IRL Press, New York.

51. Clark, C., Sinclair, J. & Baldwin, T. (1993). Folding of Bacterial Luciferase Involves a Non-native Heterodimeric Intermediate in Equilibrium with the Native Enzyme and the Unfolded Subunits. *J Biol Chem* 268, 10773-10779.

52. Towbin, H., Staehelin, T. & Gordon, J. (1979). Electrophoretic transfer of proteins from polyacrylamide gels to nitrocellulose sheets: procedure and some applications. *Proc Natl Acad Sci U S A* 76, 4350-4354.

53. Thompson, J., Shirley, B., Grimsley, G. & Pace, C. (1989). Conformational stability and mechanism of folding of ribonuclease T1. *J Biol Chem* 264, 11614-11620.

54. Royer, C., Mann, C. & Matthews, C. (1993). Resolution of the fluorescence equilibrium unfolding profile of trp aporepressor using single tryptophan mutants. *Protein Sci* 2, 1844-1852.

55. Fu, L. & Liang, J. (2002). Unfolding of human lens recombinant beta-B2 and gamma-C crystallins. *J Struct Biol* 139, 191-198.

56. Santoro, M. & Bolen, D. (1988). Unfolding free energy changes determined by the linear extrapolation method. 1. Unfolding of phenylmethanesulfonyl alpha-chymotrypsin using different denaturants. *Biochemistry* 27, 8063-8068.

57. Lackowicz, J. (1986). *Principles of Fluorescence Spectroscopy* (Orton, C., Ed.), Plenum Press, NY & London.

58. Bianchini, E., Louvain, V., Marque, P.-E., Juliano, M., Juliano, L. & Le Bonniec, B. (2002). Mapping of the catalytic groove preferences of factor Xa reveals an inadequate selectivity for its macromolecule substrates. *J Biol Chem* 277, 20527-20534.

59. Drapeau, G., Boily, Y. & Houmard, J. (1972). Purification and properties of an extracellular protease of Staphylococcus aureus. *J Biol Chem* 247, 6720-6726.

60. Ryser, S., Vial, E., Magnenat, E., Schlegel, W. & Maundrell, K. (1999). Reconstitution of caspase-mediated cell-death signalling in Schizosaccharomyces pombe. *Curr Genet* 36, 21-28.

61. Fernandes-Alnemri, T., Litwack, G. & Alnemri, E. (1994). CPP32, a novel human apoptotic protein with homology to Caenorhabditis elegans cell death protein Ced-3 and mammalian interleukin-1 beta-converting enzyme. *J Biol Chem* 269, 30761-30764.

62. Dorstyn, L., Kinoshita, M. & Kumar, S. (1998). Caspases in cell death. *Results probl cell differ* 24, 1-24.

63. Stennicke, H. R., Deveraux, Q. L., Humke, E. W., Reed, J. C., Dixit, V. M. & Salvesen, G. S. (1999). Caspase-9 can be activated without proteolytic processing. *J Biol Chem* 274, 8359-8362.

64. Van Criekinge, W., Beyaert, R., Van de Craen, M., Vandenabeele, P., Schotte, P., De Valck, D., and Fiers, W. (1996). Functional characterization of the prodomain of interleukin-1β-converting enzyme. *J Biol Chem* 271, 27245-27248.

65. Barr, P. J. & Tomei, D. L. (1994). Apoptosis and its role in human disease. *Bio-Technol* 12, 487-493.

66. Brown, C., Hong-Brown, L. & Welch, W. (1997). Strategies for correcting the delta F508 CFTR protein-folding defect. *J Bioenerg Biomembr* 29, 491-502.

67. Kelly, J. (1998). The alternative conformations of amyloidogenic proteins and their multi-step assembly pathways. *Curr Opin Struct Biol* 8, 101-106.

68. Cohen, F. E. (1999). Protein misfolding and prion diseases. *J Mol Biol* 293, 313-320.

69. Cohen, G. (1997). Caspases: the executioners of apoptosis. *Biochem J* 326, 1-16.

70. Turk, B., Turk, D. & Turk, V. (2000). Lysosomal cysteine proteases: more than scavengers. *Biochim Biophys Acta* 1477, 98-111.

71. Rozman, J., Stojan, J., Kuhelj, R., Turk, V. & Turk, B. (1999). Autocatalytic processing of recombinant human procathepsin B is a bimolecular process. *FEBS Lett* 459, 358-362.

72. Zhuang, P. & Butterfield, D. (1992). Spin labeling and kinetic studies of a membrane-immobilized proteolytic enzyme. *Biotechnol Prog* 8, 204-210.

73. Renatus, M., Stennicke, H., Scott, F., Liddington, R. & Salvesen, G. (2001). Dimer formation drives the activation of cell death protease caspase 9. *Proc Natl Acad Sci U S A* 98, 14250-14255.

74. Schellman, J. (1978). Solvent denaturation. *Biopolymers* 17, 1305-1322.

75. Alonso, D. & Dill, K. (1991). Solvent denaturation and stabilization of globular proteins. *Biochemistry* 30, 5974-5985.

76. Myers, J., Pace, C. & Scholtz, J. (1995). Denaturant m values and heat capacity changes: relation to changes in accessible surface areas of protein unfolding. *Protein Sci* 10, 2138-2148.

77. Doyle, S., Braswell, E. & Teschke, C. (2000). SecA folds via a dimeric intermediate. *Biochemistry* 39, 11667-11676.

78. Dill, K. & Chan, H. (1997). From Levinthal to pathways to funnels. *Nat Struct Biol* 4, 10-19.